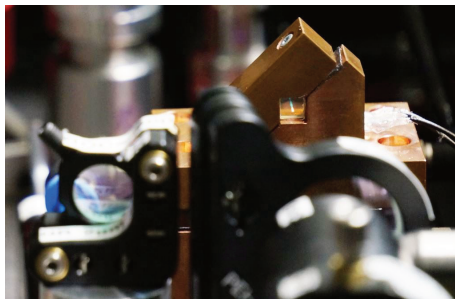# Regenerative amplification of ultrashort laser pulses with thulium- and holmium-doped materials

Von der Fakultät für Mathematik und Physik
der Gottfried Wilhelm Leibniz Universität Hannover
zur Erlangung des Grades

DOKTOR DER NATURWISSENSCHAFTEN
– **Dr. rer. nat.** –

genehmigte Dissertation von

Dipl.-Phys. Andreas Wienke

geboren am 16.03.1985 in Lüdenscheid

2016

Referent: Prof. Dr. Uwe Morgner
Korreferent: Prof. Dr. Detlev Ristau
Tag der Promotion: 12.02.2016

Kurzfassung

Andreas Wienke

Regenerative Verstärkung von ultrakurzen Laserpulsen mit Thulium- und Holmium-dotierten Materialien

Das Thema dieser Arbeit sind hochenergetische Ultrakurzpulslaserstrahlquellen bei einer Wellenlänge von 2 µm, die für viele Anwendungen im Bereich der Materialbearbeitung, zum Beispiel von Polymeren, interessant sind. Mit dem Konzept der regenerativen Verstärkung sollten hohe Pulsenergien im µJ-Bereich bei gleichzeitig ultrakurzen Pulsen erreicht werden. Das zunächst beschriebene System basierte vollständig auf Thulium-dotierten Materialien, die in einem Wellenlängenbereich von 1,9 µm bis 2,0 µm emittieren. Ein Thulium-dotierter Ultrakurzpulsfaseroszillator erzeugte Pulsdauern von 112 fs bei einer Wellenlänge von 1935 nm. Die Pulse wurden zeitlich in einer passiven Faser gestreckt, in einem Thulium-dotierten Faserverstärker auf nJ-Pulsenergien verstärkt und in einen regenerativen Verstärker eingekoppelt, der erstmalig mit Thulium-dotierten Materialien demonstriert wurde. Mit Hilfe eines Thulium:YAlO-Kristalls wurden Pulsenergien von mehr als 700 µJ erzeugt, einzig limitiert durch die Zerstörschwelle des Lasermaterials. Die Pulse konnten zu Dauern von weniger als 400 fs komprimiert werden. Der regenerative Verstärker wurde mit Stickstoffgas gespült, um die bei der Wellenlänge auftretende atmosphärische Absorption zu reduzieren. Weitere Untersuchungen bezüglich des Skalierungspotentials durch Variation der unterschiedlichen Betriebsparameter wurden durchgeführt. Ein weiteres vielversprechendes Lasermaterial sind Holmium-dotierte Fasern und Kristalle, deren Hauptemissionswellenlänge um 2,1 µm liegt. Der bisher bestehende Aufbau wurde zu einem vollständig auf Holmium basierenden System umgebaut und selbst entwickelte Thulium-dotierte Faserlaser wurden als Pumplaser verwendet. Der Holmium-dotierte Ultrakurzpulsfaseroszillator emittierte Pulsdauern von 463 fs bei einer Zentralwellenlänge von 2,1 µm, die mit einem Gitterstrecker zeitlich gestreckt und anschließend in einem Holmium-Faserverstärker auf nJ-Pulsenergie verstärkt wurden. Der nachfolgende regenerative Verstärker basierte auf einem Holmium:YAG-Kristall und verstärkte die Pulse auf ähnliche Energien von mehr als 700 µJ wie bei dem Thulium-Lasersystem, ebenfalls limitiert durch die Zerstörschwelle des Laserkristalls. Durch spektrale Formung der Seedpulse konnte eine komprimierte Pulsdauer von weniger als 1,2 ps erreicht werden. Weiterhin wurde das Skalierungsverhalten und die Verstärkungsdynamik des regenerativen Verstärkers durch Variation von unterschiedlichen Betriebsparametern untersucht. Beide Materialien liefern im direkten Vergleich fundamentale Erkenntnisse zur Auswahl des Verstärkungsmaterials in diesem Wellenlängenbereich.

Abstract

Andreas Wienke

Regenerative amplification of ultrashort laser pulses with thulium- and holmium-doped materials

The subject of this thesis are high energy ultrafast laser sources, which operate in the 2 µm wavelength range and are highly interesting for applications in material processing for example of polymers. By applying the concept of regenerative amplification, pulse energies in the µJ range should be reached with sub-ps pulse durations. The first system described was completely based on thulium-doped laser materials, which operate in the wavelength region between 1.9 µm and 2.0 µm. An ultrashort pulse thulium-doped fiber oscillator was developed, which generated pulses with durations of 112 fs at 1935 nm wavelength. Subsequent temporal stretching in a passive fiber and amplification in a thulium-doped fiber led to pulse energies in the nJ-range to seed a regenerative amplifier, which was demonstrated for the first time to operate with thulium-doped materials. By the use of a thulium:YAlO-crystal, output pulse energies of more than 700 µJ were generated. The maximum pulse energy was limited only by the damage threshold of the laser crystal. The pulses could be compressed to a duration of less than 400 fs. Purging of the regenerative amplifier cavity with nitrogen gas was necessary to reduce the strong atmospheric absorption that is present at this wavelength. Further investigations of the scaling potential in variation of round trip numbers, repetition rate, and seed energy were carried out. Another promising laser material are holmium-doped fibers and crystals, which emit wavelengths around 2.1 µm. The existing setup was changed to an entirely holmium-based system and self-developed thulium-doped fiber lasers were used as pump sources. The ultrashort pulse oscillator based on a holmium-doped fiber and delivered pulses with a duration of 463 fs at a central wavelength of 2.1 µm. The pulses were stretched in a grating stretcher and amplified in a subsequent holmium-doped fiber amplifier to the nJ energy range. After seeding the regenerative amplifier based on a holmium:YAG-crystal, similar pulse energies compared to the thulium-system of more than 700 µJ were reached, which were also limited by the damage threshold of the laser crystal. By spectrally shaping the seed pulses, a compressed pulse duration of less than 1.2 ps was achieved. The scaling behaviour and gain dynamics of the regenerative amplifier were investigated by a variation of round trip numbers, repetition rate, and seed energy. Both materials deliver in a direct comparison a fundamental understanding for the choice of the amplifying material in this wavelength range.

Für Isabel, Emilia & Leana.

Contents

Acronyms

Notation	Description
AC	autocorrelation
AR	anti reflective
ASE	amplified spontaneous emission
BFP	birefringent quartz-plate
CPA	chirped-pulse amplification
CW	continuous wave
Er	erbium
FBG	fiber Bragg grating
FR	Faraday rotator
FWHM	full width at half maximum
GDD	group delay dispersion
GVD	group velocity dispersion
HDF	holmium-doped fiber
HITRAN	high-resolution transmission molecular absorption
Ho	holmium
HR	highly reflective
HWP	half-wave plate
LD	laser diode
LMA	large mode area
LuO	Lu_2O_3
MFD	mode field diameter

Notation	Description
MIR	mid infrared
NA	numerical apertur
NDF	normal dispersion fiber
NPR	nonlinear polarization rotation
OC	output coupling
PC	Pockels cell
PCF	photonic crystal fiber
PER	polarization extinction ratio
PM	polarization maintaining
PR	partially reflective
QWP	quarter-wave plate
RA	regenerative amplifier
ROC	radius of curvature
RTP	rubidium titanyl phosphate
SA	saturable absorber
SESAM	semiconductor saturable absorber
SPM	self-phase modulation
TDF	thulium-doped fiber
TFP	thin film polarizer
Tm	thulium
Tm:YAP	thulium-doped YAlO$_3$

Notation	Description
TOD	third order dispersion
WDM	wavelength division multiplexer
YAG	$Y_3Al_5O_{12}$
YAP	$YAlO_3$
Yb	ytterbium
YLF	$YLiF_4$
ZGP	zinc-germanium-phosphide

CHAPTER 1

Introduction

Ultrafast lasers operating at a wavelength around $2\,\mu m$ have gained an increased interest in recent years because of their wide field of application in material processing, micromachining, texturing, but also applications in biology, medicine, and fundamental research technology benefit from these laser sources. Lasers operating in this wavelength region enable applications that were not addressed by commonly used $1\,\mu m$ laser systems. In the important field of industrial applications like material processing, $2\,\mu m$ lasers are used to directly process polymers without further preparation because the absorption at this wavelength is much higher than at $1\,\mu m$ [Sch10]. A novel regime for processing of semiconductor materials like silicon and gallium arsenide is enabled by utilizing their transparency range at $2\,\mu m$ wavelength. By focusing at the back surface of semiconductor wafers, material processing can be accomplished there without modification of the front surface [Geh14; Min15]. Furthermore, two- and three-photon absorption in the mid-infrared in semiconductor materials enables even in-volume processing with pulse durations around $100\,fs$ [Hur07]. Also extension of the cutoff energy in high harmonic generation [Kra92], atmospheric sensing [Kad11], and frequency conversion to longer wavelengths [Lei12; Mal15a; Pet01] are attractive topics in nowadays scientific research, which need high energy ultrashort pulses in the $2\,\mu m$ wavelength range. Especially the latter named frequency conversion is an interesting topic for resonant infrared ablation of polymers [Nai14; Nai13]. By optical parametric processes, the wavelength region above $3\,\mu m$ can be reached in which polymers have distinct absorption features. For example, the polymer PEDOT:PSS strongly absorbs at $3.03\,\mu m$, $3.40\,\mu m$ and $3.50\,\mu m$ while PET has absorption lines at $2.91\,\mu m$, $3.37\,\mu m$ and $3.43\,\mu m$. This can be exploited by selective patterning of a thin organic film in a combined structure of both polymers without damaging the other film. By this method, organic solar cells can be manufactured with very high efficiencies [Nai14].

High energy and ultrashort pulses in the wavelength region around 2 μm were not directly generated by a laser material in the past years but by several frequency conversion stages pumped with classical "workhorse" laser systems based on titanium:sapphire. The pump power to reach certain energy levels increases rapidly because several conversion stages are needed, which result in high acquisition costs, low optical-to-optical efficiencies, and complex and spacious setups.

In recent years, ultrashort fiber lasers based on rare-earth-doped optical fibers have superseded titanium:sapphire lasers in many terms. Especially the gain material ytterbium offers high pulse energies in the nJ-range directly from a compact, all-fiber oscillator and simultaneously a broad bandwidth to support comparable pulse durations (less than 30 fs). Such laser systems are much cheaper, because cost-effective pump diodes are used. For higher pulse energy levels, the amplification with laser crystals is inevitable and was realized by single- and multipass amplifiers or regenerative amplifiers generating several hundreds of μJ or even mJ pulse energy with excellent beam quality and pulse durations as short as 200 fs. However, frequency conversion stages are still needed to reach the 2 μm wavelength region and the setup becomes unwieldy.

The aim of this work was therefore the development of new ultrafast laser sources operating directly in the 2 μm wavelength region with μJ pulse energies. Two different high energy ultrashort pulse laser systems were set up at 1.94 μm and 2.1 μm wavelength, respectively. The laser system operating at 1.94 μm was completely based on thulium-doped materials and demonstrated for the first time. It consisted of a compact and straightforward solution: a self-developed ultrashort pulse seed oscillator, stretching unit, fiber preamplifier, and regenerative amplifier. The laser system was then modified to operate at 2.1 μm wavelength by changing the several stages to gain materials doped with holmium. Furthermore, special pump lasers to address the optimum absorption wavelength of the holmium-doped materials were developed.

This thesis is organized as follows: Chapter 2 gives a brief introduction into the fundamental theoretical understanding that is relevant for this work. This includes the description of pulse propagation in fibers by the nonlinear Schrödinger equation, chromatic dispersion and several nonlinear effects, as well as the generation of ultrashort pulses in fiber lasers and corresponding numerical simulations. Furthermore, the concepts of chirped-pulse amplification and especially regenerative amplification are described here. Chapter 3 gives an overview of the existing state of the art about high energy, ultrashort pulse laser systems at 2 μm.

The developed laser system at 1.94 μm wavelength is part of Chapter 4, which includes the basic properties of thulium-doped fibers and crystals, the development of an ultrashort

pulse oscillator with fiber based dispersion management and subsequent chirped-pulse amplification to the nJ-level in thulium-doped fibers. Several experiments in continuous wave and q-switched operation were carried out to determine the general behaviour of the laser cavity based on thulium-doped YAP, which was designed for regenerative amplification operation. Furthermore, the first demonstration of a regenerative amplifier based on Tm:YAP is presented. Output energies of hundreds of µJ are generated with sub-ps pulse durations. Purging of the regenerative amplifier cavity was necessary to suppress strong atmospheric absorptions. Further investigations on scaling potential of the regenerative amplifier were carried out when varying the numbers of round trips inside the regenerative amplifier cavity, the repetition rate and the input seed energy.

Chapter 5 focuses on the modification of the existing laser system to the 2.1 µm wavelength range with holmium-doped materials. The general properties of holmium-doped fibers and crystals are given and an ultrashort pulse holmium-fiber oscillator is described both experimentally and numerically. In another part of this chapter the grating stretcher and fiber preamplifier with holmium-doped fibers to generate nJ-pulses are described. For further amplification, the existing regenerative cavity was altered by changing the laser crystal to holmium-doped YAG. Proper pump lasers to address the optimum absorption wavelengths of the used holmium-doped media were developed. Continuous wave and q-switch experiments with the Ho:YAG laser cavity were performed to explore the characteristics of the laser material. When operating the laser cavity as regenerative amplifier, similar output energies compared to Tm:YAP were found. Spectral precompensation of the seed pulses was necessary to compensate the strong gain shaping inside the regenerative amplifier. The scaling behaviour and dynamics of the Ho:YAG regenerative amplifier were investigated by changing the round trip numbers, repetition rate and seed energy.

Finally, the results of this thesis are summarized and discussed in Chapter 6. Chapter 7 gives an outlook on possible further investigations.

CHAPTER 2

Fundamentals

In this chapter, the theoretical base will be addressed in the context of this thesis. Section 2.1 deals with the pulse propagation in fibers including chromatic dispersion and nonlinear effects. The ultrashort pulse generation in fiber lasers is emphasized in Section 2.2 while the basics of the corresponding numerical simulations are given in Section 2.3. The concept of chirped-pulse amplification will be explained in Section 2.4 and regenerative amplification of ultrashort pulses in Section 2.5.

2.1 Pulse propagation in fibers

An optical pulse is typically treated in the time domain as an electric field $E(t)$ of an electromagnetic wave, which undergoes a fast oscillation with a central frequency ω_0 under its pulse envelope with the amplitude $A(t)$:

$$E(t) = \frac{1}{2} \left[A(t) e^{i\omega_0 t} + c.c. \right].$$ (2.1)

The pulse envelope $A(t)$ varies only slowly compared to the electric field (s. Fig. 2.1 (a)) and is normalized such that its squared absolute value represents the average power $P = |A|^2$. The *slowly-varying envelope approximation* is an appropriate simplification for pulses with many cycles of the electric field [Ild04]. In this thesis, the pulse durations were in the range of $100\,\mathrm{fs}$ to $100\,\mathrm{ps}$, therefore this approximation is highly applicable here. The equation to describe the propagation of such a field in a fiber with negligible higher order dispersion and nonlinear effects except for self-phase modulation (SPM) is given by the nonlinear pulse propagation equation [Agr07]:

$$\frac{\partial A}{\partial z} + \beta_1 \frac{\partial A}{\partial t} + \frac{i\beta_2}{2} \frac{\partial^2 A}{\partial t^2} + \frac{\alpha}{2} A = \gamma(\omega_0) |A|^2 A,$$ (2.2)
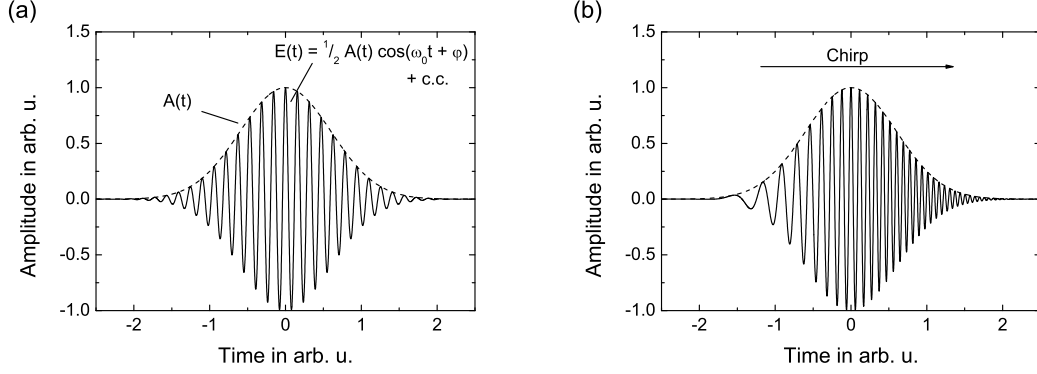
Figure 2.1: (a) Electrical field $E(t)$ of an optical pulse with envelope $A(t)$ and (b) visualized chirp on an optical pulse.

with the nonlinear parameter γ

$$\gamma(\omega_0) = \frac{n_2\omega_0}{cA_{eff}}, \tag{2.3}$$

α is the loss inside the fiber, c the velocity of light in vacuum and A_{eff} the effective mode area. The origin of the chromatic dispersion terms $\beta_{1,2}$, which affect the pulse in time, are explained in the following Subsection 2.1.1. The factor n_2 represents the nonlinear refractive index, which arises from the intensity I dependent Kerr effect (written here in its simplest form):

$$\tilde{n} = n(\omega) + n_2 I. \tag{2.4}$$

This nonlinear effect is a third-order susceptibility χ^3 effect, which is dominant in fibers because the χ^2 tensor vanishes in isotropic media (e.g. fused silica fibers). The Kerr effect leads to other nonlinear effects like SPM and nonlinear polarization rotation (NPR), which are described in Subsection 2.1.2.

If Equation (2.2) is transformed into the reference frame of the propagating pulse by $T \rightarrow t - z/v_G$ (with $v_G = 1/\beta_1$ group velocity; velocity of the pulse envelope), the following simplified equation can be attained:

$$i\frac{\partial A}{\partial z} + i\frac{\alpha}{2}A - \frac{\beta_2}{2}\frac{\partial^2 A}{\partial T^2} + \gamma\,|A|^2\,A = 0. \tag{2.5}$$

When losses are neglected ($\alpha = 0$), Equation (2.5) represents the nonlinear Schrödinger equation including second order dispersion and SPM. For this equation, the analytic solution

in terms of a soliton was found. Anyway, if the pulse duration approaches 100 fs and the pulse intensity gets higher, other nonlinear effects like Raman scattering, self-steepening, and higher order dispersion have to be included. This extended nonlinear Schrödinger equation can be solved by the split-step Fourier method (s. Section 2.3).

2.1.1 Chromatic dispersion

In general, chromatic dispersion describes the frequency dependent refractive index $n\left(\omega\right)$ of a (transparent) material. In the context of ultrashort pulses, this leads to a temporal pulse broadening (also called: chirping), when the various propagating frequencies experience each a different time delay (s. Fig. 2.1 (b)). It can be described by a Taylor expansion of the wave number $\beta\left(\omega\right)$ around the center frequency ω_0

$$\beta\left(\omega\right) = n\left(\omega\right)\frac{\omega}{c} = \beta_0 + \beta_1\left(\omega - \omega_0\right) + \frac{1}{2}\beta_2\left(\omega - \omega_0\right)^2 + \frac{1}{6}\beta_3\left(\omega - \omega_0\right)^3 + \ldots, \qquad (2.6)$$

with β_0 describing a constant phase shift, which has no further consequence on the pulse. The first order term β_1 is the inverse group velocity, which represents an overall time delay but has no influence on the pulse shape. Higher order terms contribute to temporal pulse broadening with typically strongest impact at lowest order. The second order term β_2 is called group velocity dispersion (GVD), given in s^2/m. The third order dispersion (TOD) β_3 will be important when pulse durations less than 100 fs are considered or in the absence of β_2.
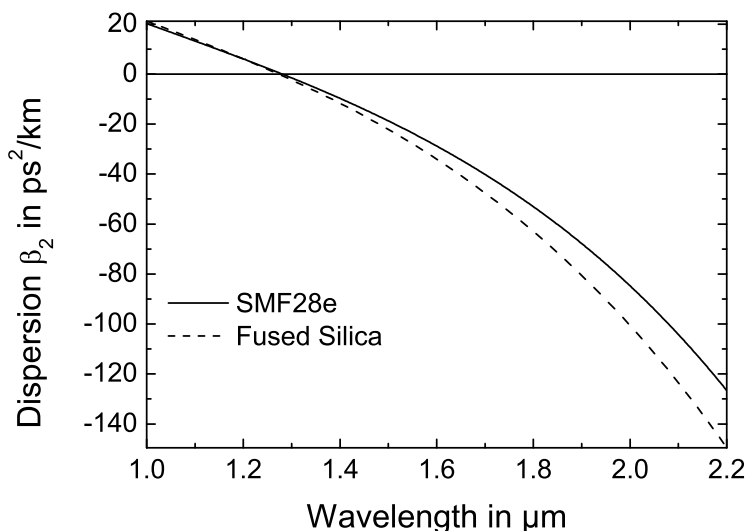

Figure 2.2: Dispersion values of SMF28e and fused silica.

The dispersion value β_2 of a standard fiber (SMF28e) in comparison to bulk fused silica in the wavelength range from $1.0\,\mu m$ to $2.2\,\mu m$ is shown in Fig. 2.2. The dispersion below $1.27\,\mu m$ wavelength is positive, so called normal dispersion, and changes to negative (anomalous) dispersion above $1.27\,\mu m$. Around $2.0\,\mu m$, this value is around $-85\,ps^2/km$. In comparison to fused silica, this value is higher because additionally to the material dispersion also waveguide dispersion has to be taken into account. This dispersion type is normal in a standard step-index single-mode fiber and can be calculated by the core radius and numerical apertur (NA) [Mit05].

2.1.2 Nonlinear effects

An ultrashort pulse propagating in a fiber with length L experiences an intensity-dependent phase shift in the presence of high peak power in combination with the nonlinear response of a material. This nonlinear phase change is called *self-phase modulation* (SPM) [Sto78], if it is induced by the pulse with the intensity $I(t) = |E(t)|^2 \sim |A(t)|^2$ itself. When another pulse is involved, one would speak of *cross-phase modulation* (XPM). The nonlinear phase change generated by SPM is then given by [Agr07]:

$$\phi_{nl}(t) = n_2 \frac{2\pi}{\lambda} L I(t).$$ (2.7)

SPM generates a change of the instantaneous frequency, which is given by the derivative of the Equation (2.7):

$$\delta\omega(t) = -\frac{\partial}{\partial t}\phi_{nl}(t) = -\frac{2\pi L}{\lambda}n_2\frac{\partial I(t)}{\partial t}.$$ (2.8)

This change is proportional to the negative derivative of the temporal pulse shape: the instantaneous frequency decreases at the leading edge of the pulse and increases at its trailing edge, respectively. Therefore, new spectral components are generated for an initially transform-limited or positively chirped pulse so that the pulse spectrum broadens. If the initial pulse is negatively chirped, these components will be annihilated and the spectrum becomes compressed.

Another consequence of the Kerr effect is the *nonlinear polarization rotation* (NPR). A pulse propagating through a Kerr medium (e.g. a fiber) experiences an intensity dependent change of its polarization state. At sufficiently high peak power (or long interaction length), the polarization at the peak of the pulse is rotated by a larger angle than its wings. If a polarizing element is placed behind the Kerr medium, the wings of the pulse can be discriminated. This acts as a fast artificial saturable absorber, which enables mode-locking

(named earlier *polarization additive-pulse mode-locking*) [Tam92]. Mode-locking by NPR was solely used for the fiber oscillators in this thesis.

For ultrashort pulses, the Kerr effect has a further impact on the pulse shape: as the refractive index becomes intensity dependent, the group velocity represented by the first term β_1 in the Taylor expansion of Equation (2.6) also becomes intensity dependent. The *self-steepening* causes the high intensity center of the pulse to travel at lower speed than the low intensity pulse wings. In consequence, the temporal pulse shape gets asymmetric with a longer leading edge of the pulse. Simultaneously, the optical spectrum of the pulse will become also asymmetric owing to the prevailing SPM.

Besides Kerr induced effects, *Raman scattering* is one of the nonlinear effects that needs to be considered when an ultrashort pulse with high peak power propagates in fibers. The photons of the pulse are scattered by optical phonons, which are associated to the vibrations of the glass matrix. During the process, the photon converts parts of its energy to a phonon so that the frequency of the photon is red-shifted. As these vibrations are not discrete in the amorphous glass matrix of a silica fiber, the resulting broadband Raman spectrum is located at a lower frequency of 13.1 THz in comparison to the central frequency of the pulse [Agr07].

2.2 Ultrashort pulse generation in fiber lasers

One possible solution of the nonlinear Schrödinger equation in case of no gain ($\alpha = 0$) and anomalous dispersion ($\beta_2 < 0$) is the soliton. In terms of ultrashort pulse generation, this optical soliton is generated by balancing anomalous dispersion and SPM [Mol80]. Under certain circumstances, these effects can cancel each other so that the pulse propagates with a constant temporal and spectral shape. The pulse evolution scheme of a soliton inside a fiber laser is depicted in Fig. 2.3 (a). The achievable pulse energy E_P and pulse duration τ are related to the soliton area theorem [Agr07] in which the nonlinear coefficient γ and the dispersion β_2 of the cavity are the contributing factors: $E_P \cdot \tau = 2 \cdot |\beta_2| / \gamma$. Typical output energies of a soliton fiber laser at $2\,\mu\text{m}$ are in the order of $0.1 - 0.5\,\text{nJ}$ with pulse durations around $500\,\text{fs} - 1\,\text{ps}$ [Kie09; Kiv07; Nel95]. As the pulse is always close to the Fourier-limit, the tolerated accumulated nonlinear phase (B-Integral) is very low (in the order of $\ll \pi$) before the pulse is destabilized [Wis08].

This constraint can be overcome by applying a dispersion compensation inside the cavity, which uses temporal breathing of the pulse to lower the average pulse intensity during one round trip [Nel97]. In an all-fiber laser, segments with alternating dispersion signs were incorporated into the cavity, which sums to an overall cavity dispersion close to zero [Tam93]. In general, the circulating pulse undergoes twofold temporal stretching

and compression during one round trip (s. Fig. 2.3 (b)), so that it reaches the minimum pulse duration in every dispersion segment. These lasers are named *stretched-pulse* or *dispersion-managed soliton* lasers. Because the pulse is chirped most of the time, the accumulated nonlinear phase is much lower than in the case of the soliton. Or other way around, the pulse can tolerate a higher nonlinear phase shift ($\sim \pi$) before it gets destabilized. Limitations arise again from nonlinearities during propagation inside the cavity: the achieved pulse duration gets quite short ($\ll 100\,\text{fs}$) at the pulse minimum positions, so high peak powers are present. In fiber lasers with fiber based dispersion managements, the achieved pulse energies are quite low ($\sim 100\,\text{pJ}$) [Nel97; Tam93; Wie12]. Much higher pulse energies of more than $1\,\text{nJ}$ and less than $100\,\text{fs}$ pulses can be achieved by applying bulk optics (gratings, prisms, etc.) for dispersion management [Hax08; Ild03], which also makes the setup more complex.

In general, further pulse propagation schemes exist (self-similar and all-normal), which require normal dispersion. This is contrary to the typical anomalous material dispersion at $2\,\mu\text{m}$ in silica fibers. Therefore, these schemes are hardly realizable at this wavelength but were accomplished by Haxsen et al. [Hax12] and Tang et al. [Tan15]. However, these schemes are not used in this work, but a good overview can be found in [Wis08].
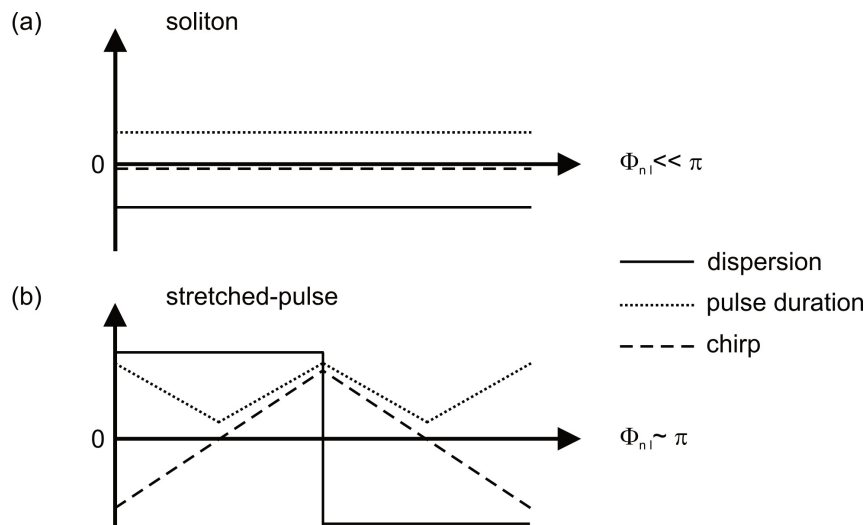

Figure 2.3: Pulse duration, dispersion, and chirp during cavity propagation [Wis08].

2.3 Numerical simulations

The numerical simulations were an essential part in this thesis when developing the fiber oscillators to find the optimal fiber lengths. The oscillators were modeled using the commercial software Fiberdesk [Sch15], which based on solving the extended nonlinear

Schrödinger equation by the split-step Fourier method. The nonlinear Schrödinger equation (2.5) is extended by the aforementioned nonlinear effects mentioned in Subsection 2.1.2:

$$\frac{\partial A}{\partial z} = -\frac{\alpha}{2} + \int_{-\infty}^{\infty} \frac{g(\omega)}{2} \tilde{A}(\omega) e^{-i\omega T} d\omega + \sum_{n \geq 1} \beta_n \frac{i^{n+1}}{n!} \frac{\partial^n}{\partial T^n} A$$

$$+ i\gamma \cdot \left(1 + i\tau_{shock} \frac{\partial}{\partial T}\right) \left(A(T) \int_{-\infty}^{\infty} R(\tau) |A(T-\tau)|^2 d\tau\right). \quad (2.9)$$

In Equation (2.9), the colored parts are losses (*red*), gain (*green*), dispersion (*blue*), SPM (*yellow*), self-steepening (*orange*), and Raman-response (*violet*). The terms for self-steepening and Raman response can be found in [Kib05]. For a numerical solution, the equation can be splitted into a linear part (dispersion and losses) and a nonlinear part. By only applying a small step, the dispersive and nonlinear part can be assumed to act independently while both parts as standalone have an analytical solution either in the frequency domain (dispersion) or the time domain (nonlinearity) [Agr07]. The switching between both parts after one step is carried out by the Fourier transformation until the solution for the whole fiber length was calculated. By following this method, a complete resonator can be modeled, which is typically set up by the scheme depicted in Fig. 2.4.
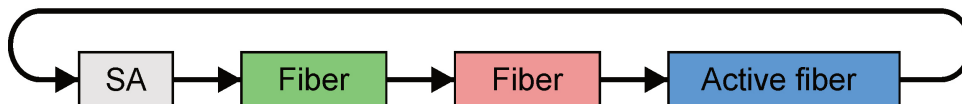

Figure 2.4: Numerical setup with alternating dispersion segments (green and red) and a active fiber (blue).

The mode-locking of the oscillator is initiated by a saturable absorber (SA), which enables and stabilizes mode-locking (white). The fiber section consists of fiber segments with alternating dispersion segments (e.g. green and red) and is terminated by an active fiber, which provides the gain (blue). The saturable absorber (SA) was based on the model developed by Kärtner et al. [Kär98] and modeled by a transfer function shown in Equation (2.10):

$$R = R_0 + \Delta R - \frac{\Delta R}{1 + \frac{|A(t)|^2}{P_{Sat}}}. \quad (2.10)$$

The parameter R_0 corresponds to the unsaturable reflectivity, ΔR is the saturable reflectivity and P_{sat} is the saturation power. Equation (2.10) describes a fast saturable absorber,

which shows no temporal limitation by a recovery time as in the case of a slow saturable absorber (e.g. semiconductor saturable absorber (SESAM)). This is a valid assumption for NPR mode-locked oscillators because the Kerr effect occurs instantaneously. The losses occurring at the SA are simultaneously the output coupling of the laser. The simulations were carried out from noise until steady state was reached, which is typically the case after several hundreds of round trips.

2.4 Chirped-pulse amplification

As already mentioned in Section 2.2, a pulse experiences strong nonlinearities if the peak power / intensity of the pulse is very high during propagation in a medium. When higher pulse energies are desired than oscillators can deliver, the pulse needs to be amplified in a scheme that avoids these nonlinearities. One way to achieve this, is the scheme of chirped-pulse amplification (CPA). The peak power is highly reduced by stretching the pulse in time before amplification. After amplification, the pulse is compressed to gain ultrashort pulses again (s. Fig. 2.5). The first realization of this concept was performed by STRICKLAND et al. [Str85] by using a 1.4 km single-mode fiber as dispersive fiber stretcher and a grating compressor to generate 2 ps, mJ-pulses.
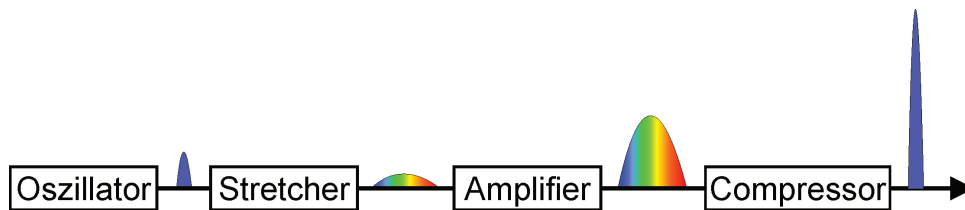

Figure 2.5: Scheme of chirped-pulse amplification.

A single pass amplifier (bulk or fiber) would be the typical example of a CPA stage, when the provided gain of the amplifier material is high (e.g. fiber amplifier with more than 20 dB gain). Besides that, multipass schemes in crystals are often applied, when the gain factor is moderate (in the order of $2-4$) [Ise02]. With multiple passes ($2-10$) through the pumped area of a crystal, the pulse can be efficiently amplified and extracts most of the energy stored in the crystal. The multiple passes are realized by a set of mirrors in a geometric order to redirect the laser beam in the crystal. This can lead to a complex and space consuming setup. If the gain of the laser material is as low as 1.1 per pass (e.g. colquiriite materials, thin-disks), much more passes through the material are needed, which can exceed 100 easily. To avoid such an overwhelming multipass setup, the concept of the regenerative amplifier (former: *injection mode-locking*) was developed by BÉLANGER et al. [Bél76] already in 1976 (s. Section 2.5).

2.5 Regenerative amplification of ultrashort pulses

For an efficient extraction of the stored energy inside the amplifier gain material, a specific input (seed) energy is needed. This saturation energy E_{Sat} represents the seed energy required to reduce the gain to $1/e$ ($\sim 37\%$) of its initial value. It can be calculated by the saturation fluence F_{Sat} multiplied with the mode field area A_{MFD} of the beam. The saturation fluence is based on the amplifier material's emission and absorption cross sections $\sigma_{em,abs}$ (for a 4-level gain medium σ_{abs} can be neglected) and the photon energy $h\nu$ with Planck's constant h at the signal frequency ν [Die06]:

$$E_{Sat} = A_{MFD} \cdot F_{Sat} = A_{MFD}\frac{h\nu}{\sigma_{em} + \sigma_{abs}}. \tag{2.11}$$

This value can be particularly much higher than the pulse energy reached by oscillators or simple amplifiers and can even outreach the damage threshold of a material. By arranging multiple passes through this medium, a much lower effective saturation is defined by E_{Sat}/N, so most of the stored energy can be extracted even with a low energy seed.
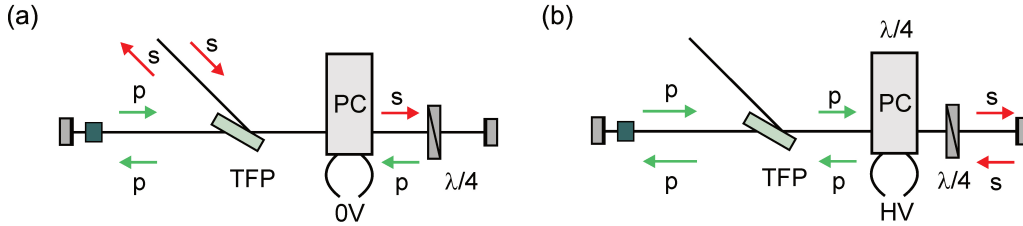

Figure 2.6: Scheme of regenerative amplification.

The number of passes through the amplifier material can be easily controlled and varied by the use of the regenerative amplification scheme because the cavity setup needs no further adjustment. By controlling the round trip numbers electro-optically, up to several hundreds of round trips and even more are possible. The scheme of a regenerative amplifier is depicted in Fig. 2.6. The cavity is similar to a standard laser cavity with highly reflective (HR) mirrors at both ends. Inside the cavity, the pulse is coupled in and out by changing its polarization state using a Pockels cell (PC), a quarter-wave plate (QWP) and a thin film polarizer (TFP). The electro-optic effect induced by high voltage (HV) applied to the PC crystals generates a change from linear polarization to circular polarization ($\lambda/4$). An incoming pulse with s-polarization is reflected at the TFP, passes twice the QWP and PC with $0\,\text{V}$ applied, so that the polarization state is changed to linear p-polarization (s. Fig. 2.6 (a)). It passes the TFP in transmission and, in the meantime in which the pulse travels through the remaining part of the cavity where it is amplified, high voltage is

applied, so that the PC state is switched to $\lambda/4$-operation (s. Fig. 2.6 (b)). In combination with the QWP this results in an effective $\lambda/2$ change of polarization state which the pulse experiences when it returns. In consequence, the pulse is sent back to the laser crystal where it is amplified in several round trips. If the desired amplification level is achieved, the pulse can be coupled out of the cavity by the same concept: the high voltage is switched off when the pulse is in the second arm of the cavity (in which no PC is). Typically, the rise time of the PC is in the few ns-range, so a following pulse needs to be timely spaced at least by this value. Furthermore, the second arm of the cavity needs to be long enough to enable switching within return of the pulse.
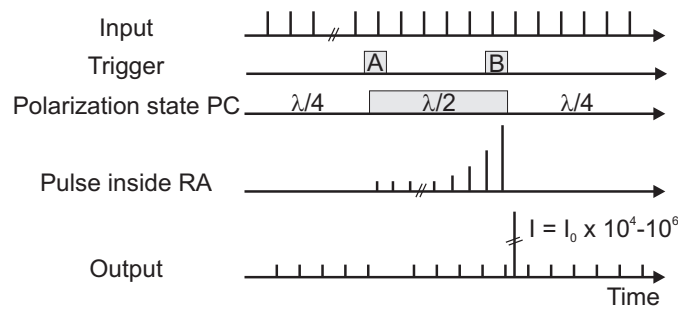
Figure 2.7: Temporal evolution during regenerative amplification with I_0: input intensity and I: output intensity (from [Ise02]).

The temporal evolution during switching of the PC is depicted schematically in Fig. 2.7. A pulse train enters the input of the regenerative amplifier. A trigger signal **A** sent to the PC sets the polarization state from $\lambda/4$ to $\lambda/2$ and a single pulse of the train is trapped inside the regenerative amplifier cavity. This state is maintained until the pulse is sufficiently amplified and a second trigger signal **B** reverses the polarization state of the PC to $\lambda/4$. Consequently, the high energy pulse is coupled out of the cavity and separated from the seed signal for example by an optical diode consisting of a Faraday rotator (FR), a half-wave plate (HWP) and a polarizer.

2.5.1 Frantz-Nodvik equations for pulse amplification

The amplification of a short pulse with a pulse duration well below the upper-state lifetime can be described by the *Frantz-Nodvik equations* [Fra63]:

$$F_{out} = F_{sat} \cdot \ln \left[1 + e^{g_0} \left(e^{F_{in}/F_{sat}} - 1 \right) \right], \tag{2.12}$$

with $F_{in,out}$ the input / output fluence of the pulse and F_{sat} the saturation fluence of Equation (2.11). As already indicated in Equation (2.11), the input / output pulse fluence

can be calculated by dividing the pulse energy E_P by the beam area A_{MFD}. The small signal gain g_0 can be calculated by $g_0 = F_{Sto}/F_{Sat}$. It has to be mentioned that for Equation (2.12) a square pulse shape is assumed [Koe06]. The stored energy fluence F_{Sto} is derived from the stored pump energy E_{abs}, the mode field of the pumped area A_{MFD} and the laser and pump wavelengths $\lambda_{l,p}$ [Ise02]:

$$F_{Sto} = \frac{E_{abs}}{A_{MFD}} \frac{\lambda_p}{\lambda_l}.$$ (2.13)

Equation (2.12) describes the single pass amplification by an amplifier medium. By calculating the output fluence after multiple passes, the output fluence of the previous run is the input of the following one. The stored energy is reduced by the amount of the extracted energy from the previous run, so the small signal gain needs to be recalculated for every pass.

The Frantz-Nodvik equations can be used for calculating the accumulated nonlinear phase shift (also called *B-Integral*) which a pulse with intensity $I(z)$ experiences during propagation through the regenerative amplifier:

$$B = \int_0^L n_2(z) I(z) \, dz.$$ (2.14)

As the pulse intensity changes with every round trip number, this equation has to be applied with the specific intensity for each round trip. A spatially varying nonlinear refractive index $n_2(z)$ of every optical element which the pulse passes has to be taken into account. With increasing round trip number and intensity during amplification, high B-Integral values in the order of $\pi - 2\pi$ result [Ise02].

CHAPTER 3

State of the art

In recent years, the number of laser systems operating at $2\,\mu m$ wavelength has increased. This is due to the aforementioned wide range of applications for which these systems are used (s. Section 1). Until now, only few systems were published at $2\,\mu m$ wavelength that produce high energies in the µJ region with sub-ps pulse durations. Generally, there are two approaches to generate such ultrashort pulses: firstly, high power Titanium:Sapphire CPA systems exist which use nonlinear difference frequency and optical parametric processes to generate multi-µJ, few-cycle pulses. But these systems lack efficiency, low costs, and compactness [Gu09; Hau07]. In addition, further scaling of the output pulse energy in parametric processes is mainly limited by the available pump power for the nonlinear processes.

The second approach is the direct use of thulium- and holmium-doped fibers and crystals, which have broad emission bandwidths at $2.0\,\mu m$ and $2.1\mu m$, respectively. Although compact seed sources for direct amplification were demonstrated quite early [Nel95], the demand for high energy ultrashort pulses at $2\,\mu m$ has increased only in the last years. A detailed state of the art concerning low pulse energy (sub-nJ) seed sources is given in the Subsections 4.2 and 5.2 respectively, in which the ultrashort pulse oscillators are described.

Singlepass amplifier architectures with thulium (Tm)-doped large mode area (LMA)-fiber amplifiers were realized already in 2010 with an output energy of 151 nJ at a repetition rate of 37.6 MHz with a pulse duration of 256 fs [Hax10]. A further increase can be achieved by using amplifier chains to reach the µJ energy level. In 2013, such a system was presented, which could deliver up to $36.7\,\mu J$ at 100 kHz repetition rate with a compressed pulse duration of 910 fs [Wan13]. Both systems utilized commercially available standard LMA fibers for reaching these high output values. In terms of high average power, STUTZKI et al. [Stu14] demonstrated a Tm-doped photonic crystal fiber (PCF) approach to achieve up to

152 W of compressed average output power with 690 fs pulse duration. However, the pulse energy is as low as 3.1 μJ because the full repetition rate of the seed oscillator of 49.1 MHz was used. Just recently, a fiber-based Tm-doped, sub-ps CPA system operating at 1910 nm was demonstrated with up to 120 μJ of compressed pulse energy at 200 kHz, generating 200 MW peak power with a pulse duration of 360 fs [Stu15]. This was attained by the use of customized Tm-doped large-pitch fibers and highly efficient dielectric gratings. Further power scaling with the used fiber is quite challenging as nonlinearities have a high impact at this peak power level and the high average power leads to unwanted thermal degradation of the beam profile [Geb15b; Stu15].

Another approach to achieve much higher output energy is the use of single- or multipass bulk amplifiers. A long pulse, singlepass amplifier was demonstrated by DERGACHEV [Der13], who used two 70 mm Ho:YLF crystals, which were pumped with up to 60 W pump power. A pulse energy of more than 11 mJ was attained with a 1 mJ, 300 ps seed. HEMMER et al. [Hem15] reached much higher output energies of 39 mJ with a pulse duration of 10 ps by cryogenic cooling of a Ho:YLF laser rod, which was seeded by a regenerative amplifier delivering up to 5.5 mJ. COLUCCELLI et al. [Col11] realized a multipass amplifier with five passes through a 50 mm long Ho:YLF crystal to achieve an output power of 1.6 W. The input was a broadband supercontinuum generated by an Er:fiber comb with a repetition rate of 100 MHz so a low pulse energy of 16 nJ at 508 fs transform limited pulse duration was reached.

As either high pulse energy or short pulses are obtained with single or multipass amplifiers, ultrafast regenerative amplifier (RA) can be used to scale nJ-pulses directly up several hundreds of μJ or even mJ of pulse energy. This was demonstrated in 2013 for the first time at a wavelength of 2.05 μm with a Ho:YLF RA with 300 ps pulse duration and an output energy of 1.7 mJ at 1 kHz repetition rate [Der13]. A much shorter pulse duration was achieved by MALEVICH et al. [Mal13] at 2.1 μm wavelength with a Ho:YAG RA, producing pulse energies up to 1 mJ at 530 fs pulse duration. This system had the aforementioned drawback of a bulky, cost-intensive and inefficient nonlinear parametric seed source, producing ultrashort pulses at 2.1 μm. By changing the seed source to a compact all-fiber PM oscillator in combination with a fiber preamplifier, the same RA produced a pulse energy of 712 μJ at 1 kHz repetition rate after compression [Mal15b]. The compressed pulse duration of 1 ps was two-times larger due to the longer seed pulses. Very recently, two publications reported Ho:YLF RAs with pulse energies of up to 7–9 mJ and pulse durations in the ps-range [Gra15; Kro15b].

In general, a clear trend was observed in the last years. Thulium as gain material is mostly used in fibers due to the high doping concentrations that can be applied in fibers.

Furthermore, laser diodes with high average power are available for direct pumping. The strong thermal issues, which become apparent by the high quantum defect, can be addressed more easily in fibers than in crystals. Anyway, thulium-doped materials are limited in lasing at wavelengths below 2025 nm. In the last years, optical parametric processes based on zinc-germanium-phosphide (ZGP) pumped at 2 µm wavelength were used to generate multi-µJ pulses in the wavelength range from 3–10 µm [Hai04; Pet01; Wan14]. This region is highly interesting for several applications (molecular fingerprint region, microstructuring and general material processing of plastic materials and semiconductors etc. [Did07; Hur07; Sch10]). ZGP is favorable for this because of its high nonlinear coefficient. Anyway, ZGP strongly absorbs at wavelengths below 2025 nm so longer wavelengths (at higher output energy) are desired, which are addressed by the aforementioned Ho:YLF and Ho:YAG bulk regenerative amplifiers. These have achieved much higher output energies in the mJ range compared to fiber-based amplifiers. The holmium crystals can be pumped by high power, continuous wave (CW) Tm-fiber lasers with excellent beam quality. Further beneficial is the small quantum defect so thermal degradation at high pump powers is low.

Regenerative amplification with thulium-doped materials

This chapter focuses on the generation and amplification of ultrashort pulses with thulium-doped fibers (TDFs) and crystals in the $2\,\mu m$ wavelength region. In comparison to existing laser systems reported in the previous Chapter 3, which typically use several stages of optical parametric processes to approach these mid infrared (MIR) wavelengths, the system presented here consisted of a compact and straight-forward solution: an ultrashort pulse fiber-based seed oscillator, a fiber-preamplifier, and a regenerative amplifier based on a thulium-doped $YAlO_3$ (Tm:YAP) crystal. These subsystems are explained in full detail in the following sections, starting with the general properties of Tm-doped fibers and crystals in Section 4.1. The generation of the seed pulses by the ultrashort pulse oscillator is described in Section 4.2, while Section 4.3 focuses on the fiber preamplification before the pulses are picked and strongly amplified with a regenerative scheme (Section 4.4).

4.1 Properties of thulium-doped fibers and crystals

Thulium (Tm) is one of the lanthanides that are a sub-group of the rare earth elements. As other classical rare earth elements such as erbium (Er), ytterbium (Yb) or neodymium (Nd), it can be doped into a variety of host materials like crystals or amorphous silica fibers for the generation and amplification of light in the $2\,\mu m$ wavelength region. The spectroscopic properties of Tm differ quite strongly depending on whether it is doped in fibers or crystals. As both types are used in this work, their properties will be described in the following subsections.

4.1.1 Silica fibers as host materials for thulium

The simplified scheme of energy levels and the corresponding cross sections of Tm-doped silica fibers are shown in Fig. 4.1. The strongest absorption line at $790\,nm$ wavelength is the $^3H_6 \rightarrow\,^3F_4$ transition which has a cross section of $8 \times 10^{-25}\,m^2$. This transition can be

easily addressed by high power multi-mode laser diodes, which deliver multiple Watts of pump power. Another strong absorption to pump into the $^3H_5$ energy level has a cross section of $4.3 \times 10^{-25}\,\text{m}^2$ at $1210\,\text{nm}$ wavelength. High power multi-mode laser diodes can also be used at this wavelength but the brightness of these is much lower compared to $790\,\text{nm}$ laser diodes. The third main absorption band around $1630\,\text{nm}$ spans broadband from $1500\,\text{nm}$ to $1700\,\text{nm}$ and has a maximum absorption cross section of $4.4 \times 10^{-25}\,\text{m}^2$. This $^3H_6 \rightarrow {}^3H_4$ transition can also be addressed by high power laser diodes operating at $1550\,\text{nm}$, but these lack also high brightness compared to $790\,\text{nm}$ laser diodes. However, single-mode Er-doped fiber lasers operating at $1540\,\text{nm} - 1580\,\text{nm}$ can be used which enables direct core pumping.
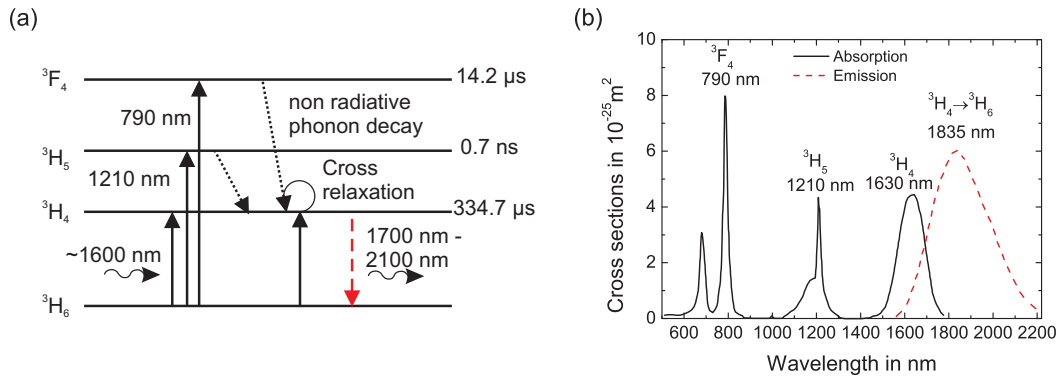
Figure 4.1: (a) Simplified energy levels with transitions and (b) corresponding absorption and emission cross sections of thulium-doped in fiber (digitized data from [Jac99]).

The Gaussian-shaped spectral emission cross section of the $^3H_4 \rightarrow {}^3H_6$ laser transition is shown as red dashed line in Fig. 4.1 (b). It is centered around $1835\,\text{nm}$, extending from $1600\,\text{nm}$ to $2200\,\text{nm}$ and overlapping with the $^3H_6 \rightarrow {}^3H_4$ absorption band. If an in-band pumping scheme for example with $1575\,\text{nm}$ as pump wavelength is used, a quantum defect of less than $17\,\%$ offers a high slope efficiency of $71\,\%$, which was shown by YAMAMOTO et al. [Yam94] already in 1994. A comparable slope efficiency of $68\,\%$ was found by WU et al. [Wu07] in 2007 when pumping with $790\,\text{nm}$ laser diodes. The possible Stokes limit of $42\,\%$ was exceeded by exploiting the beneficial cross relaxation process depicted in Fig. 4.1 (a): the energy of the non radiative decay from $^3F_4 \rightarrow {}^3H_4$ can excite a second Tm ion from the $^3H_6$ to the $^3H_4$ level. In this case, two photons at $2\,\mu\text{m}$ are generated by one pump photon (2-for-1 process) and a quantum efficiency of more than 1 can be achieved. A maximum quantum efficiency of 1.84 was demonstrated by MOULTON et al. [Mou09] with a $2.9\,\text{wt.}\,\%$ Tm-doping concentration.

When pumping at 790 nm into the $^3\mathrm{F}_4$ level, parasitic blue light emission at 470 nm is observed, which is generated by an upconversion process. These upconverted photons were assumed to cause photodarkening by the formation of permanent defects inside the fiber core, which were also observed when pumping TDFs at 1064 nm wavelength [Bro93], but experiments in recent years did not confirm this when pumping at 790 nm wavelength [Mou09].

As already mentioned, commercial grade pump laser diodes around 790 nm offer an output power of more than 35 W, which is delivered through a multi-mode fiber with a core diameter of 105 μm. Owing to the low beam quality of high power multi-mode laser diodes, these are typically used for pumping Tm-doped crystals (s. Subsection 4.1.2) or double clad fibers. The latter ones show a low pump absorption due to the limited overlap of the pump cladding with the Tm-doped core so longer fibers are needed for an efficient amplification in comparison to core-pumping. In consequence, stronger reabsorption at the emission wavelengths takes place and causes a limitation on the short wavelength side of the emission band. Due to the reabsorption effects in fibers, typical operating wavelengths are between 1860 nm and 2090 nm with a maximum around 1940 nm [Cla02].

A higher pump absorption can either be achieved by higher doping concentrations or core-pumping with single-mode Er-doped fiber lasers (e.g. at 1565 nm wavelength). Typical fibers, which are used at 2 μm wavelength, are still single-mode at this pump wavelength so that a better overlap between pump and signal mode is attained and the pump saturation is higher. Core-pumping is typically used for ultrashort pulse oscillators because the shorter active fiber reduces nonlinearities.

4.1.2 Thulium-doped crystals

Thulium as dopant material in crystals shows a different, more structured cross section shape due to the incorporation in the crystalline lattice compared to the broadband, Gaussian-like shape in TDFs. The emission cross sections of Tm doped in YAlO$_3$ (YAP), Y$_3$Al$_5$O$_{12}$ (YAG), YLiF$_4$ (YLF), and Lu$_2$O$_3$ (LuO) are shown in Fig. 4.2 (a) and the absorption cross sections in (b), respectively. As TDFs are used in this work for the generation and amplification of the pulses, the gain maximum of the amplifier crystal should fit to their lasing wavelength. With a gain maximum of 1940 nm typically achieved in TDFs (s. Subsection 4.1.1) only three materials offer suitable emission wavelengths: Tm:YAP, Tm:YAG, and Tm:LuO. Tm:YLF has its main emission wavelengths at less than 1925 nm and is therefore not suitable for amplification experiments in this work. Tm:LuO shows the highest emission cross section of $1.08 \times 10^{-20}\,\mathrm{cm}^2$ at 1940 nm, while Tm:YAP has an emission cross section of $0.49 \times 10^{-20}\,\mathrm{cm}^2$ and Tm:YAG a 4.5 times less cross section

of $0.11 \times 10^{-20}\,\mathrm{cm}^2$ at $1940\,\mathrm{nm}$. All three materials have an absorption cross section of less than $0.09 \times 10^{-20}\,\mathrm{cm}^2$, which should be taken into account for calculating the effective gain cross section with Equation (4.1). Tm:LuO was only available at the end of this work and own measurements revealed a minimum operating wavelength of $1964\,\mathrm{nm}$ with an available $3\,\mathrm{at.\,\%}$-doped crystal. This was also validated by KOOPMANN et al. [Koo11] who found the spectral tuning curve of a $1\,\mathrm{at.\,\%}$ doped Tm:LuO crystal under high power pumping between $1922\,\mathrm{nm}$ and $2134\,\mathrm{nm}$ with a maximum at $2100\,\mathrm{nm}$. At $1940\,\mathrm{nm}$, only $30\,\%$ of the maximum output power was generated. Therefore, possible parasitic lasing at $2100\,\mathrm{nm}$ can be expected when it is used as amplification material. Therefore, Tm:LuO seems less suitable for the amplification at $1940\,\mathrm{nm}$. Anyway, a closer look should be taken at the broadband emission wavelength region higher than $2050\,\mathrm{nm}$ of Tm:LuO, which is not addressed by any of the other materials doped with Tm. This could possibly be useful for further amplification in combination with holmium-doped fibers (HDFs), which operate in this wavelength region (s. Chapter 5).
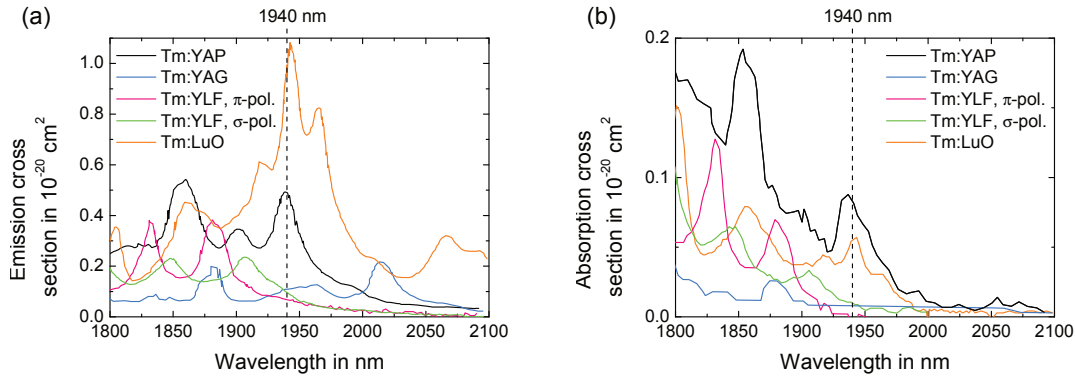
Figure 4.2: Cross sections of different Tm-doped crystals: Tm:YAP, Tm:YAG, Tm:YLF (π and σ), and Tm:LuO: (a) emission and (b) absorption (digitized data from [Koo12; Pay92; Wal98]).

In consequence, Tm:YAP was the material of choice for high power amplification at a wavelength of $1940\,\mathrm{nm}$. Additionally, Tm:YAP is the only crystal of the three that is intrinsically birefringent. This is beneficial at high pump power levels because it overcomes any thermal induced birefringence and reduces therefore depolarization losses. Table 4.1 at the end of this subsection summarizes the most important physical properties of the different host crystals, which reveals a low saturation fluence of $18\,\mathrm{J/cm}^2$ for Tm:YAP. This is also beneficial because a low seed pulse energy is required to extract most of the stored energy of the amplifier crystal. The thermal conductivity of YAP is higher than of YAG and YLF and comparable to LuO so that good heat removal is ensured.

(a)

(b)
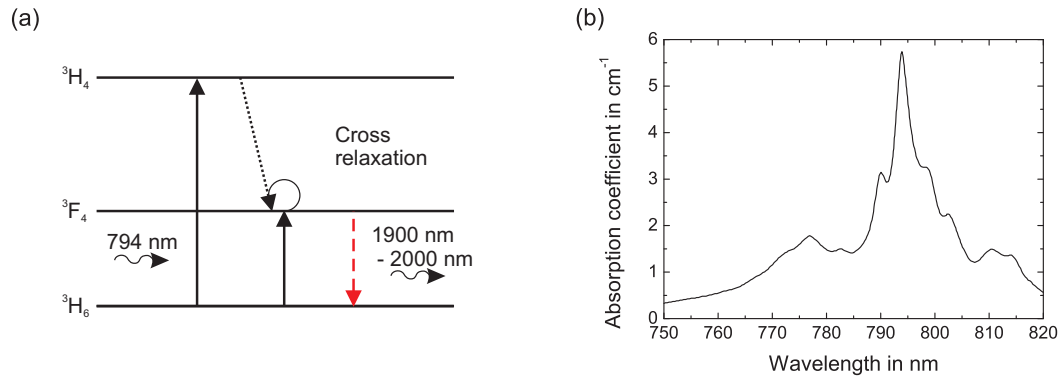
Figure 4.3: (a) Simplified energy levels with transitions [Sto95] and (b) absorption coefficients of Tm:YAP [Šul15].

Figure 4.3 shows the energy level of Tm:YAP (a) and the absorption coefficient of a 5 at. % doped Tm:YAP crystal (b). It can be effectively pumped at a wavelength of 794 nm with an absorption coefficient of $5.7\,\mathrm{cm}^{-1}$ from the $^3\mathrm{H}_6$ level into the $^3\mathrm{H}_4$ level using the same type of laser diodes as for Tm-doped fibers. The absorption cross section at 794 nm is specified to $0.7 \times 10^{-20}\,\mathrm{cm}^2$ according to the manufacturer Crytur [Šul15], which results in a pump absorption of 89 % in a 4 mm long and 4 at. % doped crystal. Similar to fibers, a 2-for-1 process by cross relaxation is possible so that two signal photons between 1.9 µm and 2.0 µm are emitted from the $^3\mathrm{F}_4$ level. In practice, such high slope efficiencies as in fibers were not attained with Tm:YAP. Only a maximum efficiency of 52 % was achieved by ČERNÝ et al. [Čer05]. This can be explained by experimental disadvantages of bulk materials in general like mismatch between pump and laser mode, imperfect anti reflective (AR)-coatings or an inefficient cooling geometry.

(a)

(b)
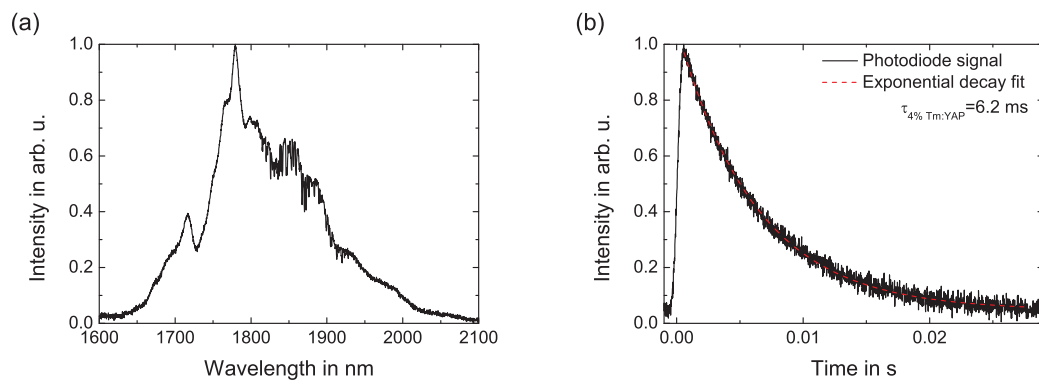
Figure 4.4: (a) Fluorescence spectrum of a 4 at. % doped Tm:YAP excited at 794 nm and (b) corresponding fluorescence lifetime measurement.

The fluorescence spectrum of a 4 at. % doped, 4 mm long Tm:YAP crystal shown in Fig. 4.4 (a) spans from 1650 nm to 2100 nm with a maximum at 1780 nm. The corresponding fluorescence lifetime of 6.2 ms (s. Fig. 4.4 (b)) was measured by chopping the continuous wave excitation beam with a mechanical chopper. This measured lifetime is longer than the literature value of 4.4 ms [Eld97], which can be explained by other doping concentrations and crystal lengths. Reabsorption effects by long laser crystals and closely located active ions can lead to radiation trapping which lengthens the effective lifetime [Sum94].

(a)

(b)
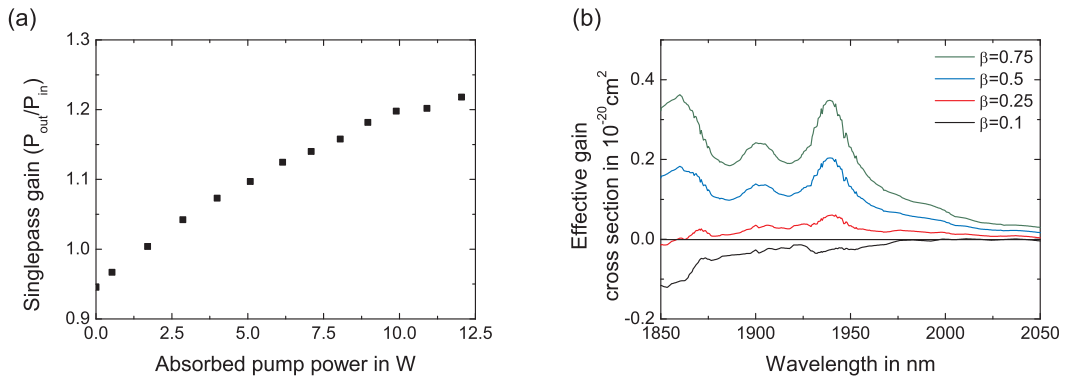
Figure 4.5: (a) Singlepass gain measurement and (b) effective gain cross section of Tm:YAP.

The singlepass gain was measured at increasing pump power in the final setup (s. Section 4.4) with a seed pulse energy of 20.7 nJ in front of the crystal (24.8 nJ in front of the RA cavity) at full repetition rate of 62.3 MHz (s. Fig. 4.5 (a)). By measuring the amplified signal power directly behind the 4 at. % doped, 4 mm long Tm:YAP crystal, a maximum singlepass power gain of 1.22 including potential losses at the AR coating of the crystal was achieved.

The effective gain spectrum depends on both emission and absorption cross section $\sigma_{em,abs}$ at a specific inversion level β:

$$\sigma_{gain}\left(\lambda\right) = \beta\sigma_{em}\left(\lambda\right) - \left(1 - \beta\right)\sigma_{abs}\left(\lambda\right). \tag{4.1}$$

Figure 4.5 (b) shows the calculated effective gain cross section by using Equation (4.1) at different inversion levels of β. At inversion levels of $\beta > 0.25$, a peak at 1940 nm appears with a full width at half maximum (FWHM) of more than 39 nm, which is sufficient for the amplification of ultrashort pulses in this wavelength region.

Table 4.1: Physical properties of the different Tm-doped crystals (the transparency range of Tm:YAP was not found in literature) [Koo12; Mat10; Pay92; Šul15; Wal98; Zen90].

Physical properties	Lu_2O_3	$Y_3Al_5O_{12}$	$YLiF_4$	$YAlO_3$
acronym	LuO	YAG	YLF	YAP
lattice	cubic	cubic	tetragonal	orthorombic
lattice constant [Å]	10.39	12.0	5.16 ∥ a	5.33 ∥ a
			10.85 ∥ c	7.38 ∥ b
				5.18 ∥ c
density [g/cm^3]	9.42	4.56	3.99	5.35
refractive index at 2 µm	1.9	1.8	1.44 ∥ a	1.93 ∥ a
(YAP only at 1.1 µm)			1.46 ∥ c	1.92 ∥ b
				1.91 ∥ c
transparency range [µm]	0.23 - 8.0	0.21 - 5.2	0.12 - 8.0	–
thermal	12.8	8.8 - 12.9	5.3 ∥ a	11.7 ∥ a
conductivity [W/(m K)]			7.2 ∥ c	10.0 ∥ b
				13.3 ∥ c
fluorescence lifetime [ms]	3.85	9.85	15.0 (π & σ)	6.2
main lasing	2100	2010	1880 ∥ σ	1990 ∥ a
wavelength [nm]			1910 ∥ σ	1940 ∥ c
absorption cross section	0.38	0.75	0.6 ∥ π	0.7
at 790 nm [$10^{-20}\,cm^2$]			0.37 ∥ σ	
absorption cross section	0.06	0.01	0.02 ∥ π	0.08
at 1940 nm [$10^{-20}\,cm^2$]			0.01 ∥ σ	
emission cross section	1.08	0.11	0.07 ∥ π	0.49
at 1940 nm [$10^{-20}\,cm^2$]			0.096 ∥ σ	
saturation	9.0	85.3	113.8 ∥ π	18.0
fluence [J/cm^2]			96.6 ∥ σ	

4.2 Ultrashort pulse oscillator

The first development of a mode-locked TDF laser was demonstrated by NELSON et al. [Nel95] in 1995 and was based on soliton propagation. This laser was passively mode-locked by NPR and emitted pulses with a duration between 350 fs to 500 fs. SHARP et al. [Sha96] achieved a pulse duration of 190 fs emitted by a soliton TDF laser with a short cavity, which resulted in a small cavity group delay dispersion (GDD).

To achieve even shorter pulses, the cavity GDD has to be compensated [Hau91], which can be accomplished by managing the dispersion inside the cavity (s. Fig. 2.3). This concept was developed and investigated in fiber lasers by TAMURA et al. [Tam93] who invented the first fiber-based realization in a stretched-pulse erbium-doped fiber laser.

Due to the lack of suitable fibers providing normal dispersion, the dispersion management in TDF lasers was achieved in the past by either chirped fiber Bragg gratings [Gum11] or

modified grating compressors [Hax08]. Although completely fiber-based, the implementation
of chirped fiber Bragg gratings in ring cavities is difficult whereas the assembly of a modified
grating compressor is not always easy to handle. Until then, the shortest pulse duration of
173 fs was generated by HAXSEN et al. [Hax08] with the use of a grating compressor inside
the laser cavity.

Recently, new fiber types providing normal dispersion at 2 μm wavelength were used
for dispersion management. A highly germanium-doped fiber was used by YANG et al.
[Yan12] for internal dispersion compensation, whereas WANG et al. [Wan10] applied 2 m of
normal-dispersion active Er-doped fiber in combination with 30 m of SMF28e in the cavity
to achieve a pulse duration of 235 fs. Another approach by HAXSEN et al. [Hax12] was to
generate pulses operating in the normal dispersion regime by utilizing a high NA, small
core fiber.

(a)

(b)
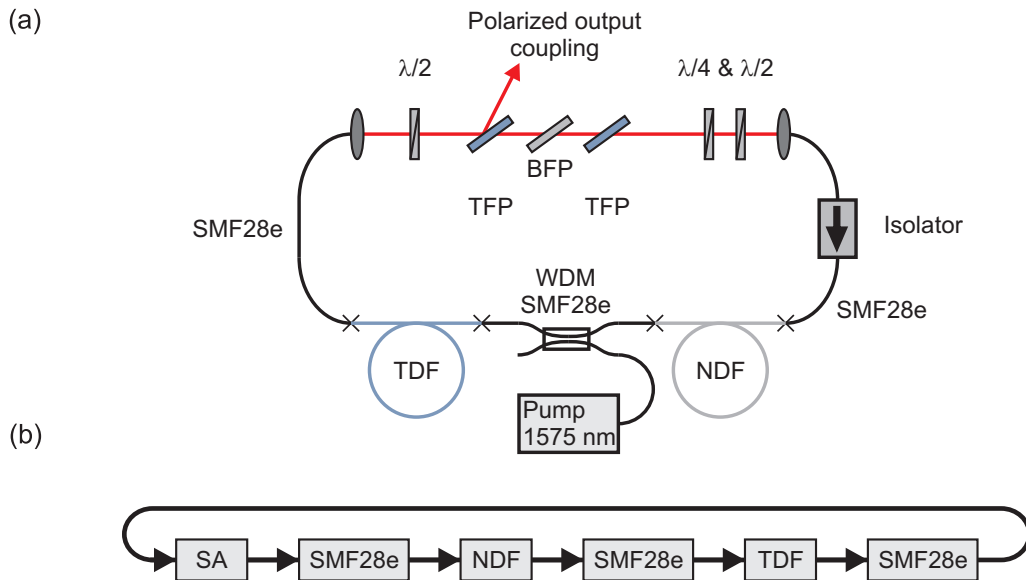
Figure 4.6: (a) Experimental thulium-doped fiber oscillator setup and (b) corresponding
numerical model (SA: saturable absorber).

For this thesis, a passively mode-locked thulium-doped fiber laser operating in the
stretched-pulse regime using the same normal-dispersion fiber for dispersion management
as in [Hax12] was developed. The experimental setup, which is comparable to [Wie12], and
the corresponding numerical model are shown in Fig. 4.6. The numerical simulations were
carried out by a commercially available software (s. Section 2.3). The simulations started
from noise until steady state was achieved. All following parameters of the experimental
setup were included into the simulation.

The cavity consisted of 0.69 m of TDF as active fiber with a mode field diameter (MFD) of 6.1 µm at a wavelength of 1940 nm. This fiber was chosen because of a very high absorption, which resulted in a short active fiber length. The TDF was core-pumped by a 1 W Er-fiber laser operating at a wavelength of 1575 nm. The pump light was delivered via a wavelength division multiplexer (WDM) designed to combine wavelengths at 1575 nm and 1950 nm. It consisted of 0.57 m standard single-mode fiber (SMF28e) with a MFD of 11.1 µm at a wavelength of 1900 nm. To achieve an optimal mode-matching from one end of the fiber section to the other, 3 cm of SMF28e were spliced to the free end of the active fiber section before the light was coupled out. The following free space section consisted of a TFP as polarized output coupling and a combination of a 3 mm birefringent quartz-plate (BFP) with a second TFP, which acted as a spectral filter. The spectral filter seemed to stabilize and start mode-locking easier in the experiment. Further included are one HWP at the beginning and a pair of HWP and QWP at the end of the free space section in order to adapt the polarization state for the mode-locked operation by NPR.

A fiber-based isolator (33 cm SMF28e fiber) was included at the input coupling of the fiber section to ensure unidirectional operation. The dispersion management was accomplished by implementing a normal dispersion fiber (NDF) inside the cavity between the isolator and the WDM. A high NA of 0.28 and a small core diameter of 2.7 µm generate a high value of waveguide dispersion, which overcompensates the negative material dispersion of the silica fiber. The normal dispersion per length of the NDF was estimated to be $\beta_{2,NDF} = +45.5\,\text{fs}^2/\text{mm}$ at a wavelength of 1940 nm. The negative dispersion of the SMF28e was $\beta_{2,SMF} = -70.0\,\text{fs}^2/\text{mm}$ and of the TDF was $\beta_{2,TDF} = -23.4\,\text{fs}^2/\text{mm}$, respectively, which were compensated by 1.53 m of NDF resulting in an estimated net cavity GDD of -0.012 ps^2. Due to the fact that TOD becomes an influential factor at compensated cavity GDD [Hau93], TOD was included into the simulation with an estimated net cavity TOD of $6.8 \cdot 10^{-4}$ ps^3. The dispersion values were calculated from the given fiber parameters taking both material and waveguide dispersion into account. The SA was modeled with the following parameters: unsaturable reflectivity $R_0 = 8\,\%$, saturable reflectivity $\Delta R = 12\,\%$ and saturation power $P_{sat} = 10\,\text{W}$. These values were obtained by a parameter study to find the optimum pulse forming mechanism inside the cavity with self-starting properties and without multi pulsing. The loss at the SA was simultaneously used as output coupling (OC). The TDF was further modeled by a gain-parameter of 4.4 per meter, a Gaussian gain profile of 100 nm FWHM around 1923 nm wavelength while the gain saturation energy was set to a value of 0.13 nJ.

The laser started mode-locking operation in the experimental setup at a pump power of 357 mW but operated in the multi-pulse regime. After the pump power was reduced

to 133 mW, single-pulse operation was attained with an average power of 9.5 mW. The repetition rate was 62.3 MHz so that the average output power corresponded to a pulse energy of 0.15 nJ. Higher pump power levels led either to the emission of continuous-wave peaks or multiple pulses.

The optical spectrum and the autocorrelation (AC) trace of the passively mode-locked laser are shown in Fig. 4.7. The power spectrum (a) offered a FWHM of the main peak of 33 nm around a peak wavelength of 1935 nm. It ranged from 1879 nm to 1985 nm at -10 dB level due to sideband-generation on the red-winged part of the main peak. Additionally, the spectrum was covered with sharp dips caused by molecular resonances [Sta03], which could be verified by the high-resolution transmission molecular absorption (HITRAN) database as molecular absorption lines (especially water) [Rot09]. These absorptions mostly took place inside the optical fibers as already reported in [Wie12]. The FWHM of the simulated optical spectrum (red dashed curve) was similar, but the spectrum showed a less pronounced sideband on the longer wavelength side.
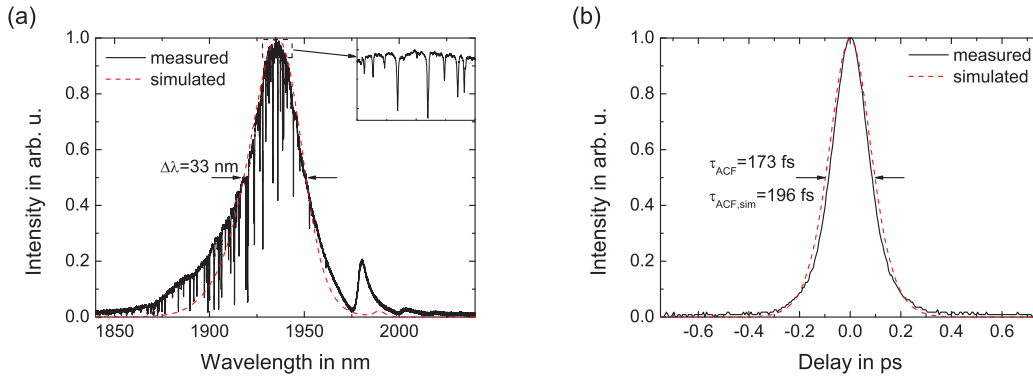
Figure 4.7: Experimental (black continuous curve) and numerical (red dashed curve) output characteristics of the TDF oscillator: (a) optical spectrum on linear scale with inset: magnification of molecular resonances and (b) AC trace of the uncompressed pulse.

Figure 4.7 (b) shows the AC trace of the uncompressed laser pulse directly out of the oscillator, which had an AC FWHM of 173 fs. This corresponded to a pulse duration of 112 fs assuming a squared hyperbolic secant shape (sech^2). A Fourier-transformation of the optical spectrum to determine the transform-limited pulse duration was not possible owing to the strong absorption lines, which interrupted the spectrum. The simulation showed a comparable FWHM spectrum, but the measured spectrum revealed more spectral features, possibly by non compensated higher order dispersion, polarization effects or phase distortions, which were not included into the simulation. Therefore, a compression of the simulated pulse led to an AC trace of 196 fs, which was 13 % longer than the measured one.

Single-pulse operation of the experimental laser was verified by measuring the output pulse train with a 12.5 GHz photodiode in combination with a 6 GHz oscilloscope and a 26.5 GHz radio-frequency (RF) spectrum analyzer (see Fig. 4.8). To observe the temporal range up to 150 ps, a commercial autocorrelator was used. Neither the long range AC trace nor the oscilloscope signal (a) showed any sign of satellite pulses. The temporal spacing of 16 ns of two following pulses (b) corresponded to the inverse of the fundamental beat note in the RF spectrum of 62.3 MHz (c). Furthermore, no signs of q-switching instabilities were visible. Figure 4.8 (d) shows the frequency comb up to 2.5 GHz, which also confirmed stable mode-locked operation.
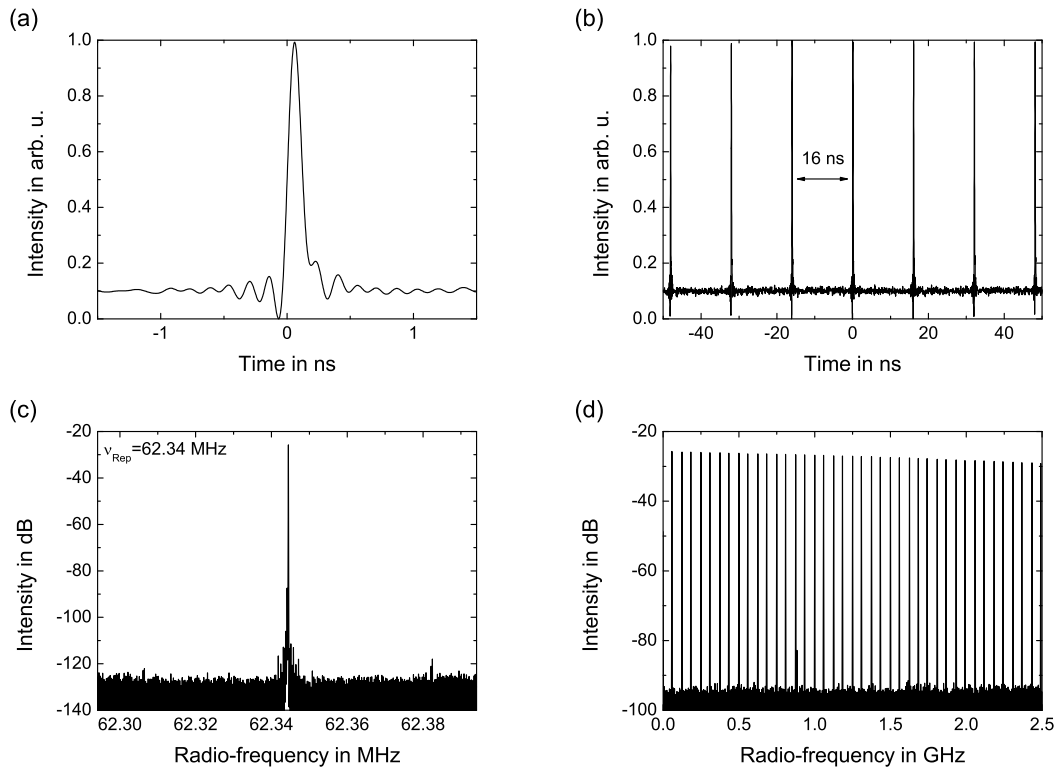
Figure 4.8: Output pulse trace and radio-frequency spectrum of the TDF oscillator: (a) single pulse, (b) pulse train, (c) fundamental beat note, and (d) frequency comb.

In summary, a passively mode-locked, stretched-pulse operating thulium-doped fiber laser was presented, which generated uncompressed sub-120 fs pulses. The dispersion management was accomplished by the use of a high NA, small core fiber, resulting in a cavity GDD of -0.012 ps^2. The average output power of the pulse was 9.5 mW, which corresponded to a pulse energy of 150 pJ at a repetition rate of 62.3 MHz. The uncompressed pulses from the oscillator were nearly transform-limited with a pulse duration of 112 fs.

The main experimental characteristics could be verified by the performed simulations, but differed in terms of sideband generation and a 13 % longer pulse duration.

4.3 Fiber preamplifier

The generated pulses from the oscillator described in the previous Section 4.2 were isolated against back reflections from the following preamplifier to avoid destabilization of the oscillator (s. Fig. 4.9 (a)). Before amplification, the pulses were stretched using a fiber stretcher consisting of several meters of polarization maintaining (PM) fiber to ensure preservation of the linear polarization state during amplification. The following amplifier consisting of a pump combiner and active fiber was designed to generate pulses at nJ-level while simultaneously offering compressibility to less than 500 fs.
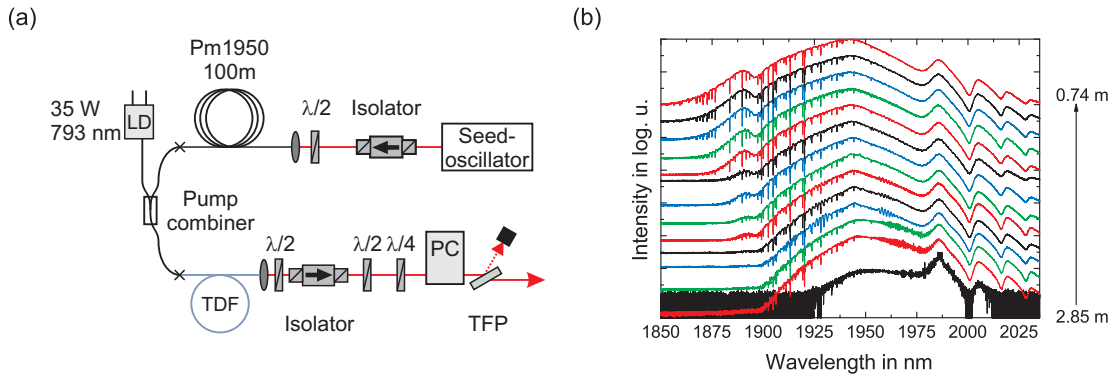
Figure 4.9: (a) Schematic setup of the TDF preamplifier and (b) optical spectrum on logarithmic scale measured at different fiber lengths to validate the optimum active fiber length.

The amplifier was seeded with an input power of 4.2 mW, measured behind the pump combiner. The cladding pumped TDF was spliced to the pump combiner and had a core diameter of 10 μm with a NA of 0.15 and a cladding diameter of 130 μm with a NA of 0.46. The pump absorption for cladding pumping at 793 nm was specified by the manufacturer to be 4.7 dB/m. Owing to the temperature sensitivity of thulium-doped fibers [Tur08], the active fiber was coiled around an aluminum-spool for passive cooling. The pump diode was fiber coupled with a multi-mode fiber, which had a core diameter of 105 μm and through which 35 W pump power were emitted at a central wavelength of 793 nm. This multi-mode fiber was spliced to the pump combiner, which coupled 89 % of the pump power into the cladding of the passive fiber resulting in a maximum available pump power of 31 W. The pump combiner had a signal fiber length of 1.88 m with the same fiber geometry as the active fiber to ensure lowest splice losses.

The optimum active fiber length of the TDF for amplification of the broadband seed signal was determined by the cut-back technique (s. Fig. 4.9 (b)). For this measurement, around 11 m of PM1950 fiber as stretching fiber were used, which resulted in a pulse duration of 11 ps. Starting with an active fiber length of 2.85 m, which ensured more than 95% absorption of the pump light, the amplified spectrum at a fixed output energy of 32 nJ revealed a red-shift of the gain spectrum by strong reabsorption in the long fiber. With decreasing fiber length in steps of less than 20 cm to 0.74 m, the amplified spectrum shifted towards the original seed spectrum with an optimum fiber length found at 0.86 m in terms of maximum FWHM.
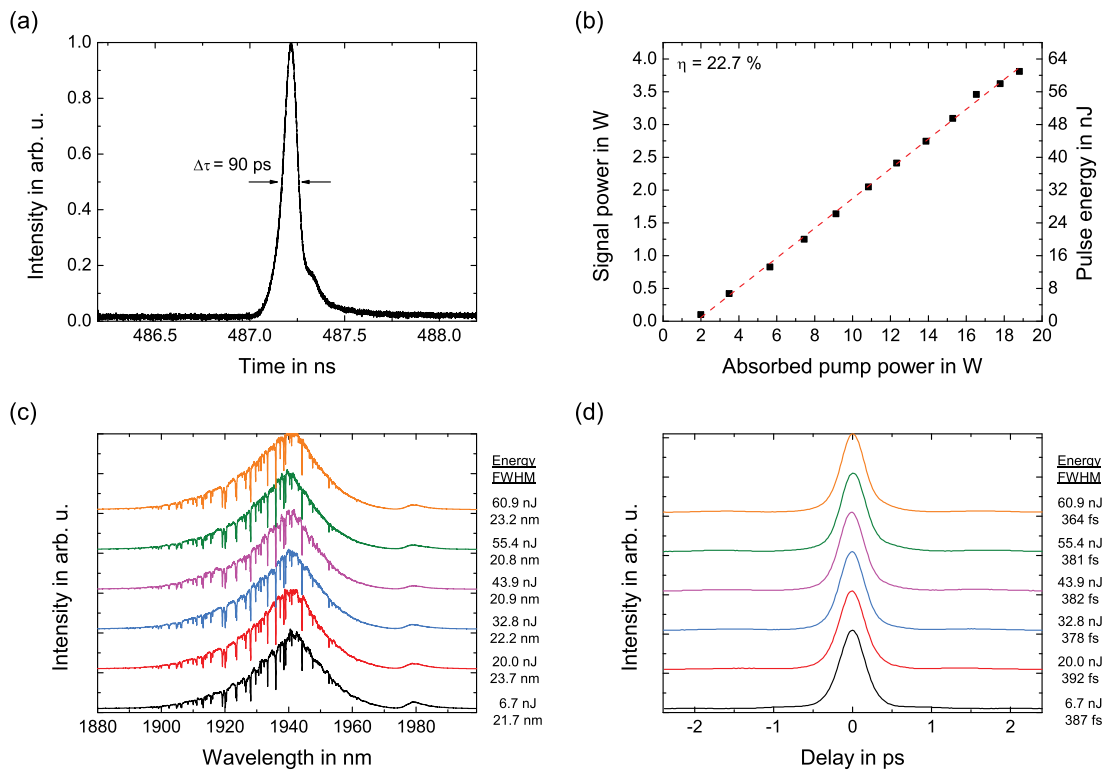
Figure 4.10: Stretched and amplified pulses after the complete fiber section consisting of 100 m PM1950 fiber, 1.88 m of the fiber pump combiner and 0.95 m Tm-doped fiber: (a) stretched pulse measured with a sampling oscilloscope (70 GHz) and fast photodiode (12.5 GHz), (b) amplifier output power vs. absorbed pump power, (c) optical spectrum at different pulse energies and (d) AC traces of the compressed pulse at different energies.

In order to stronger mitigate expected nonlinearities at higher output energies, the stretcher fiber was lengthened to 100 m in the final setup. The stretched pulse duration depicted in Fig. 4.10 (a) increased from 11 ps to 90 ps. When applying the longer stretching fiber, a slightly longer active fiber of 0.95 m could be used resulting in a higher

amplification efficiency. The pulses were amplified at an incident pump power of 26 W up to a maximum pulse energy of 61 nJ, measured behind the TFP of the pulse picker (s. Fig. 4.10 (b)). Amplification up to this pulse energy level with a gain of 29 dB showed no sign of nonlinearities or pulse degradation in the spectrum or the autocorrelation of the compressed pulses. Due to the combination of anomalous dispersion and SPM mostly in the fiber stretcher, the FWHM of the optical spectrum was reduced from initially 33 nm to 23 nm but remained nearly unchanged during the whole amplification as depicted in Fig. 4.10 (c). The pulses could still be compressed to a duration of 236 fs (364 fs AC FWHM) at 61 nJ pulse energy (s. Fig. 4.10 (d)). Parasitic lasing or amplified spontaneous emission (ASE) were not visible during the measurements. The linear polarization state after amplification was confirmed to 13 dB by measuring the polarization extinction ratio (PER). After the amplification stage, the pulse repetition rate was reduced from 62.3 MHz to 1 kHz by the use of a PC and a TFP. For example, at a pulse energy of 24 nJ this resulted in 24 µW of transmitted signal power to the RA, whereas the reflected power of 1.5 W was blocked.

4.4 Regenerative amplifier

The final experimental setup including all separate stages is shown in Fig. 4.11. In this section, only the cavity design offering the highest output energy is described. The following Subsection 4.4.1 deals with the general cavity design which is investigated in Subsection 4.4.2 under CW operation and in Subsection 4.4.3 under q-switched operation. The cavity designs for continuous wave or q-switch operation differed slightly from the final one and are described in the separate subsections but used nearly the same mode field diameters inside the cavity.
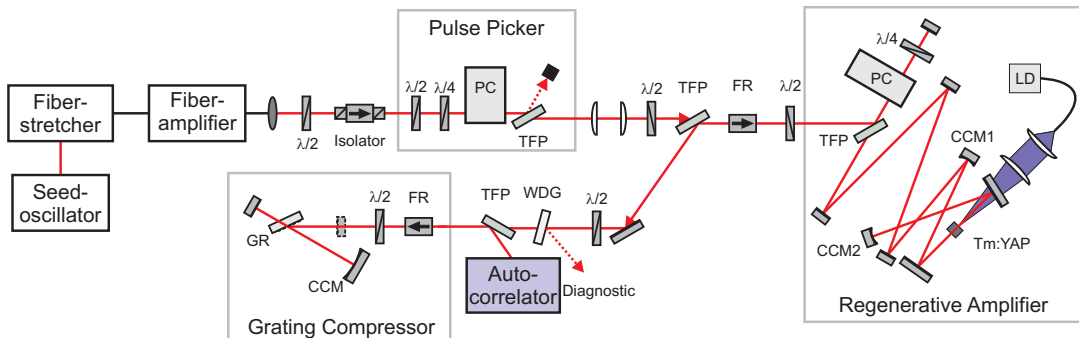
Figure 4.11: Experimental setup of the system. PC: Pockels cell, TFP: thin film polarizer, FR: Faraday rotator, CCM1: concave mirror with 600 mm ROC, CCM2: concave mirror with 300 mm ROC, WDG: wedge, GR: grating.

4.4.1 Cavity design considerations and calculations

As described in Section 4.1, the wavelength for pumping Tm:YAP is 794 nm while the emission wavelength is 1940 nm. This results in a low quantum efficiency of 41 %, which means that most of the absorbed pump light is transformed into heat inside the crystal. Therefore, thermal lensing had to be included into the design of the cavity at the position of the laser crystal. The thermal lens was measured by setting up a 80 mm plane-plane cavity as shown in Fig. 4.12 (a), which operated in a stable regime by utilizing the thermal lens as focusing element in the resonator. The pump diode was a multi-mode fiber-coupled laser diode (LD) with 35 W maximum pump power at a central wavelength of 793 nm. The output fiber of the pump diode had a core diameter of 105 µm and a NA of 0.22. The collimated pump light was focused with a 100 mm lens into the 4 mm long, 4 at. % doped Tm:YAP crystal through one of the dichroic end mirrors, which was located close to the crystal. The crystal was wrapped in indium foil and electrically cooled down to 17°C by using a Peltier element. The pump mode was measured with a rotating slit camera to a diameter of 500 µm. The measured output power (s. Fig. 4.12 (b)) dropped at a pump power of 9.45 W, which marked the position when the focal length of the thermal lens was shorter than the resonator length so that the resonator became unstable as described in [Hod97]. Therefore, a thermal lens of 80 mm at this pump power of 9.45 W was assumed for the following cavity design.
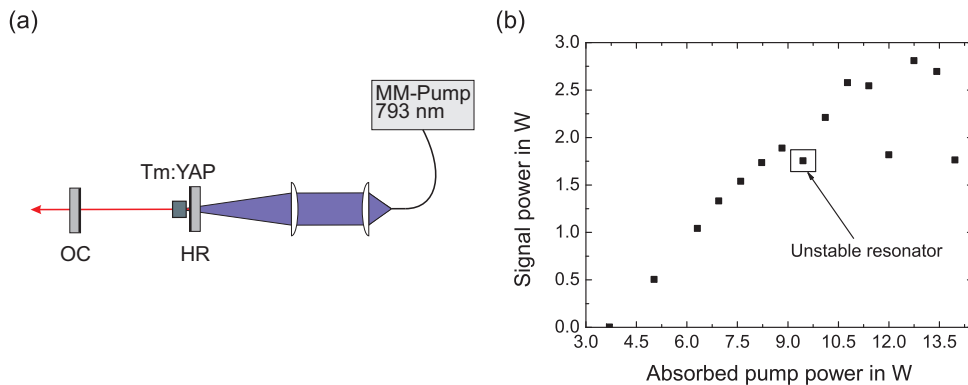
Figure 4.12: (a) Schematic setup for measuring the thermal lens and (b) laser output power vs. absorbed pump power.

Ultrashort pulse regenerative amplifier cavities have to be designed to address at least two main issues: firstly, an efficient amplification and secondly, to prevent adding strong nonlinearities to the pulses. The first issue can be coped with by using a proper MFD in the active material to reach an efficient amplification and keeping the losses inside the cavity

to a minimum. The nonlinearities can be minimized by using short optical path lengths through bulk material (crystals etc.), long stretched pulses and large MFDs. Especially the latter means that a trade-off for the MFD has to be found for an efficient amplification with reasonable nonlinearities. As Tm:YAP has a low single pass gain of 1.22 combined with a low emission cross section (s. Subsection 4.1.2), the focus here was mainly shifted to the efficient amplification part by using a small MFD inside the laser crystal. The rest of the resonator was designed so that larger MFDs can be used, especially at the position of the PC with its two 10 mm long crystals.
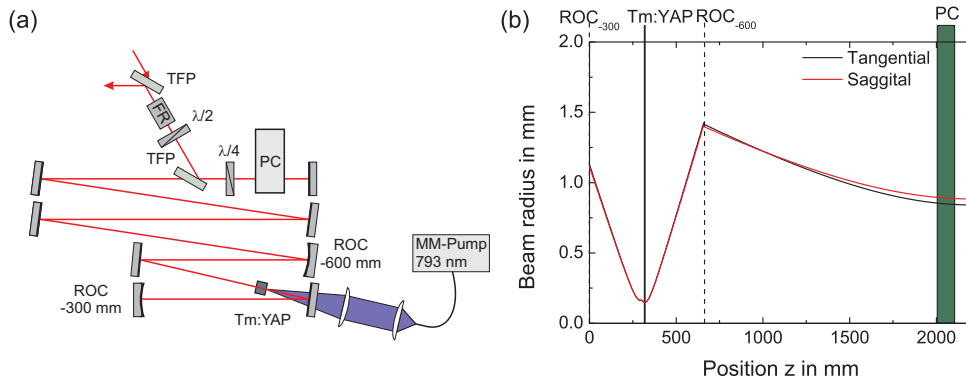
Figure 4.13: (a) Schematic setup of the RA cavity, (b) evolution of the beam inside the cavity.

The RA consisted of a 2.2 m long, standing wave cavity with two concave mirrors, which is depicted in Fig. 4.13 (a). The concave mirror CCM1 with a radius of curvature (ROC) of -600 mm was placed 35.4 cm and CCM2 with an ROC = -300 mm was placed 29.5 cm apart from the crystal. A rubidium titanyl phosphate (RTP) PC was used in combination with a TFP and a QWP as an optical switch. The evolution of the resonator mode diameters is shown in Figure 4.13 (b). The simulations of the cavity were performed with the commercial software Winlase. The MFDs were 320 µm inside the laser crystal (5×5 mm^2 aperture) and 1.7 mm inside the PC, which had an aperture of 3.2 mm. The simulation showed that for a 10 % decreased (stronger) thermal lens, the mode diameters inside the crystal and at the position of the PC increased by less than 5 %. Therefore, a nearly constant mode diameter inside the laser crystal can be assumed.

In order to understand the general operation of the designed cavity with the laser crystals, first CW and tunability experiments were performed without the optical switch. In a next step, q-switch experiments were carried out after implementing the optical switch to explore the achievable pulse energies. Finally, the cavity was seeded with ultrashort pulses for regenerative amplification.

4.4.2 Continuous wave experiments and tunability

The CW experiments were performed in an early stage of this work, therefore a different cavity design was chosen as depicted in Fig. 4.14 (a). A ROC of -800 mm was used and the second arm of the cavity with CCM2 was replaced by a dichroic mirror located as close to the crystal as possible. The MFD in the laser crystal was 800 μm and the pump mode diameter was 690 μm, which resulted in a lower thermal lensing but also in a lower efficiency due to the large MFDs. Figure 4.14 (b) shows the output power at different output coupling ratios. In the case of low ratios (1.8 % – 6 %) a maximum output power of more than 2 W was attained, which could not be achieved with high output coupling ratios (higher than 11 %). Furthermore, in all cases a drop in the output power was visible, which might be explained by a thermally induced instable resonator regime. In general, these measurements give a good qualitative overview about the CW-characteristics of a Tm:YAP laser.
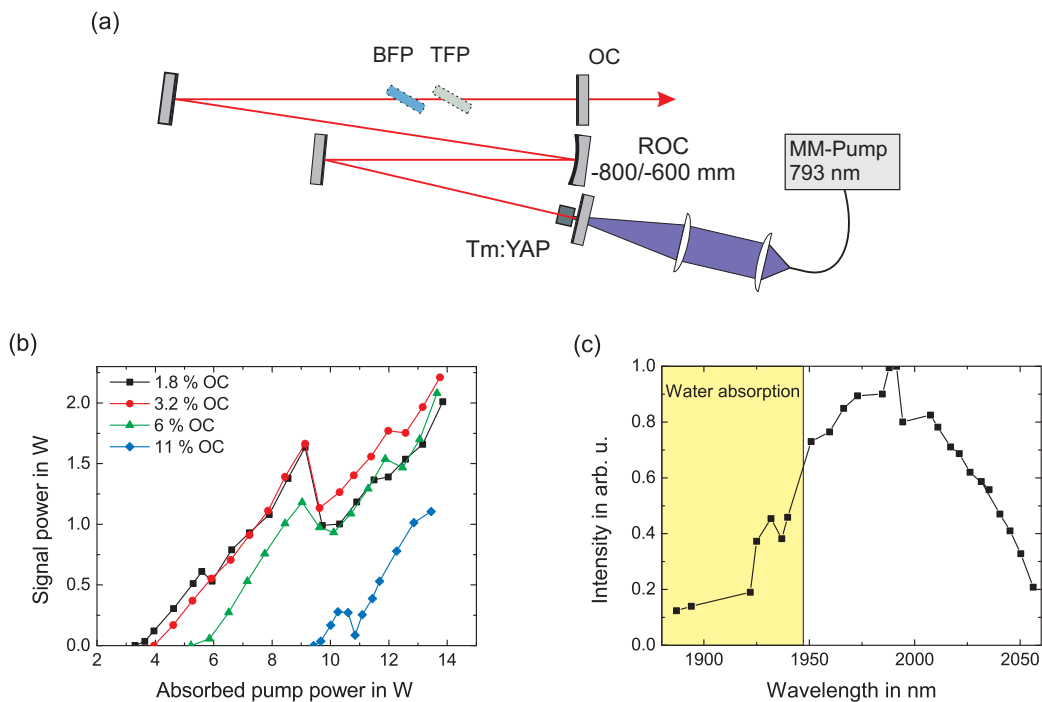
Figure 4.14: (a) Schematic setup of the cavity, (b) signal power vs. absorbed pump power at different output coupling ratios, and (c) wavelength tunability.

Tm:YAP shows a broad wavelength tuning range from 1887 nm to 2056 nm with a maximum output power of 2.1 W at a wavelength of 1991 nm (s. Fig. 4.14 (c)). This was measured by inserting a 2 mm thick BFP and a TFP in the cavity, which acted as a

tunable spectral filter. Additionally, the cavity was changed as follows: the -800 mm ROC mirror was replaced by a -600 mm ROC mirror, which resulted in a higher efficiency due to the smaller MFD of 310 μm in the laser crystal. Furthermore, the pump mode diameter was changed to 500 μm. As strong water absorption takes place in the region between 1887 - 1947 nm (marked yellow), the laser was not continuously tunable there.

4.4.3 Q-switch experiments

The cavity design for the q-switch experiments was quite similar to the final one in Fig. 4.13, except for the second arm with CCM2, which was replaced by a dichroic mirror placed as close to the laser crystal as possible and an output coupling of 3.2 %. Q-switching was achieved by using the now inserted PC, TFP, and QWP in the cavity as optical switch. The concept for q-switching is the same in the case of regenerative amplification but without seed signal (s. Fig. 2.7 in Chapter 2). The q-switch pulse builds up during the $\lambda/2$ polarization state of the optical switch.
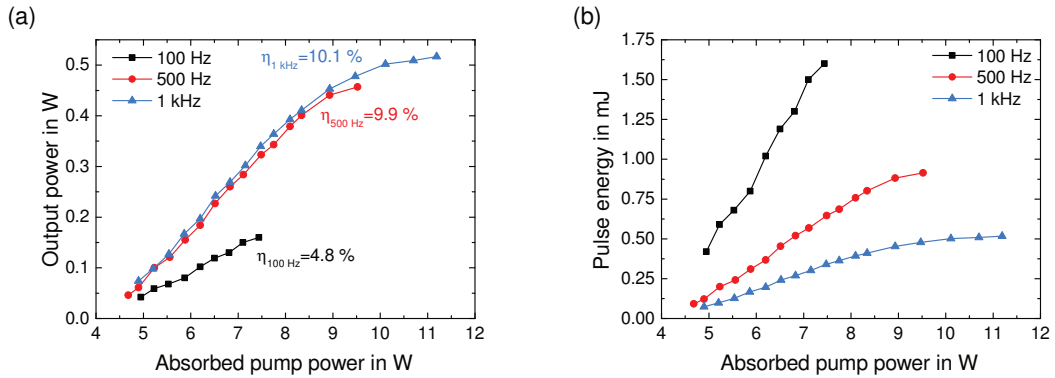
Figure 4.15: Q-switch output characteristics of Tm:YAP at different repetition rates: (a) average power and (b) pulse energy.

Figure 4.15 (a) shows the output power at different repetition rates. In case of 1 kHz and 500 Hz, an average power of more than 457 mW with a linear slope efficiency of 10 % was reached. A further increase of the pump power led to a saturation of the output power. At a repetition rate of 100 Hz, 160 mW average power at a slope efficiency of 4.8 % was attained. This resulted in the highest pulse energy of 1.6 mJ without any signs of saturation although the pump power was limited to 7.5 W to avoid a destruction of the laser crystal at these high pulse energies. Pulse energies of 914 μJ and 517 μJ were attained at 500 Hz and 1 kHz, respectively.

The pulse build up time was shortest when the resonator was perfectly aligned and / or higher pump power was applied [Ise02], because the build up time and pulse duration

in actively q-switched lasers depend on the losses and gain inside the laser cavity [Sie86]. The build up time, which was measured at 10 % of the pulse in respect to the trigger signal, decreased with increasing pump power for all three repetition rates. For 1 kHz repetition rate, the rise time decreased from 28.4 µs to 14.5 µs, which was nearly half the original value. The shortest rise time was attained at 100 Hz with 2.8 µs at highest output energy of 1.6 mJ. In the case of 1 kHz and 500 Hz, q-switch pulse operation was achieved at half the applied repetition rate at low pump power due to the low inversion in the active material. Higher pump power led to a higher inversion and the pulses were generated at the desired repetition rate. Figure 4.16 shows the representative oscilloscope trace of the pulse evolution exemplary at 1 kHz. Simultaneously to the decreased rise time, the pulse duration decreased for all three repetition rates from the µs-range over a factor 2-3 to a minimum pulse duration of 500 ns in case of 100 Hz at highest output pulse energy of 1.6 mJ.
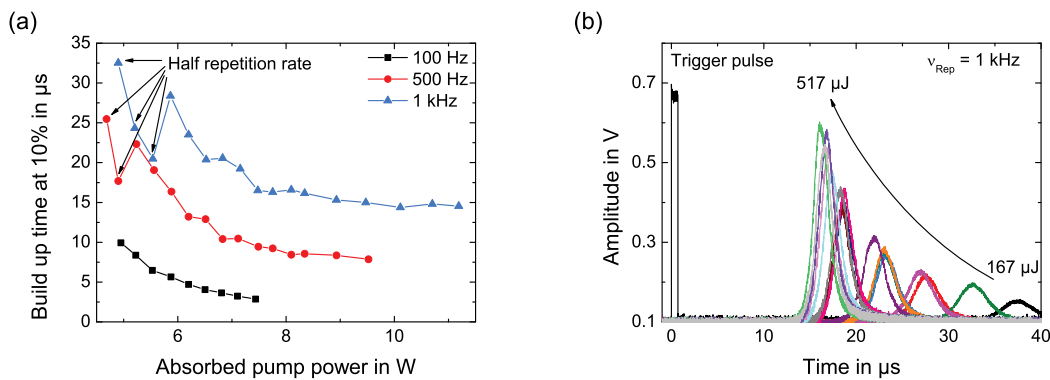
Figure 4.16: Evolution of the q-switched pulses: (a) build up time at different repetition rates and (b) oscilloscope traces of different pulse energies at 1 kHz.

4.4.4 Regenerative amplification with Tm:YAP

In the next step, after setting up and characterizing the seed oscillator, preamplifier, and the cavity of the regenerative amplifier (RA), the ultrashort pulses from the preamplifier were seeded into the RA. Parts of this chapter were already published in [Wie15a]. By setting up a magnifying telescope with a 20 mm and 30 mm lens behind the pulse picker, the MFDs of the preamplifier and the regenerative amplifier cavity were adapted to obtain a high seeding efficiency. The RA cavity was enclosed for purging with inert gas (argon, nitrogen etc.) to mitigate atmospheric absorption effects in this wavelength range [Geb15a]. After amplification, the pulses were compressed with a Martinez-type compressor [Mar84], which consisted of a single gold coated diffraction grating (600 grooves per mm, Blaze

angle: 34°), one concave mirror with a ROC = -1000 mm and two plane mirrors. The compressor efficiency of 50 % was mainly limited by the grating efficiency and the FR.
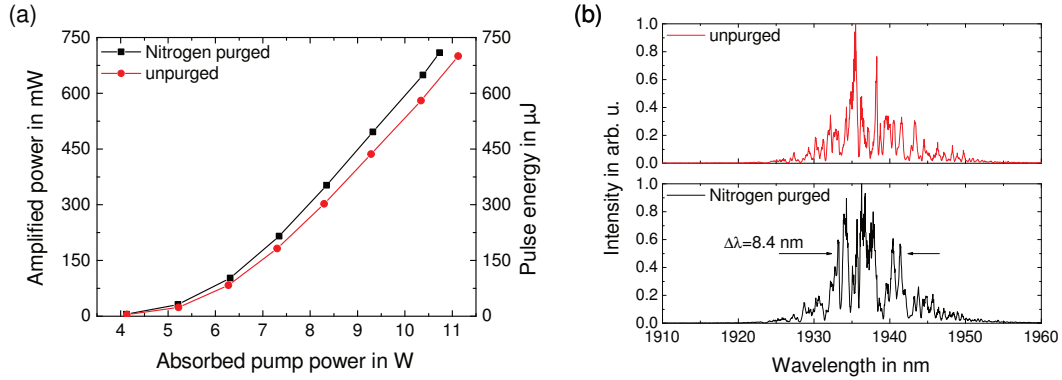
Figure 4.17: Purged (black curve) vs. unpurged cavity (red curve): (a) Uncompressed amplified power / pulse energy vs. absorbed pump power and (b) optical spectrum at 700 μJ output pulse energy.

The following experimental results were achieved with a seed pulse energy of 24.8 nJ (in front of the RA cavity) at a repetition rate of 1 kHz and with 34 round trips unless stated otherwise. At an absorbed pump power of 11.1 W a pulse energy of 700 μJ was achieved (s. Fig. 4.17 (a), red curve). As the damage threshold of the laser crystal was found during earlier experiments between a power density of $2.0 - 2.1 \, \mathrm{J/cm^2}$ the achievable pulse fluence was limited below $1.77 \, \mathrm{J/cm^2}$ in all following experiments. In this configuration, this corresponds to a pulse energy of 712 μJ. Figure 4.17 (b) (red line) shows the optical spectrum of the amplified pulses at a maximum pulse energy of 700 μJ. It was centered around 1937 nm with a bandwidth of 19 nm at -10 dB. Furthermore, it was highly structured with sharp dips, which were demonstrated in a previous publication [Wie12] and were identified by the HITRAN database [Rot09] as atmospheric absorption lines of water vapor. When purging the cavity of the RA with nitrogen gas, the relative humidity decreased from 20 % to less than 3 % and the absorption lines vanished at least partly, but the optical spectrum remained structured with a FWHM of 8.4 nm (18.5 nm at -10 dB, respectively). Additionally, the output pulse energy increased about 20 % on average at similar pump power so that a lower absorbed pump power of 10.7 W was required to reach an uncompressed pulse energy of 709 μJ (s. Fig 4.17 (a), black curve).

The output beam profile was perfectly circular at increasing pump power, but the diameter varied from 2.44 mm to 1.98 mm due to the thermal lensing effect (s. Fig. 4.18 (a)). No signs of beam profile degradation in the unpurged or purged case were observed as stated in [Geb15b]. A measurement at maximum output power in the unpurged case

revealed a beam propagation parameter M^2 in direction parallel to the optical table of 1.61 ± 0.04 and 1.57 ± 0.06 perpendicular to the optical table (s. Fig. 4.18 (b)).
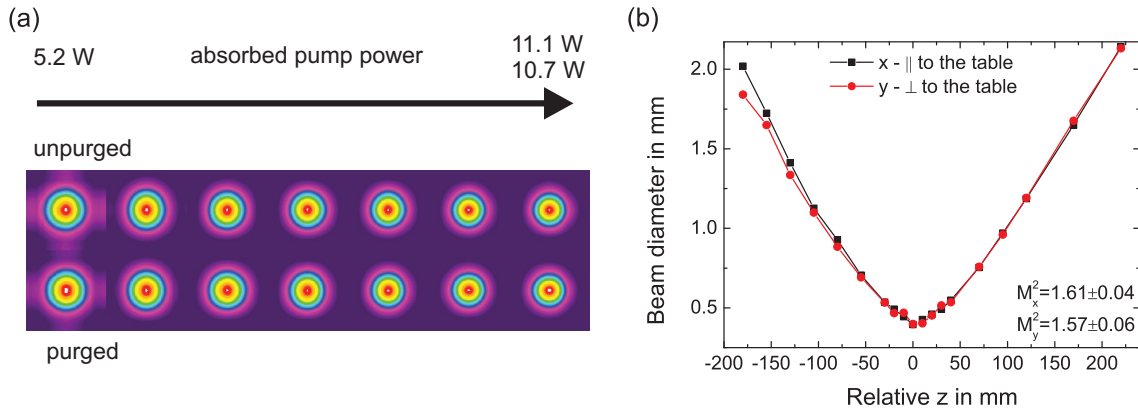
Figure 4.18: (a) Beam profile at increasing pump power levels: from $5.2\,\text{W}$ to $11.1\,\text{W}$ in unpurged case and $10.7\,\text{W}$ in purged case and (b) M^2-measurement in unpurged case at highest output power of $700\,\text{µJ}$ pulse energy.

The oscilloscope trace of the pulse during regenerative amplification with 34 round trips is shown in Fig. 4.19 (a). This was measured behind one of the HR mirrors of the RA cavity. The pulse amplification build up was clearly visible whereas the spacing of $14.8\,\text{ns}$ corresponded to the RA cavity round trip time. Only one pulse propagated inside the RA and was amplified. In Fig. 4.19 (b), the single output pulse is shown with no evidence of further satellite pulses, which were suppressed by aligning the plane-parallel laser crystal with a slight angle to the incident seed beam without any drop in efficiency or deterioration of the beam profile.
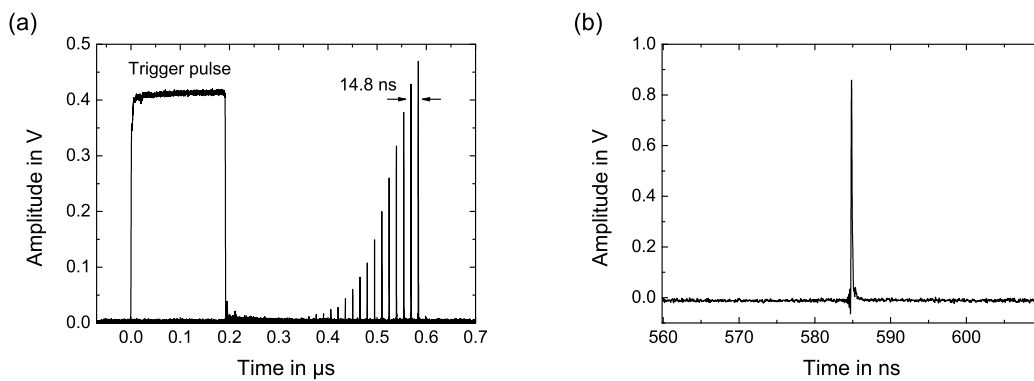
Figure 4.19: Oscilloscope trace of the RA pulses (a) during amplification at 34 round trips and (b) output pulse.

Figure 4.20 (a) shows the AC trace in a 50 ps range after pulse compression at an output pulse energy of 700 µJ. The effect of the atmospheric absorption was clearly visible in the broadband ps-pedestal (red curve), which vanished nearly completely after purging with nitrogen (black curve). These pulse quality degradation effects were observed in the MIR wavelength range between 6 µm and 8 µm at long ps pulses by SEILMEIER et al. [Sei88] already in 1988. Very recently, these effects were also investigated in the 2 µm range by GEBHARDT et al. [Geb15b]. As absorption and refractive index (and therefore dispersion) are linked together by the Kramers-Kronig relations [Kro26], a sharp absorption line at a specific wavelength causes a Fano-shaped feature in the refractive index profile. This leads to a strong spectral phase distortion across the spectrum (higher dispersion values), which forms post-pulses and a long pulse tail (broadband ps-pedestal).
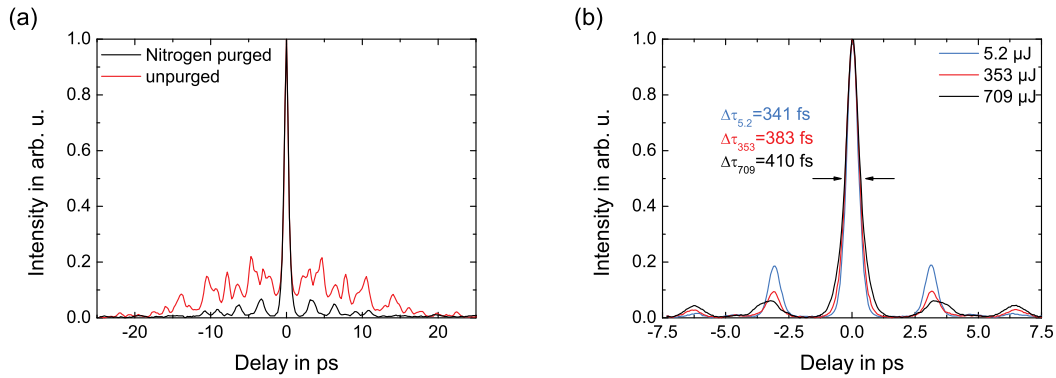
Figure 4.20: Compressed AC traces: (a) at 700 µJ output pulse energy (black curve: purged, red curve: unpurged), (b) at output pulse energies 5 µJ (blue), 353 µJ (red) and 709 µJ (black).

After purging, the only remain was a satellite pulse with a relative intensity of 6.2 % in a temporal distance of 3.2 ps, which corresponded to an optical path length of 0.96 mm. Furthermore, a second satellite pulse appeared in twice the temporal distance to the main peak. No optical element inside the cavity corresponded to the measured path length so etalon effects could be excluded as possible cause. In the experiment, the distances of the satellite pulses to the main peak did not change within measurement accuracy, but the relative intensity decreased from 19.5 % to 6.2 % with increasing pump power / pulse energy (s. Fig. 4.20 (b)). A possible explanation for this counter-intuitive behaviour was found in the different amplification levels of main and satellite pulse: if the satellite pulse was a post-pulse following the main pulse in time, then it would be amplified by the residual fraction of gain left by the main pulse. The time between main and satellite pulse left no time for the active material to recover despite continuous wave pumping. Therefore, the pulses were amplified differently and the relative intensity of the satellite pulse decreased.

For investigation of the origin of the satellite pulses, a closer look at the seed oscillator and preamplifier pulses was taken (s. Fig. 4.21 (a)), which revealed no evidence of satellite pulses. Furthermore, an AC trace after a single pass through the resonator (four passes through the PC) without regenerative amplification depicted in Fig. 4.21 (b) showed no signs of satellite pulses. When the PC inside the RA was replaced by another RTP cell from a different vendor with same crystal lengths and measured at similar output energies, more copies of the satellite pulse appeared. The temporal distance from the first satellite pulse to the main pulse shortened from 3.2 ps to 2.9 ps and the relative intensity increased in the AC trace (s. Fig. 4.21 (c)). Therefore, the generation of satellite pulses could be at least partly attributed to the PC. One possible explanation for the generation of the satellite pulse could be uncompensated birefringence of the two 90° turned RTP crystals. By various experiments with additional wave plates and thick birefringent quartz plates, it was not possible to reduce the satellite pulses. However, etalon effects inside the PC could be excluded as the two 10 mm long RTP crystals were separated by more than 5 mm from each other. Tilting the PC to achieve a static quarter wave retardation and removing the QWP of the RA showed no change in the AC trace. All in all, this indicates a resonant effect during multiple round trips caused by technical imperfection of the PC.
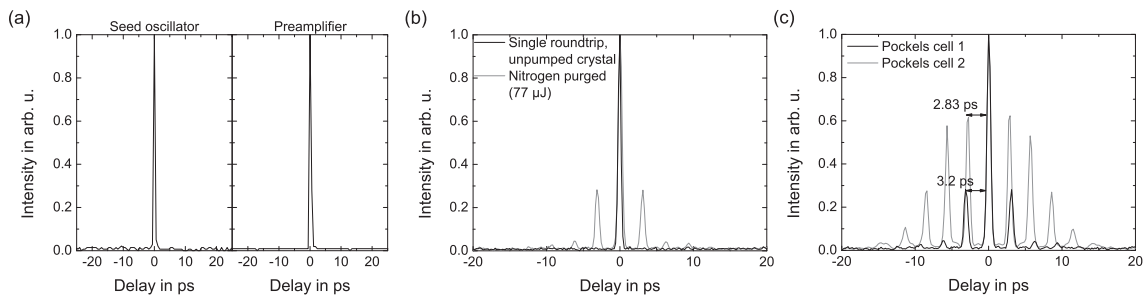
Figure 4.21: Investigation on the origin of the satellite pulses: (a) seed oscillator, preamplifier and (b) single pass through the unpumped RA revealed no signs of satellite pulses. (c) Another PC from a different vendor showed a distinct behaviour.

Another possible explanation is based on residual water absorption inside the dielectric layer coatings of the RTP-crystals [Ehl04; Jen06]. As RTP itself is non-hygroscopic [Hil14], it can be excluded as possible cause. The AR coatings on the RTP crystals, which were manufactured by electron beam evaporation [Har06], are more porous than coatings fabricated by ion assisted deposition or ion beam sputtering [Jen06]. These porous layers adsorbed water from the ambient air after the coating chamber was vented and could not be liberated. This incorporated water caused high losses, which were already measured in the 2.9 μm water window [Ehl04]. Therefore, a change to another wavelength region (e.g.

2.1 µm) without strong water absorption may result in a satellite-free autocorrelation trace
(s. Subsection 5.4.4).

After compression with the grating compressor, the duration of the compressed pulses
depicted in Fig. 4.20 (b) increased from 341 fs to 410 fs with increasing pulse energy
(assumed squared hyperbolic secant temporal profile). At the maximum output energy of
709 µJ, a fraction of 76 % was confined in the main peak. For this performance (34 round
trips, 709 µJ uncompressed output energy, 1 kHz repetition rate), a B-Integral of 7.01 was
estimated by the use of Equation (2.14) and the Frantz-Nodvik Equation (2.12). For the
calculations, a cavity loss of 6 % was applied after every round trip and a constant peak
power was assumed during one round trip. The parameters of the optical elements for the
calculations inside the cavity are shown in Table 4.2. A B-Integral of π was reached at an
output pulse energy of 429 µJ. The highest influence on the B-Integral was attributed to
the Tm:YAP crystal because of the small mode radius and high nonlinear refractive index
n_2. The RTP crystal contributes the second main fraction to the B-Integral owing to the
length of 20 mm. The nonlinear refractive index of RTP was not available in literature.
Therefore, the nonlinear refractive index of KTP (2.76×10^{-15} cm^2 / W, from [Ada89]) was
chosen for the calculations because KTP is the closest isomorph to RTP in terms of optical
and chemical properties, for which data were available.

Table 4.2: Parameters of the optical elements in the thulium-doped regenerative amplifier for
calculating the B-Integral. *The nonlinear refractive index of KTP was used instead of RTP
[Ada89].

Parameter	Tm : YAP	TFP	QWP	RTP
Length [mm]	4	7.62	1	20
Nonlinear refractive index n_2 [$\times 10^{-20}$ m^2/W]	14.6	4.91	6.12	27.6*
Mode radius [µm]	160	900	885	890
Mode area (Gaussian) [mm^2]	0.04	1.27	1.23	1.24

The linear relation of output energy to cavity round trips at a fixed absorbed pump
power of 8.5 W is shown in Fig. 4.22 (a), starting from 24 round trips with an output
energy of 47 µJ. The maximum pulse energy of 703 µJ was achieved at a round trip number
of 44. Figure 4.22 (b) compares the compressed pulse AC traces after 34, 39 and 44 round
trips at a fixed output pulse energy of ca. 700 µJ, which was achieved by applying the
appropriate pump power. The pulses could still be compressed between 404 fs and 422 fs.
Due to the higher number of round trips in the RA, the amplitude of the satellite peak
increased from 6.2 % to 15.8 % and shifted slightly from 3.2 ps to 3.6 ps. This could be
either introduced by the longer round trip time (more absorptions, more complex phase

(a)

(b)
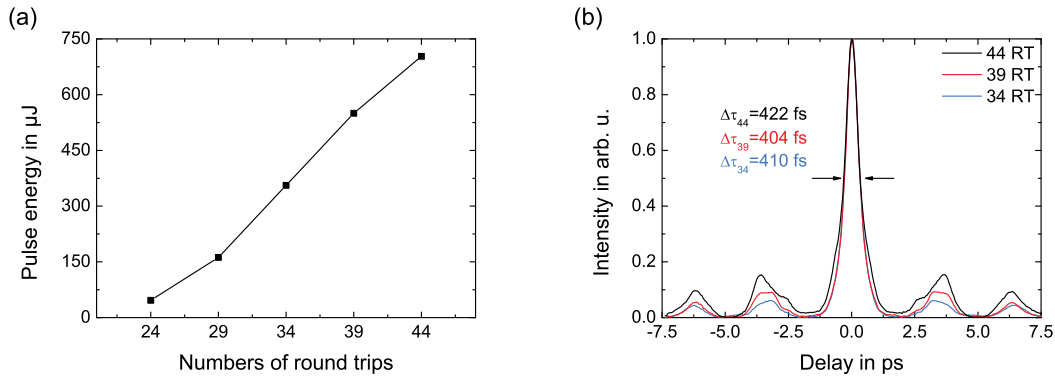
Figure 4.22: (a) Output pulse energy in relation to the number of round trips at 8.5 W absorbed pump power and (b) compressed AC traces at 34, 39 and 44 round trips (RT) at an output energy of 700 µJ.

profile) or by higher nonlinearities (B-Integral of 11.97 at 44 round trips) inside the RA cavity or even both.

If a RA is constantly pumped, it can be operated up to a repetition rate inverse to the upper state life time with a constant maximum high pulse energy [Ise02]. At higher repetition rates, the upper state level can not be pumped to full saturation, which results in a decreasing output energy. Due to the long upper state lifetime of Tm:YAP measured to 6.2 ms, this value would be around 161 Hz. The pulse energy in dependence of the repetition rate is depicted in Fig. 4.23 (a) at a fixed number of 34 round trips and an absorbed pump power of 7.5 W. Beginning at a low repetition rate of 100 Hz with a maximum output energy of 702 µJ, the pulse energy decreases nearly exponentially with increasing repetition rate up to 3 kHz to a value of 111 µJ. At this point, the pulse energy starts saturating. Higher repetition rates can not be applied to the Pockels cell to avoid strong heating of the PC driver by fast switching.

Figure 4.23 (b) shows the behaviour of the RA output while varying the seed pulse energy by operating the preamplifier at the highest output energy and reducing the pulse energy subsequently with a combination of a HWP and a TFP. The output pulse energy (black curve) increased linearly from 491 µJ at a seed energy of 12.3 nJ to a maximum pulse energy of 700 µJ at a seed energy of 48.7 nJ. Additionally, the compressed pulse duration (red curve) stayed nearly constant between 380 fs and 402 fs for the different seed pulse energies and was shortest at the highest output power. Taking the compressor efficiency of 50 % into account, these values resulted in a peak power of 700 MW with 76 % of the energy confined in the main peak. Until now, this is the highest reported peak power of an thulium-doped amplifier system. In all measurements, no bifurcation instabilities were
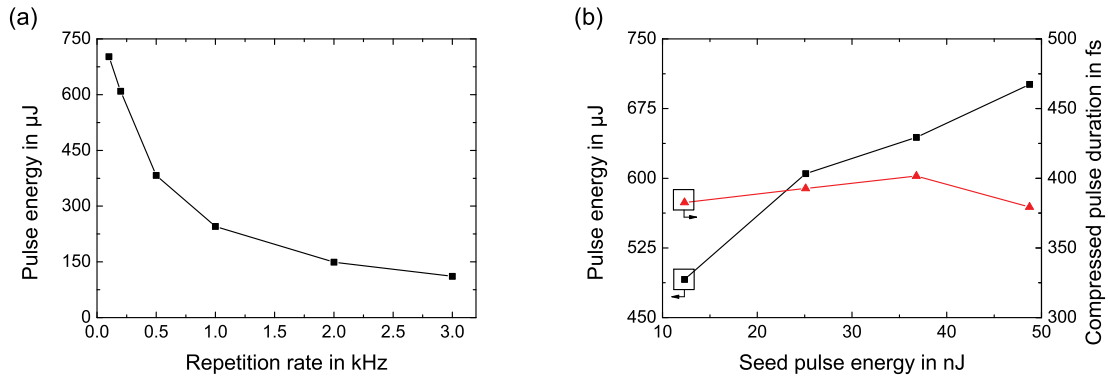
Figure 4.23: Parameter variation at 34 round trips: (a) output pulse energy vs. repetition rate at 7.5 W absorbed pump power and (b) output pulse energy and compressed pulse duration vs. seed pulse energy at 9.8 W absorbed pump power.

observed [Dör04], which could occur at repetition rates close to the inverse of the upper state lifetime.

In conclusion, an ultrafast RA system was presented, which was completely based on Tm-doped materials (fiber oscillator, fiber preamplifier, and bulk regenerative amplifier). The system delivered more than 700 µJ of output pulse energy, only limited by the damage threshold of the laser crystal. The compressed AC traces showed a ps-pedestal in the unpurged case caused by atmospheric absorption. This pedestal could be reduced by purging the cavity with nitrogen gas, whereas satellite pulses remained beside the main pulse. These satellite pulses were generated by the Pockels cell and could not be removed. Possible explanations for the origin of the satellite pulses were residual water absorption inside the porous layers of the RTP coating. Dechirping the pulses with a Martinez-type grating compressor resulted in a compressed pulse energy of 350 µJ and minimum pulse duration of 380 fs, which were calculated to a peak power of 700 MW. By variation of the round trip numbers, repetition rate, and seed energy, possible ways to increase the overall output pulse energy and efficiency were discussed. Using more appropriate gratings with higher efficiencies of more than 90 % will allow even higher output energies and peak power. This system could be used as input for a multipass amplifier with Tm:YAP to further scale the pulse energy to the multi-mJ level or as seed for an optical parametric process to gain access to the 3 µm to 10 µm wavelength range.

Regenerative amplification with holmium-doped materials

Besides thulium, holmium (Ho) is a good alternative as active material in lasers and amplifiers in the 2 µm wavelength range. Compared to thulium, its main lasing wavelength is slightly shifted towards 2.1 µm, but it offers a similar broad amplification band in fibers. Therefore, the generation and amplification of ultrashort pulses is possible. By exchanging the seed oscillator, preamplifier, and laser crystal to Holmium-doped materials, the setup is converted to operate at 2.1 µm wavelength. Furthermore, the stretching unit was adapted and proper pump lasers were developed to address the best absorption wavelength of the Ho-doped materials.

The properties of Ho in fibers and crystals are explained in the following Section 5.1 while the ultrashort pulse seed oscillator is described in Section 5.2. The stretching unit and preamplifier are depicted in Section 5.3 which amplify the seed pulses to the nJ-level. In the last Section 5.4, the regenerative amplification with Ho:YAG as active material is described.

5.1 Properties of holmium-doped fibers and crystals

Holmium is also one of the rare earth elements located in the group of the lanthanides near to Tm in the periodic table. Its spectroscopic properties are quite similar to Tm with a slightly redshifted emission band around $2.0 - 2.1$µm, depending on the host material. Subsection 5.1.1 deals with the broadband emission in HDFs while doping in crystals shows different emission characteristics, which is described in Subsection 5.1.2.

5.1.1 Silica fibers as host materials for holmium

The most commonly used absorption band of HDFs corresponds to the $^5I_8 \rightarrow {}^5I_7$ transition that is depicted in the schematic energy levels in Fig. 5.1 (a). It has a strong absorption in a broad wavelength band around 1950 nm [Jac06; Kur10]. This is easily addressed by high

power TDF lasers with multiple Watts of output power [Kim09]. Only core-pumping in the wavelength region of $2\,\mu m$ was useful in the past, because coatings with conventional low index polymers are highly absorptive at $1.95\,\mu m$ [Sim13], so that the fiber can easily be damaged when cladding pumped. New customized fiber geometries made it possible to pump directly into the cladding with a pump power of more than $1\,kW$ achieving more than $400\,W$ output power at $2.12\,\mu m$ [Hem13]. Although the absorption and emission band, which are depicted in Fig. 5.1 (b), of the $^5I_7 \rightarrow{}^5I_8$ transition have a strong overlap, the emission band is much broader and extends up to $2200\,nm$.
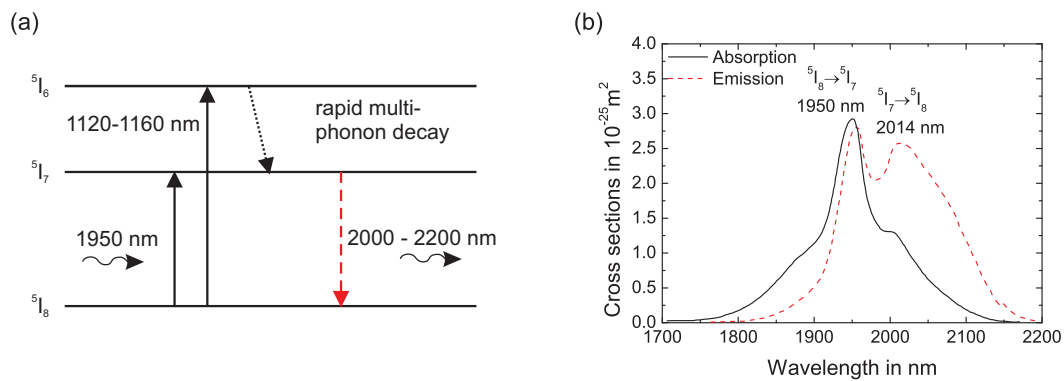
Figure 5.1: (a) Simplified energy levels of holmium-doped fibers with transitions [Jac06] and (b) corresponding absorption and emission cross sections (digitized data from [Sim13]).

Figure 5.1 (a) indicates also an excitation in the $^5I_6$ band with 1120–$1160\,nm$ sources, typically provided by high power Yb fiber lasers. With this source, a $10\,W$ all-fiber HDF laser was established, which showed a maximum slope efficiency of $30\,\%$ [Kur10]. Although noteworthy, this pumping scheme was not established. Due the remarkably low quantum defect of $7\,\%$ when pumping at $1950\,nm$, much higher pump power can be used. For this work, only core-pumping schemes are used in the ultrashort pulse oscillator and fiber preamplifier. As already mentioned in Section 4.1.1, core-pumping enables using short fiber lengths, which minimizes nonlinearities.

As shown in Fig. 5.1 (b), the broad absorption cross section of Ho in fibers reaches far into the emission band, which has two main peaks at $1955\,nm$ and $2014\,nm$ wavelength. By taking Equation (4.1) in Subsection 4.1.2 into account, the central wavelength of the effective gain cross section shifts with increasing inversion level from $2150\,nm$ towards shorter wavelengths ($2100\,nm$) by overcoming the absorption, which can be seen in Fig. 5.2 (a) for different inversion level β. Simultaneously, the FWHM of the bandwidth broadens up to more than $80\,nm$, which supports the generation of ultrashort pulses less than $100\,fs$ [Li14]. To determine the tuning behaviour of the later used HDF, a linear laser cavity

incorporating one tunable refractive grating in Littrow configuration on one side and a straight cleave with $4\,\%$ reflection as output coupling on the other side of the cavity was set up. The continuous tuning behaviour is depicted in Fig. 5.2 (b) and showed laser action between $2050\,\text{nm}$ and $2125\,\text{nm}$ with a central wavelength of $2100\,\text{nm}$.
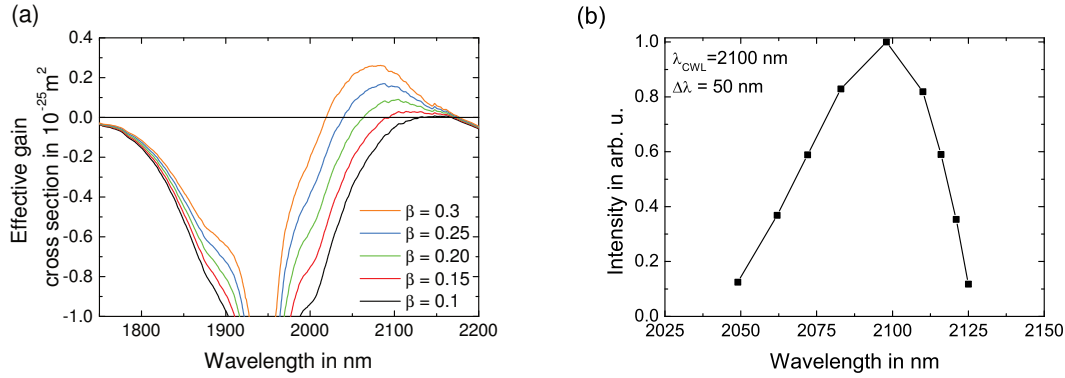
Figure 5.2: (a) Effective gain cross section at different inversion level β and (b) tuning behaviour of HDF (original data was published in [Mie14]).

5.1.2 Holmium-doped crystals

The choice of the appropriate laser crystal in the RA is comparably critical as in the case of Tm-doped crystals because the effective gain cross section has to fit to the typical lasing wavelength of the ultrashort pulse fiber oscillator around $2100\,\text{nm}$.
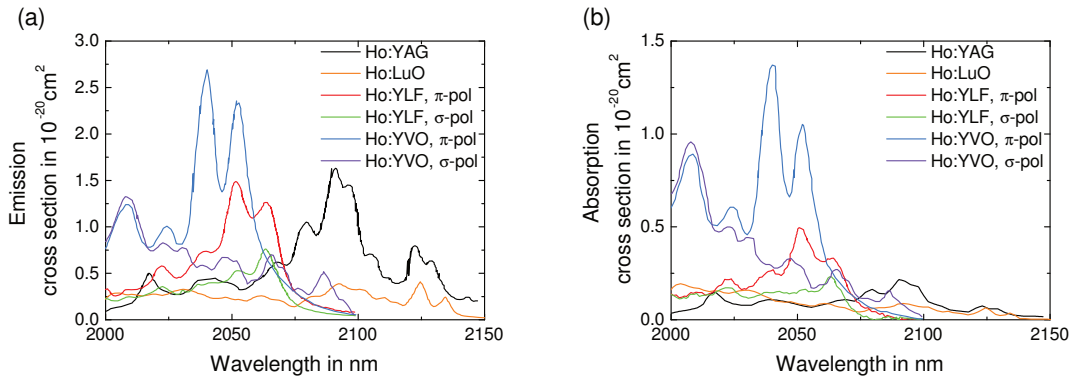
Figure 5.3: Cross sections of different materials: Ho:YAG, Ho:YLF (π and σ), Ho:YVO (π and σ) and Ho:LuO: (a) emission and (b) corresponding absorption (digitized data from [Koo12; Kwi09; Li11; Wal98]).

Figure 5.3 (a) shows the emission cross sections of different Ho-doped materials. Besides Ho:YAG, only Ho:LuO seems to be suitable for further amplification at $2100\,\text{nm}$ wavelength. Ho:YLF and Ho:YVO$_4$ (YVO or Vanadate) have only significant emission less than $2075\,\text{nm}$

and no digitizable data were found for Ho:YAP in literature. The absorption cross sections shown in Fig. 5.3 (b) for Ho:LuO and Ho:YAG are as low as $0.07 \times 10^{-20}\,\mathrm{cm}^2$ and $0.15 \times 10^{-20}\,\mathrm{cm}^2$ respectively, but Ho:YAG is favorable as amplifier material because of its highest emission cross section of $1.63 \times 10^{-20}\,\mathrm{cm}^2$.
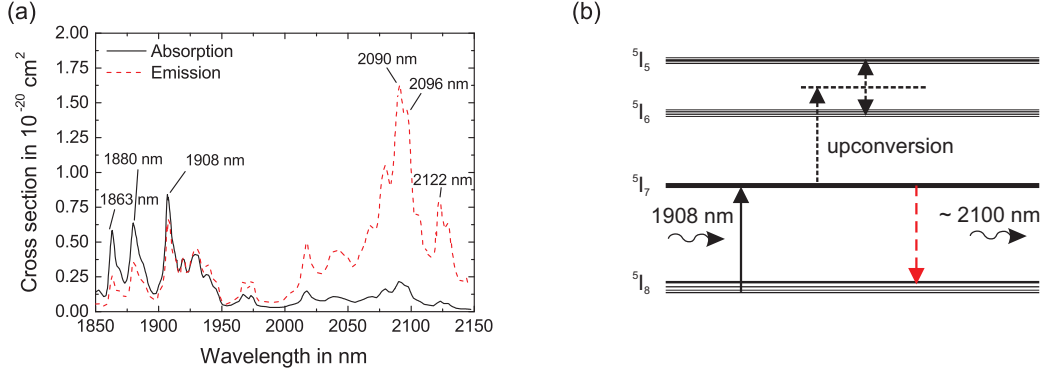
Figure 5.4: (a) Spectral cross sections of Ho:YAG (digitized data from [Kwi09]) and (b) simplified energy level with transitions of Ho:YAG ($^5I_7$ level: absorption in black, emission in red [Sch10]).

The most commonly used wavelength to pump intraband into the Ho:YAG $^5I_7$ level is 1908 nm, which can be addressed by high power Tm-fiber lasers (s. Fig. 5.4 (a)). The absorption cross section at this wavelength is $0.8 \times 10^{-20}\,\mathrm{cm}^2$, which is comparable to the one of Tm:YAP at 793 nm. The available doping concentrations were lower, in the range between 0.5 at. % and 1.6 at. %, than for the 4 at. % Tm:YAP crystal. Therefore, longer crystals of 10 mm had to be used to achieve a comparable pump absorption of up to 94 %. The corresponding emission band ranges from 2000 nm to 2150 nm but is highly structured with multiple peaks, which can be seen in Fig. 5.4 (a). In contrast to YAP, YAG is not intrinsically birefringent. But as the quantum defect is less than 10 % in Ho:YAG, thermal effects will have a lower influence and high power pumping schemes can be used as shown by MALEVICH et al. [Mal13], who used a 70 W commercial TDF laser for pumping Ho:YAG. However, Figure 5.4 (b) shows a non resonant upconversion process into the $^5I_5$ or $^5I_6$ manifold. Two closely located Ho ions are needed for this process, which are both excited to the $^5I_7$ level. This parasitic process has to be taken into account when high doping concentrations or a high population density of the $^5I_7$ level are present [Sch10]. Therefore, this is mostly important for q-switch or regenerative operation when a large amount of energy stored in the upper laser level is required.

Figure 5.5 (a) shows the fluorescence spectrum of a 0.5 at % doped Ho:YAG crystal. The spectrum looks very similar to the emission cross section depicted in Fig. 5.4 (a). This

is different from the fluorescence spectrum of Tm:YAP which differed strongly from the emission cross section spectra. The fluorescence lifetime was measured 10.6 ms as depicted in Fig. 5.5 (b) by the same method as explained in Section 4.1.2. This value is 1.7 times higher than the one of Tm:YAP, therefore much more energy can be stored inside the laser material. Compared with measured literature values of 7.8 ms, the value of 10.6 ms is slightly higher but fits to the calculated radiative lifetime of 9.8 ms [Pay92].
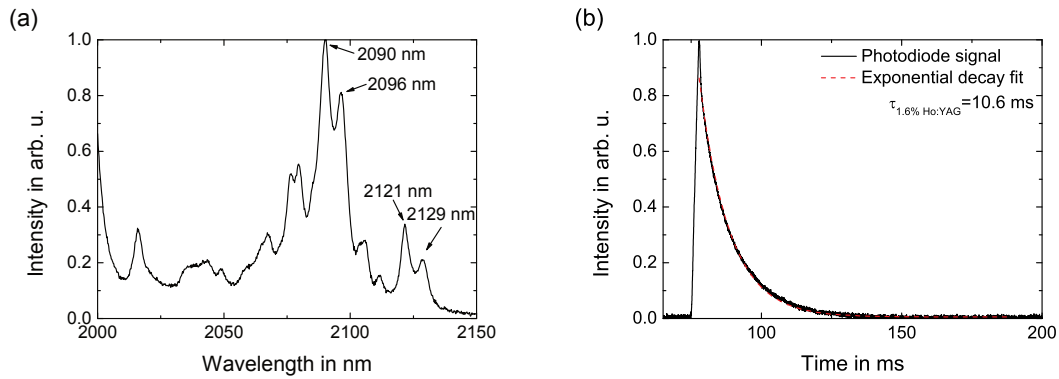
Figure 5.5: (a) Fluorescence spectrum and (b) lifetime measurement of Ho:YAG.

The singlepass gain of Ho:YAG was measured in the same way as in the case of Tm:YAP. Similar seed energies (20.8 nJ before the crystal) revealed a maximum singlepass gain of 1.82, which is nearly 1.5 times higher than the one for Tm:YAP. Furthermore, this was attained at only half the absorbed pump power compared to Tm:YAP. Due to the high singlepass gain and the low saturation fluence, Ho:YAG is a possible candidate for a high power multipass amplification scheme which could follow a regenerative amplifier to enable even higher pulse energies.
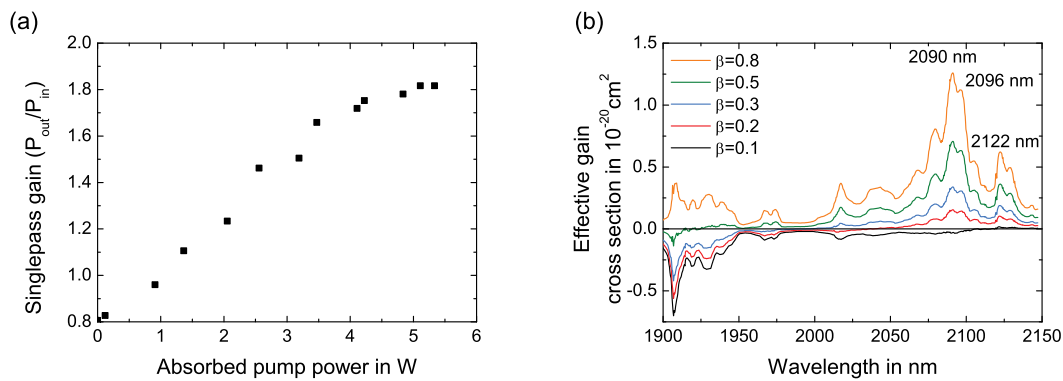
Figure 5.6: (a) Singlepass gain measurement and (b) calculated effective gain cross section of Ho:YAG.

The calculated effective gain cross section of Ho:YAG at different inversion levels β is depicted in Figure 4.5 (b). Due to the high emission and low absorption cross section of Ho:YAG, the effective gain rises above zero already at a low inversion level of $\beta = 0.2$. The main peak at 2090 nm rises stronger with increasing inversion level than the second peak at 2096 nm.

Table 5.1 summarizes the main physical properties of the mentioned Ho-doped crystals. Although Ho:YAG does not benefit from an intrinsic birefringence to overcome any thermally induced stress as Ho:YLF or Ho:YVO, it offers a high thermal conductivity, which is up to twice as large than YLF or YVO so a good heat dissipation is achieved. The saturation fluence of 5.1 J/cm^2 of Ho:YAG is much lower compared to Ho:LuO and Tm:YAP, so less round trips are needed to extract most of the energy.

Table 5.1: Physical properties of the different Ho-doped crystals (no literature data at 2.1 µm for c-cut YVO were found) [Koo12; Li11; Loi13; Pas15; Pay92; Ryb03; Wal98].

Physical properties	Lu$_2$O$_3$	Y$_3$Al$_5$O$_{12}$	YLiF$_4$	YVO$_4$
acronym	LuO	YAG	YLF	YVO
lattice	cubic	cubic	tetragonal	tetragonal
lattice constant [Å]	10.39	12.0	5.16 ∥ a	7.12 ∥ a,b
			10.85 ∥ c	6.29 ∥ c
density [g/cm^3]	9.42	4.56	3.99	4.22
refractive index at 2.1 µm	1.9	1.8	1.44 ∥ a	1.93 ∥ a,b
			1.46 ∥ c	− ∥ c
transparency range [µm]	0.23 - 8.0	0.21 - 5.2	0.12 - 8.0	0.4 - 5.0
thermal conductivity [W/(m K)]	12.8	8.8 - 12.9	5.3 ∥ a	5.10 ∥ a,b
			7.2 ∥ c	5.23 ∥ c
fluorescence lifetime [ms]	10.0	10.6	14.0	4.1
main lasing wavelength λ_{main} [nm]	2124	2090	2050 ∥ π	2040 ∥ π
			2063 ∥ σ	2007 ∥ σ
absorption cross section [10^{-20} cm^2]	1.24 at 1928 nm	0.84 at 1908 nm	0.99 ∥ π at 1940 nm	0.9 ∥ π at 1914 nm
			0.57 ∥ σ at 1945 nm	0.93 ∥ σ at 1955 nm
absorption cross section at λ_{main} [10^{-20} cm^2]	0.06	0.22	0.49 ∥ π	1.37 ∥ π
			0.23 ∥ σ	0.96 ∥ σ
emission cross section at λ_{main} [10^{-20} cm^2]	0.4	1.63	1.49 ∥ π	2.67 ∥ π
			0.76 ∥ σ	1.32 ∥ σ
saturation fluence [J/cm^2]	20.3	5.1	4.9 ∥ π	2.4 ∥ π
			9.7 ∥ σ	4.3 ∥ σ

5.2 Ultrashort pulse oscillator

Until now, only few mode-locked HDF oscillators generating femtosecond pulses were reported. A linear Ho-fiber soliton oscillator mode-locked by a SESAM was demonstrated by CHAMOROVSKIY et al. [Cha12] generating 890 fs pulses at 2085 nm wavelength. In 2014, a stretched-pulse HDF oscillator, mode-locked by NPR was realized [Li14]. In this laser, the dispersion management was accomplished by a normal dispersion fiber to achieve 160 fs pulse duration and a pulse energy of 1 nJ at 2060 nm. A subsequent nonlinear compression stage utilized by the same NDF that was already used inside the oscillator to shorten the pulses to 98 fs. Just recently, a tunable soliton oscillator was demonstrated by the same authors, which was similar to the latter mentioned but without dispersion management [Li15]. The tuning range covers wavelengths between 2040 nm and 2090 nm while maintaining pulse energies of more than 1 nJ.

(a)

(b)
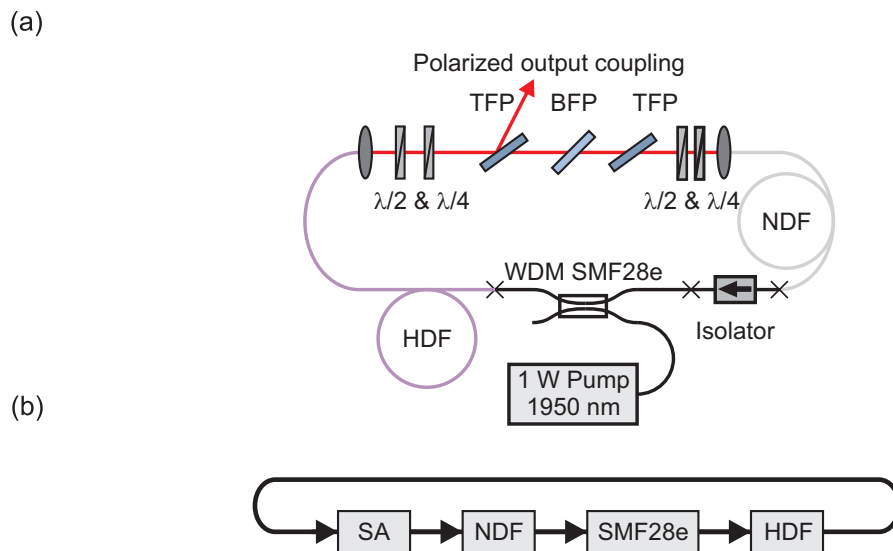
Figure 5.7: (a) Experimental oscillator setup and (b) numerical model (SA: saturable absorber).

In this work, the pulses for amplification in the Ho:YAG RA were generated by a passively mode-locked HDF-laser, which was comparable to the one described in Subsection 4.2. The experimental oscillator setup is depicted in Fig. 5.7 (a). Worth mentioning is the fact, that the here presented laser was developed simultaneously and without further knowledge to the published paper by [Li14]. The active fiber of the ring cavity was a 1.27 m double clad HDF with a core diameter of 10 μm and a NA of 0.15. It was core-pumped by a home-built 1 W 1950 nm pump laser via a WDM made of 0.35 m SMF28e. The emitted light of the

active fiber was coupled out into the free space part, which consisted of two HWP, a TFP for polarization output coupling and a spectral filter made of a BFP and a second TFP. The NDF was located at the input coupling of the free space section. It differed from the one used in Subsection 4.2 because it had a core diameter of 2.4 µm and a NA of 0.35, which resulted in a MFD of 7 µm at 2100 nm. The use of this fiber ensured lower propagation loss at 2.1 µm and lower splicing loss to SMF28e. The NDF length of 2.1 m was chosen to nearly compensate the dispersion of the SMF28e and the HDF, resulting in a calculated net cavity dispersion GDD of -0.0106 ps^2. An isolator (fiber length: 0.6 m SMF28e) was spliced between the free end of the WDM and NDF to ensure unidirectional operation.

The numerical model to simulate the oscillator is depicted in Fig. 5.7 (b) and the following parameters were included into the simulation model. The calculated dispersion parameters were $\beta_{2,NDF} = +11.3\,\mathrm{fs}^2/\mathrm{mm}$, $\beta_{2,SMF28} = +10.5\,\mathrm{fs}^2/\mathrm{mm}$ and $\beta_{2,HDF} = +11.5\,\mathrm{fs}^2/\mathrm{mm}$ at a wavelength of 2100 nm. TOD was not included into the simulations due to the prevailing GVD. The SA was modeled with the same parameters as in the case of thulium (s. Subsection 4.2): unsaturable reflectivity $R_0 = 8\,\%$, saturable reflectivity $\Delta R = 12\,\%$ and saturation power $P_{sat} = 10\,\mathrm{W}$. The loss at the SA was simultaneously used as OC. The HDF was further modeled with a gain-parameter of 3.05 per meter, a Gaussian gain profile of 100 nm FWHM around a center wavelength of 2101 nm while a gain saturation energy of 0.13 nJ was assumed.
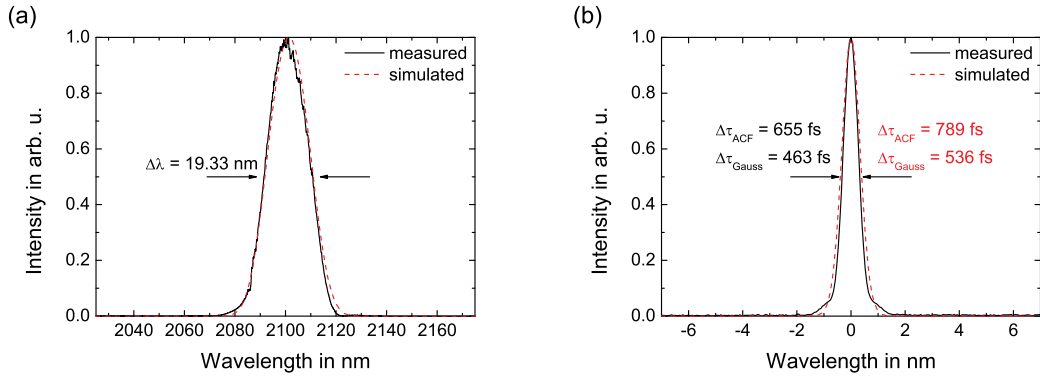
Figure 5.8: Experimental (black continuous curve) and numerical (red dashed curve) results for the HDF oscillator: (a) optical spectrum on linear scale and (b) AC trace of the uncompressed pulse.

The experimental laser operated at a central wavelength of 2100 nm with a Gaussian-shaped spectrum (s. Fig. 5.8 (a)). The FWHM of the power spectrum of the laser was 19.3 nm without any additional sidebands, which was confirmed very well by the simulations (red dashed line in Fig. 5.8 (a)). The uncompressed AC trace is shown in

Fig. 5.8 (b), which revealed a width of 655 fs. Assuming a Gaussian pulse shape, the calculated pulse duration was 463 fs. A further compression of the pulses was not carried out, as the pulses were directly used as seed for the preamplifier (s. Section 5.3), but the transform-limited pulse duration was calculated by the optical spectrum to 280 fs. The uncompressed AC of the numerical simulations were slightly longer with an AC duration of 789 fs and a corresponding pulse duration of 536 fs. Although the fiber lengths were accurately measured, the dispersion values were estimated by the MFD and NA, so that the deviation in pulse durations can be explained by this uncertainty.
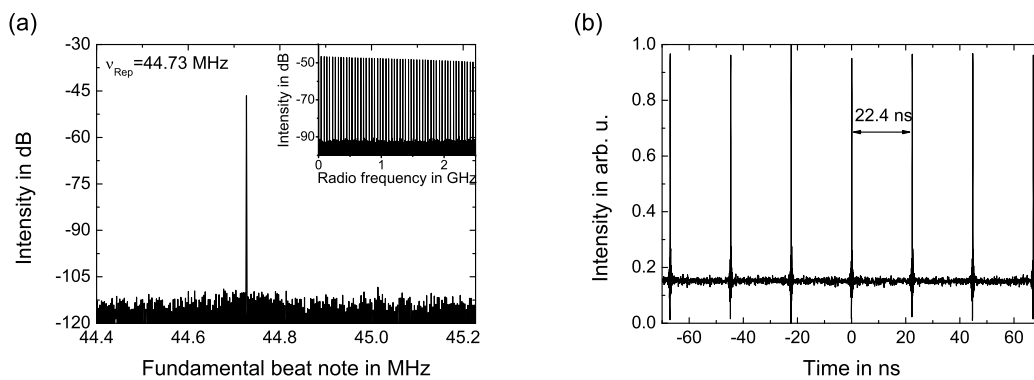
Figure 5.9: Experimental results for the HDF oscillator: (a) fundamental beat note, inset: radio frequency comb and (b) oscilloscope trace.

The fundamental beat note of 44.6 MHz in the radio frequency spectrum revealed no signs of q-switching depicted in Fig. 5.9 (a). Furthermore, the inset shows a linear decrease of the peaks in the frequency comb up to 2.5 GHz, which also confirms stable single-pulse operation. This is also verified by observation of the pulse train in the oscilloscope trace in Fig. 5.9 (b). The emitted average power of 13 mW corresponded to a pulse energy of 0.29 nJ. These pulses were seeded into the grating stretcher and the fiber preamplifier subsequently.

5.3 Fiber preamplifier

Before the pulses were amplified in the fiber preamplifier to pulse energies above 25 nJ, they were temporally stretched to 90 ps. In contrast to the fiber stretcher, which was used for the Tm-based system and described in Subsection 4.3, the losses in the PM1950 fiber were much higher at 2.1 µm wavelength than for 1.94 µm. Therefore, a Martinez-type grating stretcher was used (s. Fig. 5.10). This design had the advantage of including a focal element (focus mirror) so that the beam profile was preserved in both axis, which was important for an efficient coupling into the subsequent fiber amplifier. For the stretcher design a single gold

coated diffraction grating with 600 grooves per mm (blaze angle of 34°) and a concave silver mirror with a focal length of 200 mm were used. The input/output efficiency of the grating stretcher was 43.2 %, which was mainly limited by the low diffraction efficiency of the used grating. Subsequently, the stretched pulses were coupled into the SMF28e fiber of the WDM, which was followed by the HDF preamplifier. By using a telescope composed of a 100 mm and 30 mm lens, the input coupling efficiency into the fiber was optimized.
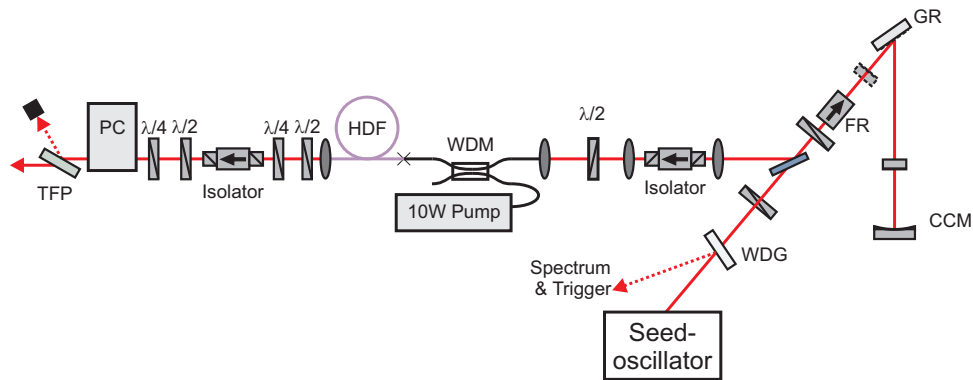
Figure 5.10: Schematic setup of the stretcher and preamplifier. PC: Pockels cell, TFP: thin film polarizer, FR: Faraday rotator, CCM: concave mirror, WDG: wedge, GR: grating, WDM: wavelength division multiplexer.

The pump laser used for the Ho-doped fiber preamplifier consisted of a Fabry-Perot laser diode with a broad emission spectrum ranging from 1900 nm to 1950 nm. The laser diode emitted a power of 5 mW, which was amplified in a single stage, double cladding pumped TDF to more than 11.5 W (s. Fig. 5.11 (a), black squares) by the use of a 35 W multi-mode laser diode operating at 793 nm. The residual pump light behind the TDF was extracted by a following pump light stripper. The losses induced by the pump stripper and the following WDM were measured 10 %, so that a maximum pump power of 10.4 W was available for the HDF preamplifier (port 1, black circles). The optical spectrum at this output power is shown on a logarithmic scale in Figure 5.11 (b) in black. Although the spectrum of the laser diode is broadband, the overlap with the absorption spectrum of HDF (red curve) is still given. The active fiber of the Ho-preamplifier was the same type that was already used for the oscillator described in Subsection 5.2 and had a length of 8.3 m. To ensure a sufficient absorption of the pump light and high amplification factors, such long fiber length was chosen as the gain spectrum shifts into the long wavelength part by reabsorption. Earlier measurements with shorter fiber lengths revealed stronger ASE and parasitic lasing in the short wavelength part (around 2050 nm), so an efficient amplification was not achieved at longer wavelengths.
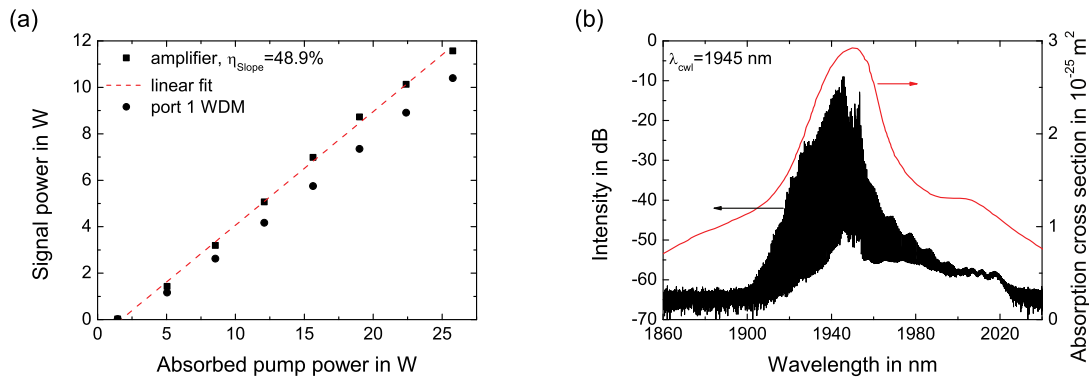
Figure 5.11: (a) Output power vs. absorbed pump power of the pump laser (black squares), linear fit (red dashed line), transmission via 1950/2100 WDM (black dots curve) and (b) optical spectrum (black curve) and absorption cross section of Ho-fiber (red curve).

The output characteristics of the Ho-doped fiber preamplifier pumped by the TDF-laser can be seen in Figure 5.12 (a): the pulses are amplified in a linear relation with a slope efficiency of 21.1 % up to a pulse energy of more than 36.8 nJ (average power of 1.64 W) at the maximum pump power of 10.4 W. The evolution of the optical spectrum is depicted in Fig. 5.12 (b), which shows a slight reduction of the FWHM from the original seed spectrum (19.3 nm) to 15.5 nm at a central wavelength of 2100 nm. The spectrum is reduced owing to gain narrowing inside the active HDF. With increasing pump power, ASE appeared in the spectrum around a wavelength of 2060 nm, but the integrated fraction is less than 5.2 % so that most of the energy is confined in the main peak. The pulses could still be compressed to a duration of 580 fs (820 fs ACF) assuming a Gaussian pulse shape with a slight pedestal, which can be attributed to uncompensated higher order dispersion (s. Fig. 5.12 (c)).

Although no PM-fiber was used for the fiber preamplifier, the linearly polarized signal was nearly preserved during amplification by adjustment of a HWP and QWP behind the HDF. Therefore, a PER of more than 19.3 dB was measured at maximum output power. After amplification, the pulses were picked with the same pulse picker used in the Tm-based system described in Subsection 4.3 and the same telescope for MFD adaption.
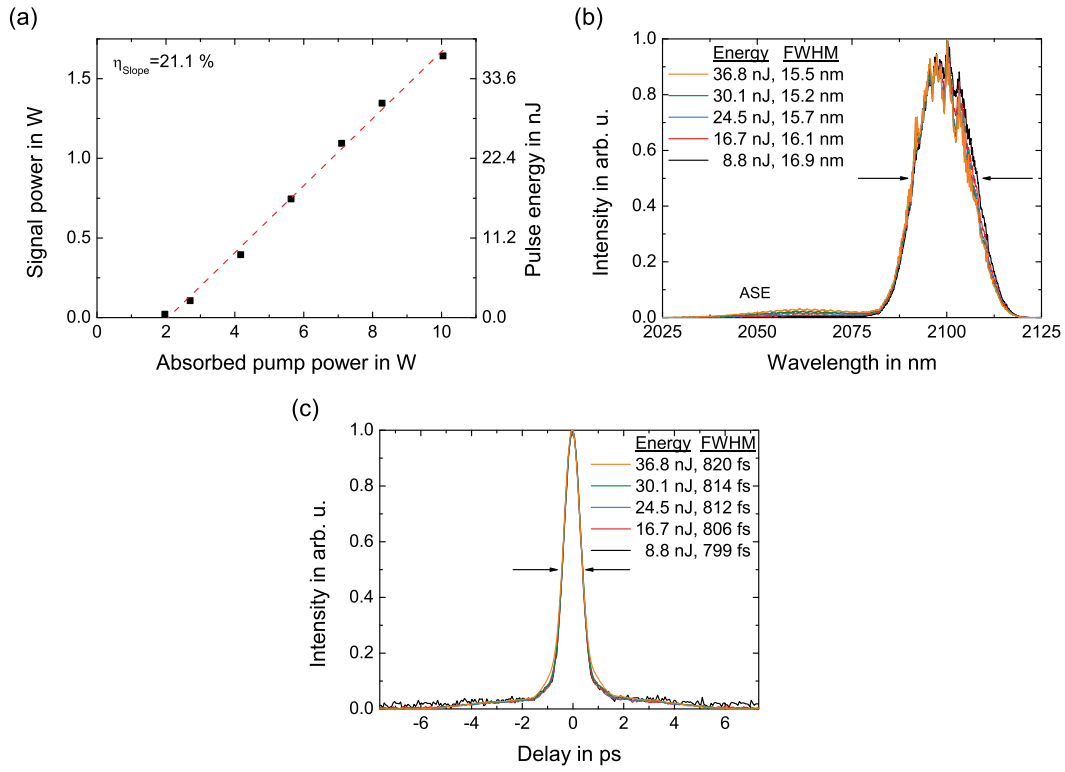
Figure 5.12: (a) Output power/pulse energy vs. absorbed pump power, (b) optical power spectrum at different pulse energies and (c) AC traces of the compressed pulse at different energies of the Ho-preamplifier.

5.4 Regenerative amplifier

The overall setup with its several stages is depicted in Fig. 5.13. The seed oscillator, stretcher unit, and preamplifier were described in the previous sections. In principle, the setup used for the regenerative amplification with Ho was quite similar to the one for the Tm-based system, but the Ho:YAG laser crystal was pumped at 1908 nm by a self-developed TDF laser. To achieve a high pump power at this wavelength, a TDF-laser was developed, which was terminated with a HR-fiber Bragg grating (FBG) on one end and with a 10 % partially reflective (PR)-FBG on the other end to generate a power of 515 mW at 1908 nm. A following single-stage TDF-amplifier amplified the isolated signal up to 13.6 W of output power (s. Fig. 5.14 (a)) with a slope efficiency of more than 50.9%. The corresponding spectrum at the maximum power is depicted in Fig. 5.14 (b). As the signal wavelength was on the low amplification band of Tm, the generation of ASE was inevitable but was suppressed to more than 53 dB so that the 1908 nm peak contains more than 99.9 % of the
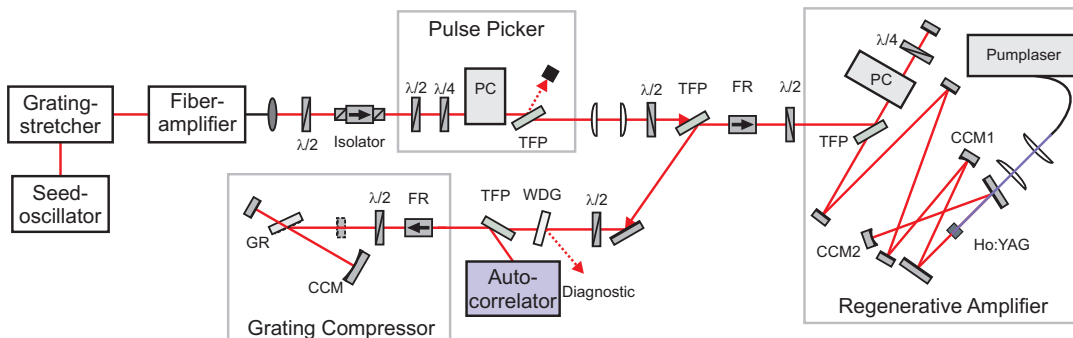
Figure 5.13: Experimental setup of the system. PC: Pockels cell, TFP: thin film polarizer, FR: Faraday rotator, CCM1: concave mirror with 600 mm ROC, CCM2: concave mirror with 300 mm ROC, WDG: wedge, GR: grating.

output power. The absorption of Ho:YAG is independent of the polarization of the pump light, therefore non-PM fibers were used for this pump laser, which resulted in random polarization of the output signal.
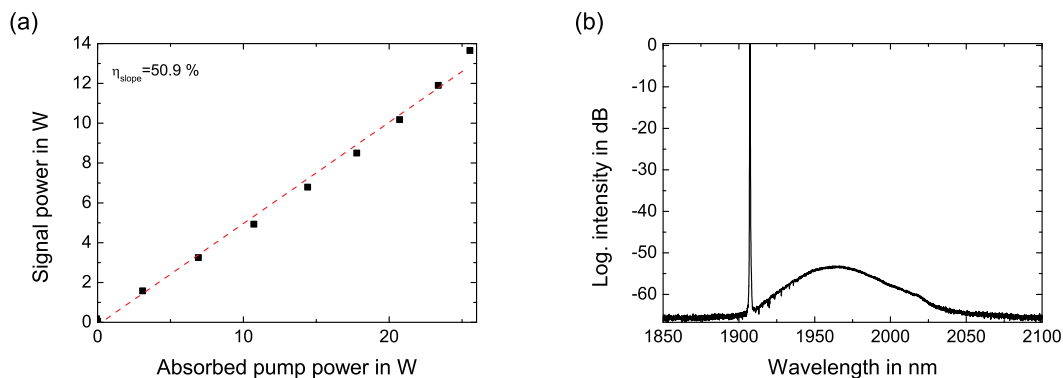
Figure 5.14: Pump laser for Ho:YAG: (a) signal power vs. absorbed pump power and (b) optical power spectrum.

5.4.1 Cavity design considerations

The pump light was delivered directly out of the single-mode TDF of the aforementioned Tm-pump laser, which is in contrast to the multi-mode fiber output of the laser diode used to pump Tm:YAP. Therefore, the pump coupling into the laser crystal had to be adapted by collimating the beam with a 8 mm focal length aspheric lens and focusing with a lens with 250 mm focal length. The generated spot had a calculated size of 320 µm in the laser crystal, which was in perfect overlap with the targeted resonator mode diameter to achieve highest efficiency in the later amplification process.

Due to the low quantum defect of less than 10% between pump and signal wavelength, a negligible thermal lens in the $10\,\text{mm}$ long Ho:YAG crystal was expected. This was determined in a similar experiment with which the thermal lens of the Tm:YAP crystal was measured. A simple $80\,\text{mm}$ plane-plane cavity was set up with the HR mirror located as close to the laser crystal as possible, which is depicted in Fig. 5.15 (a). Although the pump size is 1.5 times smaller than in the case of Tm:YAP, no influence on the stability by a thermal lens was measured as shown in Figure 5.15 (b) because the output power of the CW resonator increased nearly linear.
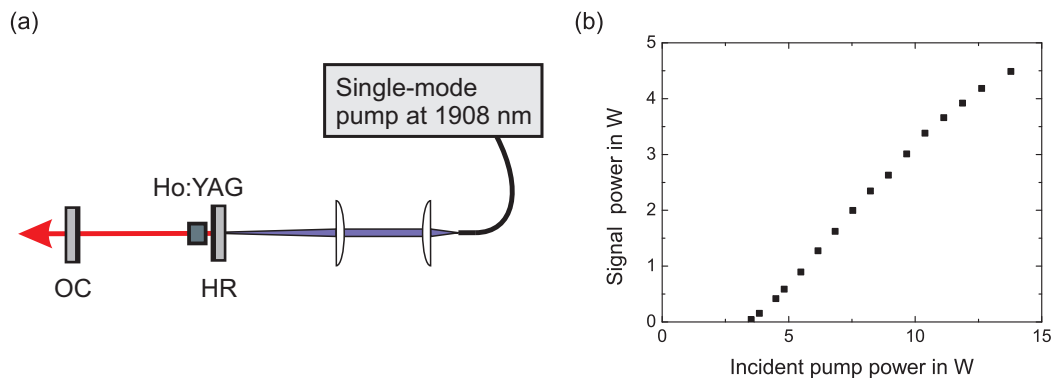
Figure 5.15: Pump laser for Ho:YAG: (a) signal power vs. absorbed pump power and (b) optical power spectrum.

The cavity design used for the regenerative amplification with Ho:YAG was only slightly altered compared to the previous Chapter 4 (s. Fig. 4.13). It was changed owing to the longer crystal ($10\,\text{mm}$) and negligible thermal lens. To achieve the same MFDs inside the cavity, the distance of the curved mirrors CCM1 and CCM2 to the laser crystal had to be adapted (CCM1: $330\,\text{mm}$ and CCM2: $297\,\text{mm}$ apart from the crystal). The evolution of the resonator mode, which was already depicted in Fig. 4.13 (b), was basically the same. This cavity design was used for all following experiments.

5.4.2 Continuous wave experiments and tunability

To determine the most suitable Ho:YAG crystal for lasing and amplification, four doping concentrations were tested ranging from $0.5\,\text{at.}\%$ to $1.6\,\text{at.}\%$ at a crystal length of $10\,\text{mm}$ (s. Fig. 5.16 (a) – (d)). In contrast to the measurements with Tm:YAP in Subsection 4.4.2, the CW laser experiments with Ho:YAG were performed with the final cavity setup described in Subsection 5.4.1, but missing out the optical switch. All doping concentrations could achieve a maximum power (red dots) of more than $4.0\,\text{W}$ with typically low output couplings (3.2% and 6%). Furthermore, slope efficiencies of more than 66% were achieved for all crystals with higher output couplings (11% to 19%). The highest slope efficiency of 83.6%

was achieved with the 0.5 at. % doped Ho:YAG crystal and 11 % output coupling (a). This laser operated at 2090 nm wavelength with a second peak at 2096 nm, which was 10 dB below the main peak. In contrast, the highest output power was achieved with the highest doping concentration of 1.6 at. % and an output coupling of 11 % (d). In fact, this laser operated at a wavelength of 2121 nm with a slope efficiency of 66 %. The crystal with 1.6 at. % doping was used for all further experiments due to the highest output power and strongest absorption.
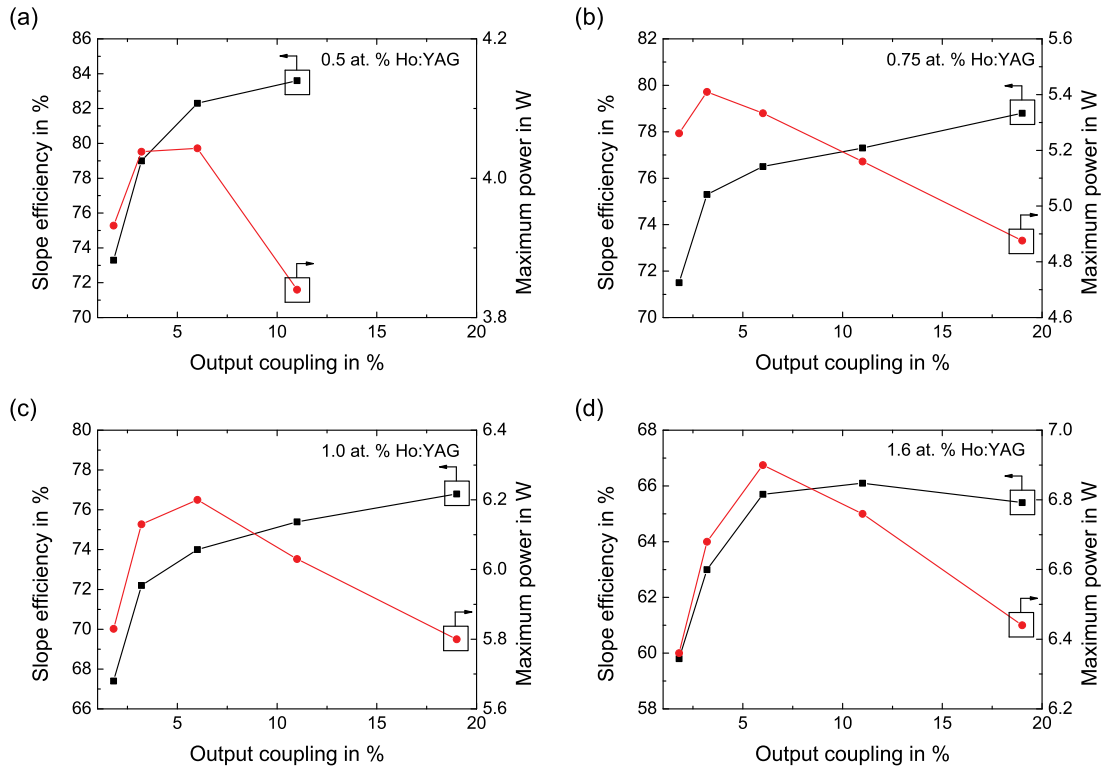
Figure 5.16: Comparison of different doping concentrations of Ho:YAG in terms of slope efficiency and maximum achieved output power vs. output coupling: (a) 0.5 at. % – (d) 1.6 at. %.

The spectral tunability was tested with the same birefringent filter, which was already used for Tm:YAP in Subsection 4.4.2. All tested configurations had in common, that the laser could not be tuned continuously but showed switching between single or multiple operating wavelength lines between 2129 nm, 2121 nm, 2096 nm, and 2090 nm, which corresponded to the peaks in the fluorescence spectrum in Fig. 5.5 (a). In general, these operating lines shifted from high wavelengths at high doping and/or low output coupling to lower wavelengths for low doping and/or high output coupling.

5.4.3 Q-switch experiments

As in the case of the Tm-based system, q-switch experiments were performed after insertion of the optical switch consisting of the PC, TFP and QWP to explore the possible pulse energies, which can be achieved in the regenerative amplification process. These experiments were carried out with the final cavity setup using the 11 % output coupler and the 1.6 at. % doped crystal as this combination has revealed the maximum CW output power (s. Subsection 5.4.2). Figure 5.17 (a) shows the output power at different repetition rates (1 kHz, 500 Hz and 100 Hz). In comparison to Tm:YAP, Ho:YAG showed higher output power in q-switch operation before saturation starts. For 1 kHz an output power of more than 1 W and a slope efficiency of 29.5 % was reached, while 594 mW could be achieved at 500 Hz with an efficiency of 21.5 %. Only the maximum output power at 100 Hz of 162 mW is comparable to Tm:YAP, because it was also limited to avoid a damage of the laser crystal at these pulse energies (1.62 mJ). Furthermore, a maximum pulse energy of more than 1 mJ could be found for every repetition rate (s. Fig. 5.17 (b)) with 1.6 mJ maximum pulse energy at 100 Hz. This is different to Tm:YAP, which showed the onset of saturation much earlier at repetition rates of more than 100 Hz.
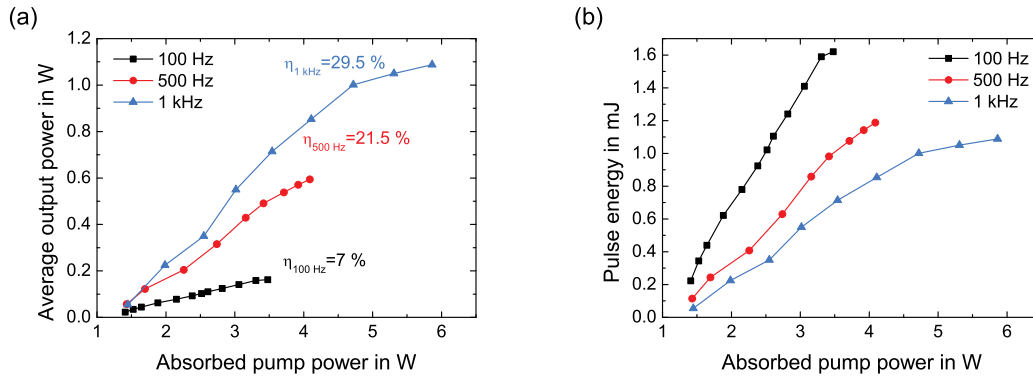
Figure 5.17: Q-switch output characteristics of Ho:YAG at different repetition rates: (a) average power and (b) pulse energy.

Contrary to the q-switched operation with Tm:YAP, Ho:YAG reached build up times (measured at 10 % in respect to the trigger signal) of less than 1 μs owing to the high gain and efficient amplification (s. Fig. 5.18 (a)). At nearly half the needed absorbed pump power in comparison to Tm:YAP, minimum build up times of 387 ns (100 Hz) to 652 ns (1 kHz) were attained at an absorbed pump power of 3.47 W (5.86 W at 1 kHz, respectively). The pulse duration decreased for all repetition rates and was lowest with 117 ns at a maximum pulse energy of 1.6 mJ at 100 Hz repetition rate (s. Fig. 5.18 (b)). This duration was 4.1 times lower than the minimum pulse duration achieved with Tm:YAP. In direct

comparison, both diagrams (a) and (b) have the same course with increasing pump powers including saturation points.
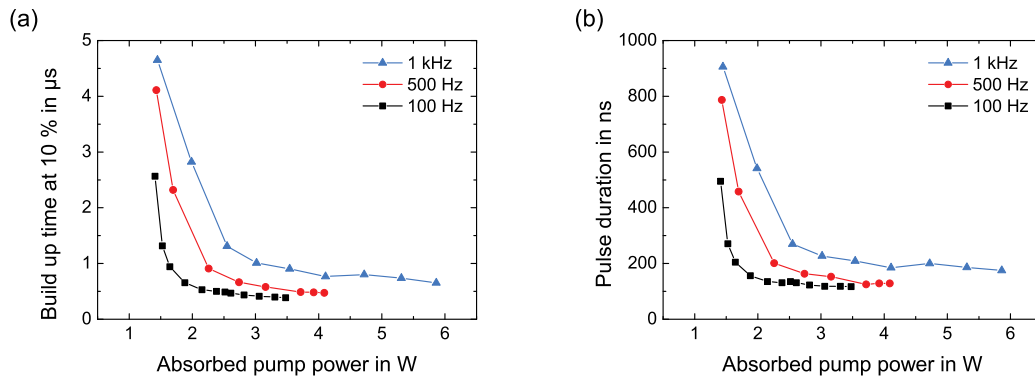
Figure 5.18: (a) Build up time and (b) pulse duration of the q-switched pulses at different repetition rates.

Figure 5.19 (a) depicts the evolution of the pulses at increasing pump power measured at a repetition rate of $1\,\mathrm{kHz}$. The pulses became more asymmetric with a strong rising edge because of its dependence on the increasing small signal gain whereas the trailing edge only depends on the cavity photon decay time. The optical spectrum (s. Fig. 5.19 (b)) of the pulses with maximum pulse energy at $1\,\mathrm{kHz}$ shows one main peak at $2089.5\,\mathrm{nm}$ with a second peak at $2095.5\,\mathrm{nm}$, which was $11\,\mathrm{dB}$ below the main peak.
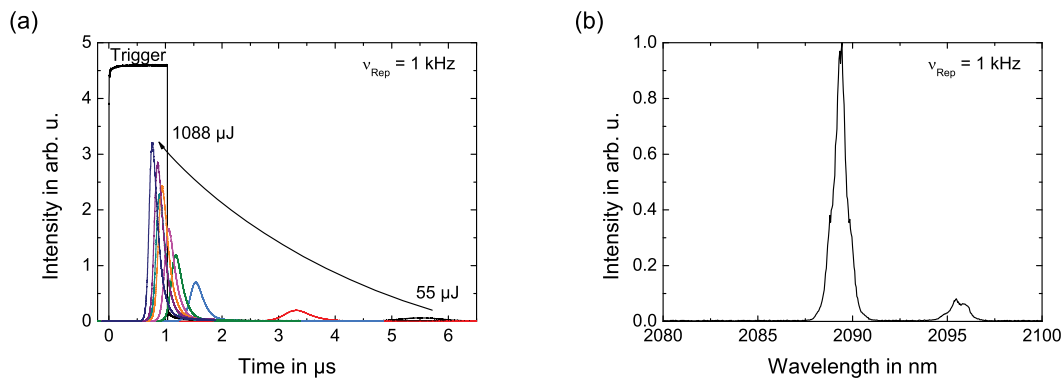
Figure 5.19: (a) Evolution of the pulses at increasing pump power at $1\,\mathrm{kHz}$ and (b) optical spectrum at $1\,\mathrm{kHz}$ and maximum output power of $1.6\,\mathrm{mJ}$.

5.4.4 Regenerative amplification with Ho:YAG

Parts of this chapter were already published in [Wie15b]. The uncompressed pulses of the preamplifier seeded the regenerative amplifier with a pulse energy of $24.4\,\mathrm{nJ}$. After ten

round trips and at 4.5 W of absorbed pump power, a maximum pulse energy of 714 µJ at 1 kHz was reached (s. Fig. 5.20 (a), blue dots). This energy was again limited by the damage threshold of the crystal, which was found at a comparable power density as in the case of Tm:YAP. The pulses were amplified with an efficiency of 31.2 %.
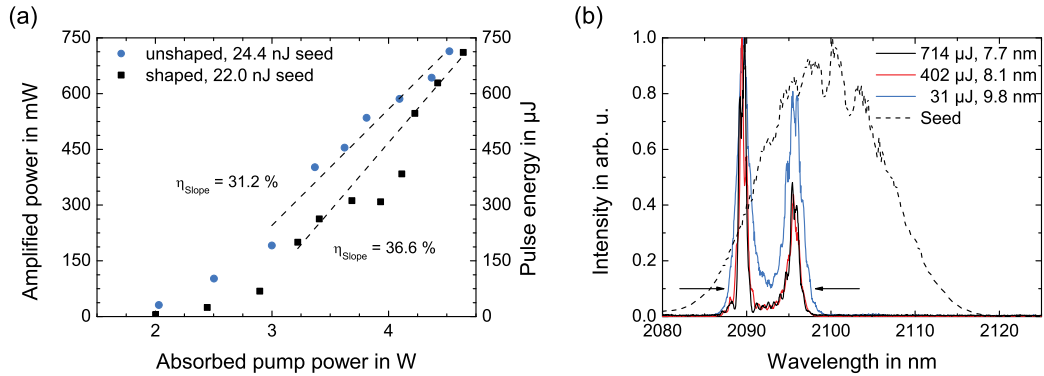
Figure 5.20: (a) Uncompressed amplified power / pulse energy vs absorbed pump power and (b) evolution of the optical spectrum with increasing pulse energy.

The optical spectrum is depicted in Fig. 5.20 (b) for three different pulse energies, which were attained at distinct pump powers. The spectrum showed a strong deformation of the Gaussian-shaped seed spectrum. Mainly visible in the spectrum were the well-known emission peaks of Ho:YAG at 2090 nm and 2096 nm, which already appeared in the fluorescence spectrum and q-switched spectrum. In here, gain narrowing was visible for both peaks separately, which effectively reduced the overall width at -10 dB level of the optical spectrum from 9.8 nm to 7.7 nm.
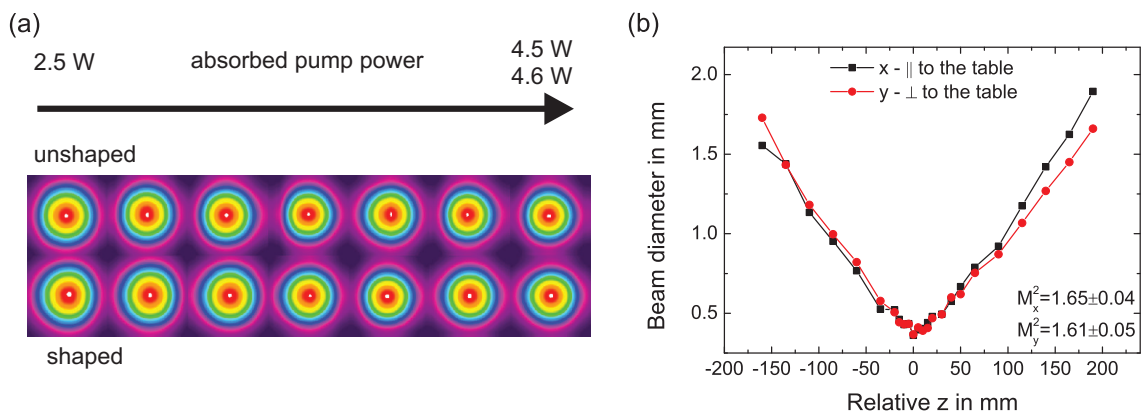
Figure 5.21: (a) Beam profile at different pump power levels from 2.5 W to 4.5 W in the unshaped case and 4.6 W in the shaped, (b) M^2-measurement at highest output power of 714.

The laser cavity had to be readjusted for every pump power step in case of Ho:YAG to find the maximum output power. This was not induced by a transversal mode hopping but by a slight misalignment of the crystal's angle to the incoming pump light to avoid back reflections into the non-isolated pump laser. The output beam profile is depicted in Fig. 5.21 (a), which was perfectly circular and did not change during the increase of the pump power as expected due to the low thermal lensing. Furthermore, the beam propagation parameter M^2 is comparably good as in the case of Tm:YAP with a value of 1.65 ± 0.04 parallel and 1.61 ± 0.05 perpendicular to the table (s. Fig. 5.21 (b)) at an output energy of $714\,\mu J$.
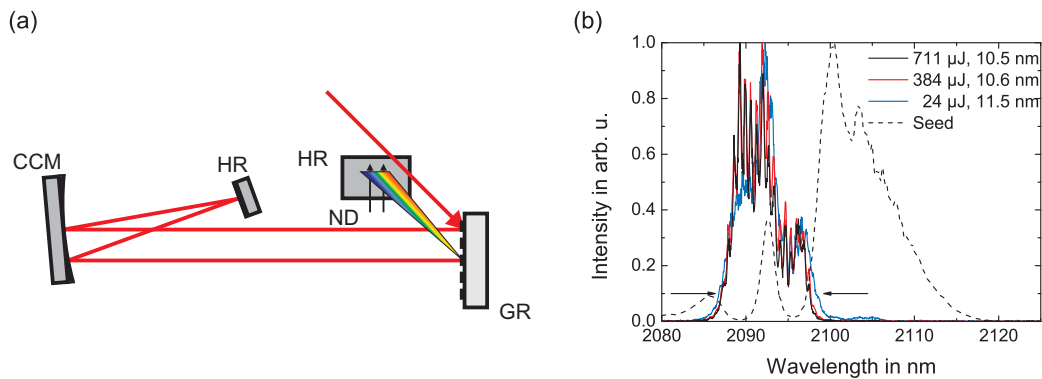
Figure 5.22: (a) Side view of the setup with spectral shaping in the grating stretcher (GR: Grating, HR: mirror, CCM: concave mirror, ND: Needles for hard cut), (b) shaped optical spectrum after regenerative amplification.

Owing to the strong gain shaping, a mechanical shaper was included into the grating stretcher shown in Fig. 5.22 (a) to suppress the two main emission wavelengths at $2090\,nm$ and $2096\,nm$ with two pins. The shaped seed spectrum is depicted as black dashed line in Figure 5.22 (b), which showed the two incisions. Due to this spectral precompensation, the amplified spectrum in the RA was different than in the unshaped case with emission bands between the two main wavelengths at $2090\,nm$ and $2096\,nm$. Additionally, it broadens up to a width of $10.5\,nm$ at $-10\,dB$ level at an output energy of $711\,\mu J$. Anyway, the spectrum is still highly structured, because the seed shaping method with two pins is rather coarse. A better solution for this might be a spatial light modulator with which amplitude and phase of the pulse can be modified [Wei00].

The seed energy of the RA was reduced from $24.4\,nJ$ to $22.0\,nJ$ by inserting the mechanical shaper, therefore slightly more absorbed pump power was required to reach the maximum pulse energy of $711\,\mu J$ at an absorbed pump power of $4.6\,W$ (s. Fig. 5.20 (a), black squares). The slope efficiency in the shaped case was measured to $36.6\,\%$ without taking into account

the two datapoints at 3.93 W and 4.11 W of absorbed pump power, which were assumed to be outliers due to the readjustment of the cavity at every pump power step. However, the calculated B-Integral for this measurement was only 2.51 whereas the parameters of the optical elements in Table 5.2 were used. Although the laser crystal was 2.5 times longer than in the case of Tm:YAP, the lower B-Integral can be explained by the 3.4 times lower number of round trips (B-Integral of 7.01 in the Tm:YAP case). The small mode radius and high nonlinear refractive index of Ho:YAG were the main attributing factors to the B-Integral.

Table 5.2: Parameters of the optical elements in the holmium-doped regenerative amplifier for calculating the B-Integral. *The nonlinear refractive index of KTP was used instead of RTP [Ada89].

Parameter	Ho : YAG	TFP	QWP	RTP
Length [mm]	10	7.62	1	20
Nonlinear refractive index n_2 [$\times 10^{-20}$ m^2/W]	12.7	4.91	6.12	27.6*
Mode radius [µm]	160	910	890	895
Mode area (Gaussian) [mm^2]	0.04	1.3	1.26	1.24
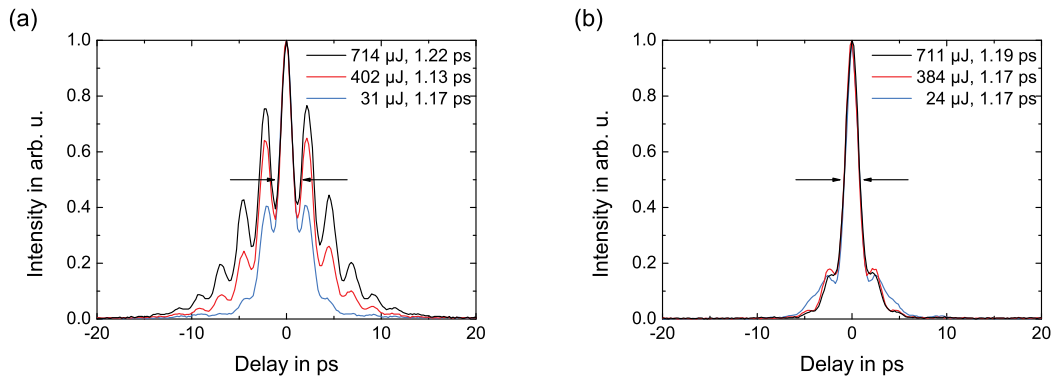
Figure 5.23: Autocorrelation traces of the compressed pulse at different pulse energies in the unshaped case (a) and in the shaped case (b).

The advantage of the spectral shaping is clearly visible in the AC traces in Fig. 5.23. The multi-pulse like structure (a) disappeared in the shaped case and a single pulse appeared in the AC trace (b) with a slight pedestal below the main pulse. The duration of the compressed pulses at a maximum energy of 711 µJ was 1.19 ps, which was constant over amplification. This pulse duration was nearly a factor of 3 higher than for Tm:YAP. Obviously, the narrow gain spectrum of Ho:YAG was responsible for the longer compressed pulse duration of Ho:YAG despite spectral precompensation. However, no atmospheric absorption lines are

present at 2.1 μm, therefore purging was not necessary. Worth mentionable is the fact, that no visible satellite pulse occurred at this wavelength although the same Pockels cell was used as in the case of Tm:YAP (s. Subsection 4.4.4). This fact supports the explanation of adsorbed water in the coating of the RTP crystal as a cause for satellite pulses, as no discrete absorption lines of water are present at 2.1 μm wavelength. Therefore, no strong phase distortions occurred, which could generate post-pulses [Geb15b; Sei88].

The oscilloscope trace of the pulse during regenerative amplification at 10 round trips is shown in Fig. 5.24 (a). Due to the slightly differed cavity design mentioned before, the round trip time is now 14.5 ns corresponding to a cavity length shortened by 45 mm in comparison to the case of thulium. Only one pulse propagated inside the RA and was amplified. Figure 5.24 (b) shows the single-pulse output of the RA revealing no evidence of pre- or post pulses.
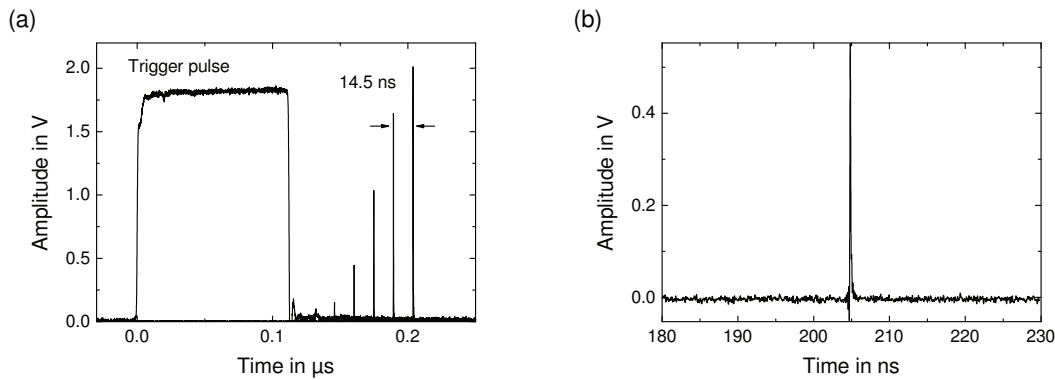
Figure 5.24: Oscilloscope trace of the RA pulses (a) during amplification at 10 round trips and (b) temporal signal of the output pulse behind the RA.

Although the spectral precompensation has worked out for regenerative amplification with Ho:YAG to clean the AC trace, the following measurements were carried out without spectral precompensation as it had no influence on the maximum achievable pulse energy. To verify the dynamics of the RA operating in the linear regime, the cavity round trips were varied between 6 and 16 round trips (s. Fig. 5.25 (a)). At a pump intensity of $83.1\,\mathrm{MW/m^2}$, which corresponds to an absorbed pump power of 3.34 W, the RA output energy increased linearly up to 14 round trips and saturated after 15 round trips with a maximum single-pulse energy of 492 μJ (black curve). A further increase of round trips led to bifurcation instabilities, which were suppressed by applying a higher pump intensity of $98.2\,\mathrm{MW/m^2}$ (3.95 W of absorbed pump power, red curve). This also resulted in a higher pulse energy of 686 μJ after 14 round trips. When more round trips were applied, bifurcation instabilities did not occur, but the pulse energy saturated.

(a)

(b)
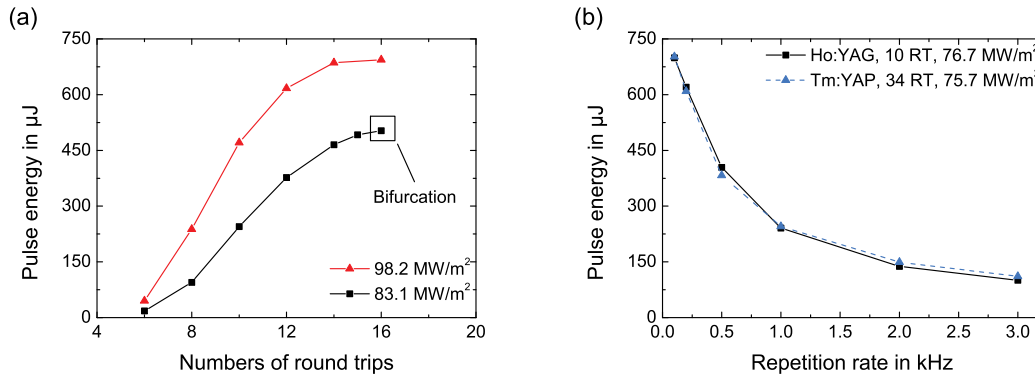
Figure 5.25: (a) Pulse energy vs. different round trip numbers, (b) pulse energy vs. repetition rate (RT: round trips).

Figure 5.25 (b) shows the variation of repetition rate at a pump intensity of $76.7\,\mathrm{MW/m^2}$ (black squares), which corresponded to $3.08\,\mathrm{W}$ absorbed pump power. When a repetition rate of $100\,\mathrm{Hz}$ was applied to the RA, the maximum achievable pulse energy of $699\,\mathrm{\mu J}$ was reached. Reducing it to a repetition rate of $3\,\mathrm{kHz}$ resulted in a pulse energy of $100\,\mathrm{\mu J}$. As already pointed out in Subsection 4.4.4, a regenerative amplifier can be operated with a constant maximum pulse energy up to the inverse of the upper state laser level. With the upper state lifetime of $10.6\,\mathrm{ms}$, this corresponds to a value of $94\,\mathrm{Hz}$. The following decrease in pulse energy was clearly visible. In direct comparison to the Tm:YAP system (blue dots), which was operated at nearly the same pump intensity of $75.7\,\mathrm{MW/m^2}$, both systems performed identically, although the number of round trips to achieve similar pulse energies was different.

The variation of the seed energy was performed with a slightly different oscillator operating at $2090\,\mathrm{nm}$ with a Gaussian-like spectral shape and a FWHM of $17.3\,\mathrm{nm}$. The results of regenerative amplification after ten round trips and at $1\,\mathrm{kHz}$ repetition rate are depicted in Fig. 5.26 (a). The output pulse energy (black curve) increased nearly linear from $526\,\mathrm{\mu J}$ at a seed energy of $7.1\,\mathrm{nJ}$ to a maximum pulse energy of $705\,\mathrm{\mu J}$ at a seed energy of $31.2\,\mathrm{nJ}$. The duration of the compressed pulses (red curve) varied between $1.20\,\mathrm{ps}$ and $1.12\,\mathrm{ps}$ for the different seed pulse energies and was shortest at $20.6\,\mathrm{nJ}$ pulse energy. Due to the different seed oscillator with distinct spectral precompensation, the AC traces of the compressed pulses shown in Fig. 5.26 (b) differed in shape from the ones presented in Fig. 5.23 (b). Although showing similar compressed pulse durations, higher sidelobes were visible in the AC trace, which were not suppressed by stronger filtering. One explanation for this behaviour could be a different spectral phase occurring inside the grating stretcher

and fiber preamplifier due to the changed seed oscillator: as the oscillator used before was operated at a wavelength of 2100 nm, the spectral shaping occurred mostly in the wings of the pulse to suppress the highest peak at 2090 nm. The oscillator operating at 2090 nm was shaped in the center of its emission spectrum. Therefore, the following fiber preamplifier induced a stronger phase change on the stretched pulses, which could not be compensated by the grating compressor. A spatial light modulator inside the stretcher could help to further suppress the sidelobes.
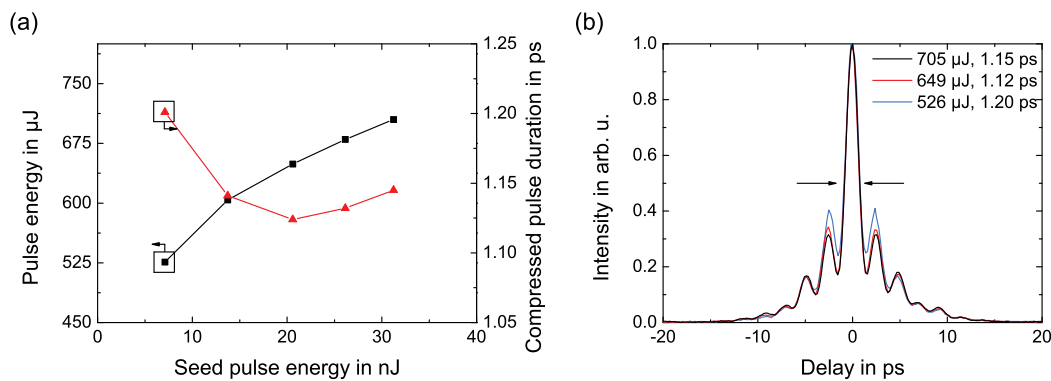
Figure 5.26: Ho:YAG RA: variation of seed energy after 10 round trips. (a) output pulse energy and compressed pulse duration at 4.5 W absorbed pump power and (b) AC traces of the compressed pulse at different seed energy.

In conclusion, the ultrafast regenerative amplifier system presented here was completely based on holmium-doped materials. The complete setup consisted of a HDF ultrashort pulse seed oscillator operating at 2100 nm, a grating stretcher, HDF-preamplifier, and a RA based on a Ho:YAG crystal. Appropriate TDF pump lasers were developed to address the optimum absorption wavelengths of the Ho-doped materials. The RA system showed a similar limitation of the pulse energy in terms of the damage threshold of the amplifier crystal compared to Tm:YAP. The achieved output pulse energy exceeded 700 µJ, but the gain spectrum of Ho:YAG caused a strong deformation of the seed signal. In consequence, a multipulse-like structure was visible in the AC trace. This issue could be resolved by hard-cut spectral filtering inside the grating stretcher to achieve compressed pulse durations of 1.2 ps at a compressor efficiency of 50 %. Due to the narrow gain spectrum, these pulses are 3 times longer than in the case of Tm:YAP. Anyway, no satellite pulses are visible in the AC trace although the same RA cavity was used to amplify the pulses, which can be explained by the absence of strong atmospheric absorption lines at 2.1 µm. During variation of round trip numbers, the RA system showed bifurcation instabilities at low pump powers. Higher pump power led to suppression of the bifurcation instabilities but

also to the onset of gain saturation. The variation of repetition rate revealed a nearly exponential increase of output pulse energy with decreasing repetition rate. Furthermore, a variation of the seed energy showed a linear increase of the output energy.

CHAPTER 6

Conclusion

In this thesis, two different regenerative amplifier systems were presented, which were based on thulium- and holmium-doped materials and operated at 1.94 µm and 2.1 µm wavelength, respectively. For both systems, individual ultrashort pulse fiber oscillators, stretching units, fiber preamplifiers, and pump lasers were developed. Similar seed pulses for the subsequent regenerative amplifiers in terms of pulse energy, pulse duration, and optical spectrum were used for a feasible comparison between both regenerative amplifier materials.

At 1.94 µm, the ultrashort pulse seed oscillator was based on a thulium-doped fiber and utilized the concept of stretched-pulse operation by the use of a normal dispersion fiber. The laser emitted low energy pulses with an uncompressed duration of 112 fs at a peak wavelength of 1935 nm. The output characteristics were confirmed by numerical simulations and showed good agreement. After stretching the pulses in a fiber stretcher, they were amplified in a subsequent thulium-doped fiber amplifier to a maximum pulse energy of 61 nJ. A pulse picker consisting of a Pockels cell and a TFP reduced the repetition rate from MHz to kHz range. The achieved pulse duration is one of the shortest compared with existing passively mode-locked ultrashort pulse TDF oscillators [Hax08; Wan10]. Only JIANG et al. [Jia12] demonstrated a much lower pulse duration of 58 fs directly out of the oscillator by the use of a very short fiber section, but the high repetition rate of 500 MHz makes pulse picking nearly unfeasible and therefore unsuitable for regenerative amplification.

For the design of the regenerative amplifier, several issues had to be considered like the targeted mode field diameters and the strong thermal lens in the Tm:YAP crystal. The designed cavity of the regenerative amplifier was firstly investigated in terms of continuous wave operation and tunability. Secondly, experiments in q-switch operation were performed to explore the possibly achievable pulse energies for the regenerative amplification operation which were found up to the mJ-range.

Finally, regenerative amplification was demonstrated for the first time with thulium-doped materials. The regenerative amplifier based on the Tm:YAP crystal was seeded with the pulses of the thulium-preamplifier at a pulse energy of around 25 nJ and 1 kHz repetition rate. The laser system delivered more than 700 µJ output pulse energy, which was limited by the damage threshold of the laser crystal. Strong atmospheric absorption lines were present at the wavelength of 1937 nm of the pulses, which imposed the optical spectrum strongly and caused post-pulses and a long ps-pedestal in the autocorrelation trace of the compressed pulses. Purging the regenerative amplifier cavity with nitrogen gas reduced these atmospheric absorption and the pedestal in the autocorrelation trace, whereas satellite pulses remained beside the main pulse. These satellite pulses were generated possibly by residual water absorption in the porous e-beam coatings of the RTP crystals of the PC. However, the pulses could be dechirped in a Martinez grating compressor to a minimum pulse duration of 410 fs with an efficiency of 50 %. The variation of round trip numbers for scalability revealed a linear behaviour of the output energy without any signs of gain saturation or bifurcation instabilities. By increasing the repetition rate from 100 Hz to 3 kHz, an exponential decrease of output energy was revealed, which was explained by the long lifetime of Tm:YAP. When varying the seed energy, the output energy of the regenerative amplifier increased linearly up to 700 µJ. The compressed pulse duration was shortest with 380 fs at this highest output energy which resulted in a maximum peak power of 700 MW after compression. Until now, this was the highest peak power demonstrated at this wavelength with thulium-doped materials. Comparable pulse duration but lower pulse energy of 120 µJ was achieved by STUTZKI et al. [Stu15] by the use of Tm-doped large-pitch fibers.

The overall system was then modified to operate at 2.1 µm wavelength with holmium-doped materials. The seed oscillator was changed to an ultrashort pulse holmium-doped fiber oscillator, which based on the same pulse evolution scheme as the thulium-doped oscillator. The emitted duration of the low energy, single pulses was 463 fs at a central wavelength of 2100 nm, which was supported by numerical simulations. As the propagation losses in silica fibers are higher at 2.1 µm in comparison to 1.94 µm, a grating stretcher was used before the holmium-doped fiber preamplifier, which amplified the pulses up to a pulse energy of 36.8 nJ. The following pulse picking and mode field adaption scheme was the same that was already applied in the thulium-doped system. Shorter pulse durations of less than 160 fs were attained in ultrashort pulse HDF oscillators with an optimized dispersion management [Hoo13; Li14].

The cavity of the following regenerative amplifier based on Ho:YAG was the same which was already used for Tm:YAP with only few changes to ensure a good comparability

between both systems. Four different doping concentrations were tested in continuous wave experiments for maximum output power which was found at the 1.6 at. % doped crystal. Q-switch experiments revealed pulse energies of more than 1 mJ for various repetition rates.

Although the optical seed spectrum was slightly narrower, the pulse parameters used for seeding the Ho:YAG regenerative amplifier were comparable to the case of Tm:YAP. The spectral shape, pulse energy, stretched pulse duration, and chirp-sign were similar, which enabled a good comparison between both regenerative amplifier laser materials. Ho:YAG showed a higher amplification efficiency compared to Tm:YAP, so less round trips were used. At seed parameters similar to Tm:YAP, a comparable output energy of more than 700 μJ was attained of the regenerative amplifier based on the Ho:YAG crystal before it was limited by the crystal's damage threshold. The gain spectrum of Ho:YAG caused a strong gain shaping of the input pulses which induced a multipulse-like structure in the AC trace. This was mitigated by spectral precompensation of the seed pulses and the resulting duration was 1.2 ps without any signs of multiple pulses or long-term background. The achieved pulse duration was three times longer than in the case of Tm:YAP because of the narrower gain spectrum of Ho:YAG. When varying the round trip numbers to scale the output energy, limitations arose, which were in contrast to the linear relation found in Tm:YAP. Bifurcation instabilities appeared at low pump power which could be suppressed at higher pump power, but the maximum output energy saturated. The variation of repetition rate revealed the same course of lines at similar pump intensity as in the case of Tm:YAP during an increase from 100 Hz to 3 kHz. The variation of the seed energy was performed with a slightly different seed oscillator and showed a linear relation of the output energy.

In general, both systems delivered comparable experimental results in terms of output energy but Ho:YAG performed more efficiently. Higher output energy was demonstrated with Ho:YLF regenerative amplifiers with multiple mJ output energy by the use of much higher pump power [Der13; Gra15; Kro15b], but the pulse durations were in range of few to hundreds of ps. Only MALEVICH et al. [Mal13] demonstrated a Ho:YAG regenerative amplifier with mJ output energy and a pulse duration of 530 fs by the use of a broadband seed source and spectral precompensation. In terms of pulse duration, this was surpassed by the here described Tm:YAP regenerative amplifier, which was demonstrated for the first time and offered a duration less than 410 fs because of the generally broader gain spectrum in Thulium-doped crystals.

CHAPTER 7

Outlook

The developed laser systems described in this thesis represent the next generation of high energy ultrashort pulse lasers. Significant progress was achieved in understanding of thulium- and holmium-based regenerative amplifier systems. The achieved results show that pulse energies of hundreds of μJ can easily be reached at 2 μm wavelength by overcoming the technical difficulties and physical effects arising at this wavelength. The compressed pulse durations are comparable to existing ytterbium amplifier systems operating at 1 μm wavelength [Bal11; Bue09; Chi09; Liu02; Ric10; Say09]. However, there are some aspects for further research, which could be considered.

Further scaling of the pulse energy can be accomplished by subsequent singlepass crystal amplifier stages to boost the pulse energy into the multi-mJ region. DERGACHEV [Der13] showed this in principle with hundreds of ps pulse duration in Ho:YLF crystals at a wavelength of 2.05 μm, which supports only a small spectral bandwidth. The transfer to femtosecond amplifier systems was not demonstrated yet and must be clarified, also with regard to the strong structured gain spectrum of holmium-doped crystals, which is a basic problem in those crystals. The here demonstrated spectral shaping of the seed signal to overcome the spectral gain deformation is rather course and should be optimized, for example by the use of spatial light modulators to affect amplitude and phase independently.

Anyway, high power pump sources for these holmium amplifiers are commercially available. The drawback of these sources are mainly the costs as well as noise influences by atmospheric absorptions at this wavelength. These can have a strong impact on the beam profile and the whole beam line for the pump laser needs to be purged as consequence.

Bifurcation instabilities in regenerative amplifiers are a general problem [Dör04], but KROETZ et al. [Kro15a] showed just recently that with a detailed numerical analysis specific stability points can be obtained, which offer a higher pulse energy and very low noise

operation while simultaneously suppressing bifurcation instabilities.

Further improvement in terms of shorter pulses can be attained by the use of a nonlinear compression stage in a gas-filled hollow-core photonic crystal fiber, which was demonstrated by BALCIUNAS et al. [Bal15] and GEBHARDT et al. [Geb15a] at 2 µm wavelength. The optical spectrum of a high energy pulse (tens of µJ) can be broadened to support tens of fs or even sub-cycle pulse duration. The attained intensity is in the order of ionization ($\sim 10^{14}\,\mathrm{W/cm^2}$), which is sufficient for strong-field applications like high harmonics generation.

In terms of application, the presented laser systems are suitable as front-end for frequency conversion stages to longer wavelengths [Der08; Lei12; Mal15a; Pet01]. Optical parametric processes based on nonlinear crystals like ZGP, AGS, AGSe etc. to generate multi-µJ, wavelength tunable pulses in the range from $3-10\,\mu\mathrm{m}$ are important features for further studies. As already mentioned, this region is highly interesting for several applications like resonant infrared ablation of polymers, microstructuring and general material processing of semiconductors [Did07; Hur07; Sch10].

Bibliography

[Ada89]   R. Adair, L. L. Chase, and S. A Payne: "Nonlinear refractive index of optical crystals". *Phys. Rev. B* **39** (5), pp. 3337–3350 (1989).

[Agr07]   G. P. Agrawal: *Nonlinear fiber Optics.* 4th ed. Academic Press (2007).

[Bal15]   T. Balciunas, C. Fourcade-Dutin, G. Fan, T. Witting, A. A. Vorin, A. M. Zheltikov, F. Gerome, G. G. Paulus, A. Baltuska, and F. Benabid: "A strong-field driver in the single-cycle regime based on self-compression in a kagome fibre". *Nat. Commun.* **6**, p. 6117 (2015).

[Bal11]   T. Balčiunas, O. D. Mücke, P. Mišeikis, G. Andriukaitis, A. Pugžlys, L. Giniunas, R. Danielius, R. Holzwarth, and A. Baltuška: "Carrier envelope phase stabilization of a Yb:KGW laser amplifier". *Opt. Lett.* **36** (16), pp. 3242–3244 (2011).

[Bél76]   P.-A. Bélanger and J. Boivin: "Gigawatt peak-power pulse generation by injection of single short pulse in a regenerative amplifier above threshold (RAAT)". *Can. J. Phys.* **54** (6), pp. 720–727 (1976).

[Bro93]   M. M. Broer, D. M. Krol, and D. J. DiGiovanni: "Highly nonlinear near-resonant photodarkening in a thulium-doped aluminosilicate glass fiber". *Opt. Lett.* **18** (10), pp. 799–801 (1993).

[Bue09]   U. Buenting, H. Sayinc, D. Wandt, U. Morgner, and D. Kracht: "Regenerative thin disk amplifier with combined gain spectra producing 500 µJ sub 200 fs pulses". *Opt. Express* **17** (10), pp. 8046–8050 (2009).

[Čer05]   P. Černý and D. Burns: "Modeling and experimental investigation of a diode-pumped Tm:YAlO$_3$ laser with a- and b-cut crystal orientations". *IEEE J. Sel. Topics Quantum Electron.* **11** (3), pp. 674–681 (2005).

[Cha12]   A. Chamorovskiy, A. V. Marakulin, S. Ranta, M. Tavast, J. Rauti-
ainen, T. Leinonen, A. S. Kurkov, and O. G. Okhotnikov: "Femtosecond
mode-locked holmium fiber laser pumped by semiconductor disk laser". *Opt.
Lett.* **37** (9), pp. 1448–1450 (2012).

[Chi09]   N. B. Chichkov, U. Bünting, D. Wandt, U. Morgner, J. Neumann, and
D. Kracht: "Spatially dispersive regenerative amplification of ultrashort laser
pulses". *Opt. Express* **17** (26), pp. 24075–24083 (2009).

[Cla02]   W. A. Clarkson, N. P. Barnes, P. W. Turner, J. Nilsson, and D. C.
Hanna: "High-power cladding-pumped Tm-doped silica fiber laser with wave-
length tuning from 1860 to 2090 nm". *Opt. Lett.* **27** (22), pp. 1989–1991 (2002).

[Col11]   N. Coluccelli, A. Gambetta, D. Gatti, M. Marangoni, A. Di Lieto, M.
Tonelli, G. Galzerano, and P. Laporta: "1.6-W self-referenced frequency
comb at 2.06 µm using a Ho:YLF multipass amplifier". *Opt. Lett.* **36** (12),
pp. 2299–2301 (2011).

[Der13]   A. Dergachev: "High-energy, kHz-rate, picosecond, 2-µm laser pump source
for mid-IR nonlinear optical devices". *Proc. SPIE 8599, Solid State Lasers
XXII: Technology and Devices*, 85990B (2013).

[Der08]   A. Dergachev, D. Armstrong, A. Smith, T. Drake, and M. Dubois:
"High-power, high-energy ZGP OPA Pumped by a 2.05-µm Ho:YLF MOPA
System". *Proc. SPIE 6875, Nonlinear Frequency Generation and Conversion:
Materials, Devices, and Applications VII*, p. 687507 (2008).

[Did07]   S. A. Diddams, L. Hollberg, and V. Mbele: "Molecular fingerprinting with
the resolved mode of a femtosecond laser frequency comb". *Nature* **445** (7128),
pp. 627–630 (2007).

[Die06]   J.-C. Diels and W. Rudolph: *Ultrashort Laser Pulse Phenomena.* 2nd ed.
Academic Press (2006).

[Dör04]   J. Dörring, A. Killi, U. Morgner, A. Lang, M. Lederer, and D. Kopf:
"Period doubling and deterministic chaos in continuously pumped regenerative
amplifiers". *Opt. Express* **12** (8), pp. 1759–1768 (2004).

[Ehl04]   H. Ehlers, T. Gross, M. Lappschies, and D. Ristau: "Ion-assisted deposi-
tion processes for precision and laser optics". *Proc. SPIE 5250, Advances in
Optical Thin Films*, pp. 519–527 (2004).

[Eld97]   I. F. ELDER and J. PAYNE: "Diode-pumped, room-temperature Tm:YAP laser".
           Appl. Opt. **36** (33), pp. 8606–8610 (1997).

[Fra63]   L. M. FRANTZ and J. S. NODVIK: "Theory of pulse propagation in a laser
           amplifier". *J. Appl. Phys.* **34** (8), pp. 2346–2350 (1963).

[Geb15a]   M. GEBHARDT, C. GAIDA, S. HÄDRICH, F. STUTZKI, C. JAUREGUI, J. LIMPERT,
           and A. TÜNNERMANN: "Nonlinear compression of an ultrashort-pulse thulium-
           based fiber laser to sub-70 fs in Kagome photonic crystal fiber". *Opt. Lett.* **40**
           (12), pp. 2770–2773 (2015).

[Geb15b]   M. GEBHARDT, C. GAIDA, F. STUTZKI, S. HÄDRICH, C. JAUREGUI, J. LIMPERT,
           and A. TÜNNERMANN: "Impact of atmospheric molecular absorption on the
           temporal and spatial evolution of ultra-short optical pulses". *Opt. Express* **23**
           (11), pp. 13776–13787 (2015).

[Geh14]   N. GEHLICH, T. BONHOFF, L. SISKEN, M. RAMM, C. GAIDA, M. GEBHARDT,
           I. MINGAREEV, L. SHAH, and M. C. RICHARDSON: "Utilizing the transparency
           of semiconductors via backside machining with nanosecond 2 µm Tm:fiber
           laser". *Proc. SPIE 8968, Laser-based Micro- and Nanoprocessing VIII*, 89680W
           (2014).

[Gra15]   L. VON GRAFENSTEIN, M. BOCK, U. GRIEBNER, and T. ELSAESSER: "8 mJ, 1
           kHz, Picosecond Ho:YLF Regenerative Amplifier". *Advanced Solid State Lasers.*
           Optical Society of America, AW4A.8 (2015).

[Gu09]   X. GU, G. MARCUS, Y. DENG, T. METZGER, C. TEISSET, N. ISHII, T. FUJI, A.
           BALTUSKA, R. BUTKUS, V. PERVAK, H. ISHIZUKI, T. TAIRA, T. KOBAYASHI,
           R. KIENBERGER, and F. KRAUSZ: "Generation of carrier-envelope-phase-stable
           2-cycle 740-µJ pulses at 2.1-µm carrier wavelength". *Opt. Express* **17** (1), pp. 62–
           69 (2009).

[Gum11]   R. GUMENYUK, I. VARTIAINEN, H. TUOVINEN, and O. G. OKHOTNIKOV:
           "Dissipative dispersion-managed soliton 2 µm thulium/holmium fiber laser".
           Opt. Lett. **36** (5), pp. 609–611 (2011).

[Hai04]   S. HAIDAR, K. MIYAMOTO, and H. ITO: "Generation of tunable mid-IR (5.5–9.3
           µm) from a 2-µm pumped ZnGeP$_2$ optical parametric oscillator". *Opt. Commun.*
           241 (1-3), pp. 173–178 (2004).

[Har06]   K. S. HARSHA: *Principles of Physical Vapor Deposition of Thin Films.* Elsevier
           Ltd. (2006).

[Hau07] C. P. HAURI, R. B. LOPEZ-MARTENS, C. I. BLAGA, K. D. SCHULTZ, J. CRYAN, R. CHIRLA, P. COLOSIMO, G. DOUMY, A. M. MARCH, C. ROEDIG, E. SISTRUNK, J. TATE, J. WHEELER, L. F. DIMAURO, and E. P. POWER: "Intense self-compressed, self-phase-stabilized few-cycle pulses at 2 µm from an optical filament". *Opt. Lett.* **32** (7), pp. 868–870 (2007).

[Hau91] H. A. HAUS, J. G. FUJIMOTO, and E. P. IPPEN: "Structures for additive pulse mode locking". *J. Opt. Soc. Am. B* **8** (10), pp. 2068–2076 (1991).

[Hau93] H. A. HAUS, J. D. MOORES, and L. E. NELSON: "Effect of third-order dispersion on passive mode locking". *Opt. Lett.* **18** (1), pp. 51–53 (1993).

[Hax08] F. HAXSEN, A. RUEHL, M. ENGELBRECHT, D. WANDT, U. MORGNER, and D. KRACHT: "Stretched-pulse operation of a thulium-doped fiber laser". *Opt. Express* **16** (25), pp. 20471–20476 (2008).

[Hax10] F. HAXSEN, D. WANDT, U. MORGNER, J. NEUMANN, and D. KRACHT: "Pulse energy of 151 nJ from ultrafast thulium-doped chirped-pulse fiber amplifier". *Opt. Lett.* **35** (17), pp. 2991–2993 (2010).

[Hax12] F. HAXSEN, D. WANDT, U. MORGNER, J. NEUMANN, and D. KRACHT: "Monotonically chirped pulse evolution in an ultrashort pulse thulium-doped fiber laser". *Opt. Lett.* **37** (6), pp. 1014–1016 (2012).

[Hem15] M. HEMMER, D. SÁNCHEZ, M. JELÍNEK, V. SMIRNOV, H. JELINKOVA, V. KUBEČEK, and J. BIEGERT: "2-µm wavelength, high-energy Ho:YLF chirped-pulse amplifier for mid-infrared OPCPA". *Opt. Lett.* **40** (4), pp. 451–454 (2015).

[Hem13] A. HEMMING, N. SIMAKOV, A. DAVIDSON, S. BENNETTS, M. HUGHES, N. CARMODY, P. DAVIES, L. CORENA, D. STEPANOV, J. HAUB, R. SWAIN, and A. CARTER: "A monolithic cladding pumped holmium-doped fibre laser". *CLEO: 2013.* Optical Society of America, CW1M.1 (2013).

[Hil14] A. HILDENBRAND-DHOLLANDE and F. R. WAGNER: "Laser-Induced Damage in Optical Materials". Ed. by DETLEV RISTAU. CRC Press. Chap. Materials for Lasers: Frequency Conversion, Q-Switching, and Active Materials (2014).

[Hod97] N. HODGSON and H. WEBER: *Optical resonators.* Springer-Verlag London (1997).

[Hoo13] H. HOOGLAND, A. THAI, D. SÁNCHEZ, S. L. COUSIN, M. HEMMER, M. ENGELBRECHT, J. BIEGERT, and R. HOLZWARTH: "All-PM coherent 2.05 µm Thulium/Holmium fiber frequency comb source at 100 MHz with up to 0.5 W average power and pulse duration down to 135 fs". *Opt. Express* **21** (25), pp. 31390–31394 (2013).

[Hur07] W. C. HURLBUT, Y.-S. LEE, K. L. VODOPYANOV, P. S. KUO, and M. M. FEJER: "Multiphoton absorption and nonlinear refraction of GaAs in the mid-infrared". *Opt. Lett.* **32** (6), pp. 668–670 (2007).

[Ild04] F. Ö. ILDAY: "Theory and Practice of High-Energy Femtosecond Fiber Lasers". PhD thesis. Cornell University (2004).

[Ild03] F. Ö. ILDAY, J. R. BUCKLEY, H. LIM, F. W. WISE, and W. G. CLARK: "Generation of 50-fs, 5-nJ pulses at 1.03 µm from a wave-breaking-free fiber laser". *Opt. Lett.* **28** (15), pp. 1365–1367 (2003).

[Ise02] A. ISEMANN: "Diodengepumpte Ultrakurzpuls-Laser und -Verstärkersysteme auf Colquiriite-Basis". PhD thesis. University of Hannover (2002).

[Jac06] S. D. JACKSON: "Midinfrared holmium fiber lasers". *IEEE J. Quantum Electron.* **42** (2), pp. 187–191 (2006).

[Jac99] S. D. JACKSON and T. A. KING: "Theoretical modeling of Tm-doped silica fiber lasers". *J. Lightwave Technol.* **17** (5), pp. 948–956 (1999).

[Jen06] L. JENSEN, M. JUPÉ, H. MÄDEBACH, H. EHLERS, K. STARKE, D. RISTAU, W. RIEDE, P. ALLENSPACHER, and H. SCHROEDER: "Damage threshold investigations of high-power laser optics under atmospheric and vacuum conditions". *Proc. SPIE 6403, Laser-Induced Damage in Optical Materials*, 64030U (2006).

[Jia12] JIE JIANG, CHRISTIAN MOHR, JENS BETHGE, ANDREW MILLS, WILL MEFFORD, INGMAR HARTL, MARTIN E. FERMANN, CHIEN-CHUNG LEE, S. SUZUKI, THOMAS R. SCHIBLI, NICK LEINDECKER, KONSTANTIN L. VODOPYANOV, and PETER G. SCHUNEMANN: "500 MHz, 58fs highly coherent Tm fiber soliton laser". *Conference on Lasers and Electro-Optics 2012*. Optical Society of America, CTh5D.7 (2012).

[Kad11] P. KADWANI, R. SIMS, J. CHIA, F. ALTAT, L. SHAH, and M. RICHARDSON: "Atmospheric Propagation Testing Using Broadband Thulium Fiber Systems". *Advances in Optical Materials*. Optical Society of America, FWB3 (2011).

[Kär98]   F. X. KÄRTNER, J. AUS DER AU, and U. KELLER: "Mode-Locking with Slow and Fast Saturable Absorbers - What's the difference?" *IEEE J. Sel. Topics Quantum Electron.* **4** (2), pp. 159–168 (1998).

[Kib05]   B. KIBLER, J.M. DUDLEY, and S. COEN: "Supercontinuum generation and nonlinear pulse propagation in photonic crystal fiber: influence of the frequency-dependent effective mode area". *Appl. Phys. B* **81** (2–3), pp. 337–342 (2005).

[Kie09]   K. KIEU and F.W. WISE: "Soliton Thulium-Doped Fiber Laser With Carbon Nanotube Saturable Absorber". *IEEE Phot. Technol. Lett.* **21** (3), pp. 128–130 (2009).

[Kim09]   J. W. KIM, A. BOYLAND, J. K. SAHU, and W. A. CLARKSON: "Ho-doped silica fibre laser in-band pumped by a Tm-doped fibre laser". *2009 European Conference on Lasers and Electro-Optics - European Quantum Electronics Conference*, pp. 1–1 (2009).

[Kiv07]   S. KIVISTÖ, T. HAKULINEN, M. GUINA, and O. G. OKHOTNIKOV: "Tunable Raman Soliton Source Using Mode-Locked Tm-Ho Fiber Laser". *IEEE Phot. Technol. Lett.* **19** (12), pp. 934–936 (2007).

[Koe06]   W. KOECHNER: *Solid-state Laser Engineering.* Ed. by W. T. RHODES. 6th ed. Springer-Verlag (2006).

[Koo12]   P. KOOPMANN: "Thulium- and Holmium-Doped Sesquioxides for 2 µm Lasers". PhD thesis. University of Hamburg (2012).

[Koo11]   P. KOOPMANN, S. LAMRINI, K. SCHOLLE, P. FUHRBERG, K. PETERMANN, and G. HUBER: "Efficient diode-pumped laser operation of $Tm:Lu_2O_3$ around 2 µm". *Opt. Lett.* **36** (6), pp. 948–950 (2011).

[Kra92]   J. L. KRAUSE, K. J. SCHAFER, and K. C. KULANDER: "High-order harmonic generation from atoms and ions in the high intensity regime". *Phys. Rev. Lett.* **68** (24), pp. 3535–3538 (1992).

[Kro15a] P. KROETZ, A. RUEHL, G. CHATTERJEE, A.-L. CALENDRON, K. MURARI, H. CANKAYA, P. LI, F. KÄRTNER, I. HARTL, and R. J. D. MILLER: "Overcoming Bifurcation Instability in High-Repetition-Rate Ho:YLF Regenerative Amplifiers". *Opt. Lett.* **40** (23), pp. 5427–5430 (2015).

[Kro15b] P. Kroetz, A. Ruehl, G. Chatterjee, P. Li, K. Murari, H. Cankaya, A.-L. Calendron, F. Kärtner, I. Hartl, and R. J. D. Miller: "Ho:YLF Regenerative Amplifier with 6.9 mJ at 1 kHz Overcoming Bifurcation Instability". *Advanced Solid State Lasers.* Optical Society of America, ATh3A.4 (2015).

[Kro26] R. de L. Kronig: "On the theory of dispersion of X-Rays". *J. Opt. Soc. Am.* **12** (6), pp. 547–556 (1926).

[Kur10] A. S. Kurkov, V. V. Dvoyrin, and A. V. Marakulin: "All-fiber 10 W holmium lasers pumped at $\lambda = 1.15$ µm". *Opt. Lett.* **35** (4), pp. 490–492 (2010).

[Kwi09] J. Kwiatkowski, J. K. Jabczynski, L. Gorajek, W. Zendzian, H. Jelínková, J. Šulc, M. Němec, and P. Koranda: "Resonantly pumped tunable Ho:YAG laser". *Laser Phys. Lett.* **6** (7), pp. 531–534 (2009).

[Lei12] N. Leindecker, A. Marandi, R. L. Byer, K. L. Vodopyanov, J. Jiang, I. Hartl, M. Fermann, and P. G. Schunemann: "Octave-spanning ultrafast OPO with 2.6-6.1µm instantaneous bandwidth pumped by femtosecond Tm-fiber laser". *Opt. Express* **20** (7), pp. 7046–7053 (2012).

[Li11] G. Li, B. Q. Yao, P. B. Meng, X. M. Duan, Y. L. Ju, and Y. Z. Wang: "Diode-pumped efficient laser operation and spectroscopy of Tm,Ho:YVO$_4$". *Opt. Mater.* **33** (6), pp. 937–941 (2011).

[Li15] P. Li, A. Ruehl, C. Bransley, and I. Hartl: "Passively Mode-locked Holmium-doped Fiber Oscillators Optimized for Ho:YLF Amplifier Seeding". *CLEO: 2015.* Optical Society of America, STh1L.4 (2015).

[Li14] P. Li, A. Ruehl, U. Grosse-Wortmann, and I. Hartl: "Sub-100 fs passively mode-locked holmium-doped fiber oscillator operating at 2.06 µm". *Opt. Lett.* **39** (24), pp. 6859–6862 (2014).

[Liu02] H.-H. Liu, J. Nees, and G. Mourou: "Directly diode-pumped Yb:KY(WO$_4$)$_2$ regenerative amplifiers". *Opt. Lett.* **27** (9), pp. 722–724 (2002).

[Loi13] P. A. Loiko, K. V. Yumashev, V. N. Matrosov, and N. V. Kuleshov: "Dispersion and anisotropy of thermo-optic coefficients in tetragonal GdVO$_4$ and YVO$_4$ laser host crystals". *Appl. Opt.* **52** (4), pp. 698–705 (2013).

[Mal13]   P. Malevich, G. Andriukaitis, T. Flöry, A. J. Verhoef, A. Fernández, S. Ališauskas, A. Pugžlys, A. Baltuška, L. H. Tan, C. F. Chua, and P. B. Phua: "High energy and average power femtosecond laser for driving mid-infrared optical parametric amplifiers". *Opt. Lett.* **38** (15), pp. 2746–2749 (2013).

[Mal15a]   P. Malevich, T. Kanai, G. Gitzinger, R. Maksimenka, N. Forget, A. Baltuska, and A. Pugzlys: "Broadband ZGP OPA Pumped by Femtosecond Ho:YAG Chirped Pulse Amplifier". *CLEO: 2015.* Optical Society of America, SM1P.3 (2015).

[Mal15b]   P. Malevich, T. Kanai, H. Hoogland, R. Holzwarth, A. Baltuska, and A. Pugzlys: "Millijoule 1-ps Pulses from a kHz Ho:YAG Regenerative Amplifier Seeded with a Tm,Ho-Fiber Laser". *CLEO: 2015.* Optical Society of America, SM1P.4 (2015).

[Mar84]   O. E. Martinez, J. P. Gordon, and R. L. Fork: "Negative group-velocity dispersion using refraction". *J. Opt. Soc. Am. A* **1** (10), pp. 1003–1006 (1984).

[Mat10]   Scientific Materials: *Yttrium Orthoaluminate.* Scientific Materials Corp. 2010. URL: http://scientificmaterials.com/downloads/YALO.pdf (visited on 11/03/2015).

[Mie14]   M. Miebach: "Aufbau und Charakterisierung eines passiv modengekoppemode Ultrakurzpuls-Laser mit Holmium-Faser". Bachelor's Thesis. Münster University of Applied Sciences (2014).

[Min15]   I. Mingareev, N. Gehlich, T. Bonhoff, A. Abdulfattah, A. M. Sincore, P. Kadwani, L. Shah, and M. Richardson: "Principles and applications of trans-wafer processing using a 2-µm thulium fiber laser". English. *Int. J. Adv. Manuf. Technol.* Pp. 1–12 (2015).

[Mit05]   F. Mitschke: *Glasfasern.* Elsevier GmbH (2005).

[Mol80]   L. F. Mollenauer, R. H. Stolen, and J. P. Gordon: "Experimental Observation of Picosecond Pulse Narrowing and Solitons in Optical Fibers". *Phys. Rev. Lett.* **45**, pp. 1095–1098 (1980).

[Mou09]   P. F. Moulton, G. A. Rines, E. V. Slobodtchikov, K. F. Wall, G. Frith, B. Samson, and A. L. G. Carter: "Tm-Doped Fiber Lasers: Fundamentals and Power Scaling". *IEEE J. Sel. Topics Quantum Electron.* **15** (1), pp. 85–92 (2009).

[Nai14]   S. Naithani, C. Duterte, M. Levichkova, A. Grisard, D. Schaubroeck, E. Lallier, Y. Hernandez, K. Walzer, and G. Van Steenberge: "Mid-infrared resonant ablation for selective patterning of thin organic films". *Proc. SPIE 9135, Laser Sources and Applications II*, 91350K-01–91350K-12 (2014).

[Nai13]   S. Naithani, A. Grisard, D. Schaubroeck, E. Lallier, and G. Van Steenberge: "Mid-infrared resonant ablation of PMMA". *Proceedings of 6th International Congress on Laser Advanced Materials Processing.* Niigata, Japan, pp. 1–5 (2013).

[Nel95]   L. E. Nelson, E. P. Ippen, and H. A. Haus: "Broadly tunable sub-500 fs pulses from an additive-pulse mode-locked thulium-doped fiber ring laser". *Appl. Phys. Lett.* **67** (1), pp. 19–21 (1995).

[Nel97]   L. E. Nelson, D. J. Jones, K. Tamura, H. A. Haus, and E. P. Ippen: "Ultrashort-pulse fiber ring lasers". English. *Appl. Phys. B* **65** (2), pp. 277–294 (1997).

[Pas15]   R. Paschotta: *RP Photonics Encyclopedia.* RP Photonics Consulting GmbH. 2015. URL: http://www.rp-photonics.com (visited on 11/03/2015).

[Pay92]   S. A. Payne, L. L. Chase, L. K. Smith, W. L. Kway, and W. F. Krupke: "Infrared cross-section measurements for crystals doped with Er^{3+}, Tm^{3+}, and Ho^{3+}". *IEEE J. Quantum Electron.* **28** (11), pp. 2619–2630 (1992).

[Pet01]   V. Petrov, F. Rotermund, and F. Noack: "Generation of high-power femtosecond light pulses at 1 kHz in the mid-infrared spectral range between 3 and 12 µm by second-order nonlinear processes in optical crystals". *J. Opt. A: Pure Appl. Opt.* **3** (3), R1 (2001).

[Ric10]   S. Ricaud, F. Druon, D. N. Papadopoulos, P. Camy, J.-L. Doualan, R. Moncorgé, M. Delaigue, Y. Zaouter, A. Courjaud, P. Georges, and E. Mottay: "Short-pulse and high-repetition-rate diode-pumped $Yb:CaF_2$ regenerative amplifier". *Opt. Lett.* **35** (14), pp. 2415–2417 (2010).

[Rot09]   L. S. Rothman et al.: "The HITRAN 2008 molecular spectroscopic database". *J. Quant. Spectrosc. Radiat. Transf.* **110** (9–10), pp. 533–572 (2009).

[Ryb03]   W. Ryba-Romanowski: "YVO_4 – crystal puzzles and challenges". *Crys. Res. Technol.* **38** (3–5), pp. 225–236 (2003).

[Say09]   H. SAYINC, U. BUENTING, D. WANDT, J. NEUMANN, and D. KRACHT: "Ul-
           trafast high power Yb:KLuW regenerative amplifier". *Opt. Express* **17** (17),
           pp. 15068–15071 (2009).

[Sch10]   K. SCHOLLE, S. LAMRINI, P. KOOPMANN, and P. FUHRBERG: "Frontiers in
           Guided Wave Optics and Optoelectronics". Ed. by B. PAL. InTech. Chap. 2 µm
           Laser Sources and Their Possible Applications, pp. 471–500 (2010).

[Sch15]   T. SCHREIBER: *Fiberdesk*. 2015. URL: http://www.fiberdesk.com/ (visited
           on 11/03/2015).

[Sei88]   A. SEILMEIER, M. WÖRNER, H.-J. HÜBNER, and W. KAISER: "Distortion of
           infrared picosecond pulses after propagation in atmospheric air". *Appl. Phys.
           Lett.* **53** (25), pp. 2468–2470 (1988).

[Sha96]   R. C. SHARP, D. E. SPOCK, N. PAN, and J. ELLIOT: "190-fs passively mode-
           locked thulium fiber laser with a low threshold". *Opt. Lett.* **21** (12), pp. 881–883
           (1996).

[Sie86]   A. SIEGMAN: *Lasers*. Ed. by A. KELLY. University Science Books (1986).

[Sim13]   N. SIMAKOV, A. HEMMING, W. A. CLARKSON, J. HAUB, and A. CARTER: "A
           cladding-pumped, tunable holmium doped fiber laser". *Opt. Express* **21** (23),
           pp. 28415–28422 (2013).

[Sta03]   A. STARK, L. CORREIA, M. TEICHMANN, S. SALEWSKI, C. LARSEN, V. M
           BAEV, and P. E TOSCHEK: "Intracavity absorption spectroscopy with thulium-
           doped fibre laser". *Opt. Commun.* **215** (1-3), pp. 113–123 (2003).

[Sto78]   R. H. STOLEN and C. LIN: "Self-phase-modulation in silica optical fibers".
           Phys. Rev. A **17** (4), pp. 1448–1453 (1978).

[Sto95]   R. C. STONEMAN and L. ESTEROWITZ: "Efficient 1.94 µm Tm:YALO laser".
           IEEE J. Sel. Topics Quantum Electron. **1** (1), pp. 78–81 (1995).

[Str85]   D. STRICKLAND and G. MOUROU: "Compression of amplified chirped optical
           pulses". *Opt. Commun.* **55** (6), pp. 447–449 (1985).

[Stu15]   F. STUTZKI, C. GAIDA, M. GEBHARDT, F. JANSEN, C. JAUREGUI, J. LIMPERT,
           and A. TÜNNERMANN: "Tm-based fiber laser-system with more than 200 MW
           peak power". *Opt. Lett.* **40** (1), pp. 9–12 (2015).

[Stu14]   F. STUTZKI, C. GAIDA, M. GEBHARDT, F. JANSEN, A. WIENKE, U. ZEITNER,
            F. FUCHS, C. JAUREGUI, D. WANDT, D. KRACHT, J. LIMPERT, and A. TÜN-
            NERMANN: "152 W average power Tm-doped fiber CPA system". *Opt. Lett.* **39**
            (16), pp. 4671–4674 (2014).

[Šul15]   J. ŠULC, H. JELÍNKOVÁ, P. ČERNÝ, K. NEJEZCHLEB, and V. ŠKODA: *Tm:YAP
            and Tm:YAG*. Aug. 2015. URL: http://www.crytur.cz/app/webroot/files/
            editor/file/import/Tm-YAP&YAG.pdf (visited on 11/03/2015).

[Sum94]   D. S. SUMIDA and T. Y. FAN: "Effect of radiation trapping on fluorescence
            lifetime and emissioncross section measurements in solid-state laser media".
            Opt. Lett. **19** (17), pp. 1343–1345 (1994).

[Tam92]   K. TAMURA, H. A. HAUS, and E. P. IPPEN: "Self-starting additive pulse
            mode-locked erbium fibre ring laser". *Electron. Lett.* **28** (24), pp. 2226–2228
            (1992).

[Tam93]   K. TAMURA, E. P. IPPEN, H. A. HAUS, and L. E. NELSON: "77-fs pulse
            generation from a stretched-pulse mode-locked all-fiber ring laser". *Opt. Lett.*
            18 (13), pp. 1080–1082 (1993).

[Tan15]   Y. TANG, A. CHONG, and F. W. WISE: "Generation of 8 nJ pulses from a
            normal-dispersion thulium fiber laser". *Opt. Lett.* **40** (10), pp. 2361–2364 (2015).

[Tur08]   G. TURRI, V. SUDESH, M. RICHARDSON, M. BASS, A. TONCELLI, and M.
            TONELLI: "Temperature-dependent spectroscopic properties of Tm^{3+} in ger-
            manate, silica, and phosphate glasses: A comparative study". *J. Appl. Phys.*
            103 (9), p. 093104 (2008).

[Wal98]   B. M. WALSH, N. P. BARNES, and B. DI BARTOLO: "Branching ratios, cross
            sections, and radiative lifetimes of rare earth ions in solids: Application to Tm^{3+}
            and Ho^{3+} ions in $LiYF_4$". *J. Appl. Phys.* **83** (5), pp. 2772–2787 (1998).

[Wan13]   P. WAN, L.-M. YANG, and J. LIU: "High pulse energy 2 μm femtosecond fiber
            laser". *Opt. Express* **21** (2), pp. 1798–1803 (2013).

[Wan14]   S. WANDEL, G. XU, and I. JOVANOVIC: "Development of a high-peak-power
            5-μm parametric source for dielectric laser acceleration". *Proceedings of In-
            ternational Particle Accelerator Conference (IPAC)*, TUPME045-1460–1462
            (2014).

[Wan10]   Q. WANG, T. CHEN, and K. P. CHEN: "Mode-Locked Ultrafast Thulium Fiber Laser with All-Fiber Dispersion Management". *CLEO: 2010.* Optical Society of America, CFK7 (2010).

[Wei00]   A. M. WEINER: "Femtosecond pulse shaping using spatial light modulators". *Rev. Sci. Instrum.* **71** (5), pp. 1929–1960 (2000).

[Wie12]   A. WIENKE, F. HAXSEN, D. WANDT, U. MORGNER, J. NEUMANN, and D. KRACHT: "Ultrafast, stretched-pulse thulium-doped fiber laser with a fiber-based dispersion management". *Opt. Lett.* **37** (13), pp. 2466–2468 (2012).

[Wie15a] A. WIENKE, D. WANDT, U. MORGNER, J. NEUMANN, and D. KRACHT: "700 MW peak power of a 380 fs regenerative amplifier with Tm:YAP". *Opt. Express* **23** (13), pp. 16884–16889 (2015).

[Wie15b] A. WIENKE, D. WANDT, U. MORGNER, J. NEUMANN, and D. KRACHT: "Comparison Between Tm:YAP and Ho:YAG Ultrashort Pulse Regenerative Amplification". *Advanced Solid State Lasers.* Optical Society of America, ATh2A.39 (2015).

[Wis08]   F. W. WISE, A. CHONG, and W. H. RENNINGER: "High-energy femtosecond fiber lasers based on pulse propagation at normal dispersion". *Laser & Photon. Rev.* **2** (1-2), pp. 58–73 (2008).

[Wu07]   J. WU, Z. YAO, J. ZONG, and S. JIANG: "Highly efficient high-power thulium-doped germanate glass fiber laser". *Opt. Lett.* **32** (6), pp. 638–640 (2007).

[Yam94]   T. YAMAMOTO, Y. MIYAJIMA, and T. KOMUKAI: "1.9 μm Tm-doped silica fibre laser pumped at 1.57 μm". *Electron. Lett.* **30** (3), pp. 220–221 (1994).

[Yan12]   L.-M. YANG, P. WAN, V. PROTOPOPOV, and J. LIU: "2 μm femtosecond fiber laser at low repetition rate and high pulse energy". *Opt. Express* **20** (5), pp. 5683–5688 (2012).

[Zen90]   Z. ZENG, H. SHEN, M. HUANG, H. XU, R. ZENG, Y. ZHOU, G. YU, and C. HUANG: "Measurement of the refractive index and thermal refractive index coefficients of Nd:YAP crystal". *Appl. Opt.* **29** (9), pp. 1281–1286 (1990).

List of Figures

List of Tables

Publications

Peer reviewed publications

1. **Andreas Wienke**, Frithjof Haxsen, Dieter Wandt, Uwe Morgner, Jörg Neumann, and Dietmar Kracht: "Ultrafast, stretched-pulse thulium-doped fiber laser with a fiber-based dispersion management". *Opt. Lett.* **37** (13), pp. 2466–2468 (2012).

2. Frithjof Haxsen, **Andreas Wienke**, Dieter Wandt, Jörg Neumann, and Dietmar Kracht: "Tm-doped mode-locked fiber lasers". *Opt. Fiber Technol.* **20** (6), pp. 650–656 (2014).

3. Fabian Stutzki, Christian Gaida, Martin Gebhardt, Florian Jansen, **Andreas Wienke**, Uwe Zeitner, Frank Fuchs, Cesar Jauregui, Dieter Wandt, Dietmar Kracht, Jens Limpert, and Andreas Tünnermann: "152 W average power Tm-doped fiber CPA system". *Opt. Lett.* **39** (16), pp. 4671–4674 (2014).

4. **Andreas Wienke**, Dieter Wandt, Uwe Morgner, Jörg Neumann, and Dietmar Kracht: "700 MW peak power of a 380 fs regenerative amplifier with Tm:YAP". *Opt. Express* **23** (13), pp. 16884–16889 (2015).

5. **Andreas Wienke**, Dieter Wandt, Uwe Morgner, Jörg Neumann, and Dietmar Kracht: "Comparison between Tm:YAP and Ho:YAG ultrashort pulse regenerative amplification". *Opt. Express* **24** (8), pp. 8632–8640 (2016).

International conference contributions

1. **Andreas Wienke**, Frithjof Haxsen, Dieter Wandt, Uwe Morgner, Jörg Neumann, and Dietmar Kracht: "Fiber based dispersion management in an ultrafast thulium-doped fiber laser and external compression with a normal dispersive fiber". *Lasers, Sources, and Related Photonic Devices*. Optical Society of America, AT4A.26 (2012).

2. **Andreas Wienke**, Frithjof Haxsen, Dieter Wandt, Uwe Morgner, Jörg Neumann, and Dietmar Kracht: "Stretched-pulse operation of a thulium-doped fiber laser with a fiber-based dispersion management". *CLEO: 2012*. Optical Society of America, CM1B.7 (2012).

3. Sébastien Guillemet, Yves Hernandez, Dirk Mortag, Frithjof Haxsen, **Andreas Wienke**, Dieter Wandt, Lasse Leick, and Wolfgang Richter: "High energy and low repetition rate picosecond thulium-doped all-fibre laser with photonic-crystal fibre amplifier". *Advanced Solid-State Lasers*. Optical Society of America, ATu1A.5 (2013).

4. Christian Gaida, Martin Gebhardt, Fabian Stutzki, Florian Jansen, **Andreas Wienke**, Uwe Zeitner, Frank Fuchs, Cesar Jauregui, Dieter Wandt, Dietmar Kracht, Jens Limpert, and Andreas Tünnermann: "Tm-Doped Fiber CPA System with 152 W Average Power and Sub-700 fs Pulse Duration". *Advanced Solid State Lasers*. Optical Society of America, AW4A.4 (2014).

5. **Andreas Wienke**, Dieter Wandt, Uwe Morgner, Jörg Neumann, and Dietmar Kracht: "Regenerative Amplification of Ultrashort Pulses at 2 μm with a Thulium-doped YAP Crystal". *CLEO: 2014*. Optical Society of America, STh4E.1 (2014).

6. Christian Gaida, Fabian Stutzki, Martin Gebhardt, Florian Jansen, **Andreas Wienke**, Uwe D. Zeitner, Frank Fuchs, Cesar Jauregui, Dieter Wandt, Dietmar Kracht, Jens Limpert, and Andreas Tünnermann: "Sub-700fs pulses at 152 W average power from a Tm-doped fiber CPA system". *Proc. SPIE 9344, Fiber Lasers XII: Technology, Systems, and Applications*, 93441K (2015).

7. Sébastien Guillemet, Yves Hernandez, Dirk Mortag, Frithjof Haxsen, **Andreas Wienke**, Dieter Wandt, Lasse Leick, and Wolfgang Richter: "High energy sub-nanosecond thulium-doped all-fibre laser based on a rod-type photonic-crystal fibre amplifier". *Advanced Solid State Lasers*. Optical Society of America, ATh2A.27 (2015).

8. **Andreas Wienke**, Dieter Wandt, Uwe Morgner, Jörg Neumann, and Dietmar Kracht: "Comparison Between Tm:YAP and Ho:YAG Ultrashort Pulse Regenerative Amplification". *Advanced Solid State Lasers*. Optical Society of America, ATh2A.39 (2015).

9. **Andreas Wienke**, Dieter Wandt, Uwe Morgner, Jörg Neumann, and Dietmar Kracht: "Femtosecond High Energy Regenerative Amplifier Operating at 1937 nm". *CLEO/Europe-ECEQ 2015*. European Physcial Society, CA–4 (2015).

Curriculum Vitae

Personal details   Andreas Wienke
16.03.1985 in Lüdenscheid
married, 2 children, German

University education

03/2011 – 03/2016	PhD. student in physics at the Leibniz Universität Hannover
04/2005 – 10/2010	Studies of Physics at the Westfälische Wilhelms-Universität Münster, degree: "Diplom-Physiker" Diploma thesis title: "Construction and characterisation of a passively mode-locked Titanium:Sappire-Laser for low pump powers"

Community service

08/2004 – 04/2005	Hellmig-hospital in Kamen

Education

06/2004	Abitur, Municipal High School in Kamen

Professional affiliations

01/2016 – present	Development engineer at Venteon Laser Technologies GmbH
02/2011 – 12/2015	Research scientist at Laser Zentrum Hannover e. V.
05/2009 – 09/2010	Teaching assistant for programming in LabVIEW at Westfälische Wilhelms-Universität Münster
11/2007 – 09/2010	Teaching assistant at Westfälische Wilhelms-Universität Münster

Acknowledgments

Auch wenn man sich schon länger kennt, lernt man doch immer neue und unbekannte Seiten kennen. Daher danke ich meinem Bürokollegen Gabriel Pelegrina Bonilla für eine ausgezeichnete Atmosphäre im Büro und auch außerhalb der Arbeit.

Trotz aller bisher genannten, gebührt der größte Dank meiner Frau Isabel. Sie begleitet mich seit meiner gesamten Studien- und Promotionszeit, motiviert mich immer weiter zu machen und beflügelt mein Wesen mit ihrer einzigartigen Art.